

**EARLY POSTNATAL CARDIAC DEVELOPMENT IN ATRIAL
NATRIURETIC PEPTIDE GENE-DISRUPTED MICE**

by

Janette Samantha Leroux

A thesis submitted to the Department of Anatomy and Cell Biology

In conformity with the requirements for

the degree of Master of Science

Queen's University

Kingston, Ontario, Canada

(January, 2010)

Copyright © Janette Samantha Leroux, 2010

Abstract

The natriuretic peptide system (NPS) is a hormonal system critical to mammalian cardiovascular homeostasis. The purpose of the present study was to investigate the role of ANP during early postnatal cardiac development by i) monitoring the development of cardiac hypertrophy during early postnatal development of the ANP^{-/-} mice, and ii) comparing morphologic, morphometric and molecular differences in ANP^{+/+} mice compared to ANP^{-/-} mice during this developmental period. Age matched male ANP^{+/+} and ANP^{-/-} mice, aged day 1 and weeks 1 to 5, were evaluated. Body weight, organ weights and hematocrit were recorded. RNA was isolated and quantitative real-time RT-PCR was used to monitor cardiac gene expression. An additional cohort of animals was used for morphologic and morphometric analysis. Heart weight to body weight ratio (HW/BW) was dramatically higher in ANP^{-/-} animals at all time points, indicating cardiac hypertrophy is established before the advent of adult blood pressure. Molecular analysis of gene expression revealed a compensatory response of the NPS in the ANP^{-/-} mice. Specifically an up-regulation of BNP expression in ANP^{-/-} mice was noted throughout postnatal development. Similarly, NPR-A and NPR-C demonstrated compensatory action for the lack of ANP, as expressional levels also varied throughout development. Morphological analysis of cardiac vasculature revealed striking structural differences between ANP^{+/+} and ANP^{-/-} mice. Quantitative stereological analysis of LM images indicated a greater vessel volume in ANP^{-/-} compared to ANP^{+/+} mice. This study demonstrates that alterations in early molecular events, such as changes in NPS expression, may be responsible for the maintenance and progression of cardiac hypertrophy during early postnatal development in the ANP^{-/-} mice. The absence of ANP during this critical period of development has a profound impact on final cardiac structure leading to future pathological states.

Co-Authorship

The research described in this thesis was conducted by Janette Leroux, in collaboration with Dr Yat Tse under the supervision of Dr. Stephen Pang, who conceived the studies described herein. Janette Leroux and Dr Yat Tse performed all tissue collection. Janette Leroux, Dr Yat Tse, and Dr Stephen Pang together performed the vascular cast technique. Janette Leroux performed all histological tissue processing, stereological counting and analysis, and performed all molecular techniques and molecular analysis. Janette Leroux and Dr Yat Tse designed all primers used for molecular analysis.

Acknowledgements

First and foremost I offer my sincerest gratitude to my supervisor, Dr Stephen Pang, who has supported me throughout both my undergraduate and graduate degrees. He has always selflessly given encouragement and mentorship, and has exemplified for me a life of integrity, humility and purpose. My life has been greatly enriched by Dr Pang's influence beyond any scientific pursuit or professional career. It is with pleasure that I will perpetuate the "pay-it-forward" approach that he so graciously embodies.

This work would not have been possible without the constant support of my lab supervisor and friend, Dr Yat Tse. Yat's brilliance in the lab, patience with dilemmas and trouble shooting, and never-ending humour have been a high point over the past few years. It has been a pleasure to work with Yat, and I know that I will continue to learn from him for many years to come. Thanks to my labmates Mr Dave Armstrong and Mr Phil Wong, as well as my neighbour labmates, Ms Carolina Venditti, Ms Alanna Mihic and Ms Lindsay Zara – for their camaraderie, friendship and support along the way.

The opportunities that I have gained through my time in the Department of Anatomy and Cell Biology is remarkable - I cannot begin to express the gratitude I feel for the guidance and friendship offered by faculty and staff. In particular, thank you to Drs Richard Oko, Les Mackenzie, Conrad Reifel, Dave Andrew, Ron Easteal, Fred Kan and Charles Graham. I am very thankful for the special friendship that I share with Mrs Marilyn McCauley – I thoroughly enjoyed our many chats and lunches. I would also like to thank Mrs Anita Lister for her uplifting attitude, patience and listening ear. I thoroughly appreciate the opportunity that Mr Wayne Lyons gave me as a high school co-op student, and then Mr Rick Hunt as a summer student worker in

the Anatomy Lab. I have enjoyed working with Mr Earl Donaldson – Earl’s great sense of humour made any task enjoyable.

I am also greatly appreciative of Dr Mark Rosenberg from the Department of Geography for helping me realize my interests in social epidemiology, and Dr Selim Akl from the School of Computing for his insights into the world of computer sciences.

Thank you to Dr Katherine Kilpatrick at the Health for Life Medical Centre for the opportunity to work at the most progressive health clinic in town, and thank you to Tanya Harrington at Feel Yoga Studio for the beautiful community and positive space in which I have had the opportunity to practice for the past three years.

And finally, I want to thank my family for their undying support in my pursuit of learning. Thank you Aunt Jackie and Uncle John for being more than a niece could ever hope for. Thank you to Heather Adams - I cherish the childhood we shared, and the fun we always have. Dad, Mom, Jeff, Shelle, Davin; I love you and appreciate your dedication, and the sacrifices you have made on my behalf.

Table of Contents

Abstract.....	ii
Co-Authorship	iii
Acknowledgements.....	iv
Table of Contents.....	vi
List of Figures.....	ix
Chapter 1 Introduction.....	1
Chapter 2 Literature Review.....	3
2.1 Burden of Cardiovascular Disease.....	3
2.2 Cardiac Hypertrophy.....	3
2.3 Cellular Makeup of the Developing and Adult Heart.....	6
2.4 Developing and Mature Cardiac Vasculature.....	10
2.5 The Heart as an Endocrine Organ.....	14
2.6 ANP, BNP, CNP.....	15
2.7 NPR-A, NPR-B, NPR-C.....	18
2.8 The NPS in Cardiovascular Function and Disease.....	21
2.9 The NPS during Prenatal Development.....	24
2.10 Cardiovascular Fluid Homeostasis during Postnatal Development.....	25
2.11 Blood Pressure Establishment.....	27
2.12 The NPS during Postnatal Development.....	28
Chapter 3 Objectives, Hypothesis, Specific Aims.....	29
3.1 Experimental Design & Objectives.....	29
3.2 Hypothesis.....	29
3.3 Specific Aims.....	29
Chapter 4 Materials & Methods.....	31
4.1 Animals.....	31
4.2 Genotyping.....	31
4.3 Plasma and Tissue Collection.....	32
4.4 RNA Isolation and Preparation.....	33
4.5 Reverse Transcription of mRNA.....	35
4.6 Production of Primers.....	36
4.7 Testing of Sequenced PCR products.....	36

4.8 Real-time RT-PCR.....	38
4.9 Gene Expression Analysis	39
4.10 Vascular Casting	40
4.11 Vascular Imaging	40
4.12 Histology.....	42
4.13 Histological Imaging and Analysis.....	42
Chapter 5 Results	44
5.1 Physical Data	44
5.2 Vascular Organization and Composition	50
5.2.1 Morphological Analysis.....	50
5.2.2 Morphometric (Stereological) Analysis.....	50
5.3 Molecular Analysis	53
5.3.1 Expression of ANP during postnatal development	53
5.3.2 Expression of BNP during postnatal development	57
5.3.3 Expression of NPR-A during postnatal development	57
5.3.4 Expression of NPR-B during postnatal development	57
5.3.5 Expression of NPR-C during postnatal development	59
Chapter 6 Discussion & Conclusion	60
6.1 Rationale for Examining Postnatal Age, ANP ^{-/-} Mouse Model, and Whole Heart.....	60
6.2 Results Interpretation	61
6.2.1 Physical data	61
6.2.2 Vascular organization and composition.....	64
6.2.3 Morphological analysis.....	65
6.2.4 Stereological analysis.....	66
6.2.5 Molecular analysis	68
6.2.5.1 Exclusion of CNP from Analysis.....	69
6.2.5.2 Expression of ANP	70
6.2.5.3 Expression of BNP.....	71
6.2.6 Total NP Ligand Effect.....	72
6.2.6.1 Expression of NPR-A	75
6.2.6.2 Expression of NPR-B.....	76
6.2.6.3 Expression of NPR-C.....	77
6.2.7 Total NP Ligand-Receptor Effect	78

6.2.8 Overview of Current Results with Overall Implications in the Literature.....	79
6.3 Relationship to Disease in Human Populations	86
6.4 Conclusion	89
Chapter 7 Future Directions.....	90
Bibliography	95
Appendix A: High Pure RNA Isolation	118
Appendix B: Gene Expression Analysis using LightCycler 480 [®] real-time RT-PCR.....	119
General Background	119
Appendix C: Novel Experimental Vascular Casting Technique.....	122
Materials	122
Experimental Modifications.....	123
Appendix D: Stereological Analysis of Cardiac Tissue.....	125
Appendix E: Wet Lung Weight/Dry Lung Weight Chart	131

List of Figures

Figure 1. Schematic representation of cardiac hypertrophy.....	5
Figure 2. Depiction of myocardial fibres.....	8
Figure 3. Depiction of coronary vasculature of mammalian heart.....	11
Figure 4. Diagrammatic of cardiomyocyte and microvessel interaction.	12
Figure 5. Secondary protien structure of ANP, BNP, CNP.....	16
Figure 6. Schematic of structure/function of NPR-A, NPR-B, NPR-C.....	19
Figure 7. Intracellular signaling cascade of NPR-A/NPR-B by NP ligands.....	20
Figure 8. Diagrammatic comparison of embyronic and adult NPS.....	26
Figure 9. Overview of molecular biology techniques used.....	34
Figure 10. Methodological images of polymer injection.....	41
Figure 11. Effect of <i>pro</i> ANP gene-disruption on heart weight to body weight ratios.....	45
Figure 12. Effect of <i>pro</i> ANP gene-disruption on hematocrit.	49
Figure 13. Representative LM images of coronary vascular casts.....	51
Figure 14. Stereological analysis of absolute and relative vessel volume.....	52
Figure 15. Representative LM images of 5 week ANP ^{+/+} and ANP ^{-/-} vasculature.	54
Figure 16. Analysis of absolute myocyte and “other volume.	55
Figure 17. ANP, BNP mRNA expression.....	56
Figure 18. NPR-A, NPR-B, NPR-C mRNA expression.	58
Figure 19. A diagrammatic representation of myocyte proliferation and differentiation.....	74
Figure 20. A schematic of diverse properties of ANP.....	81
Figure 21. A diagrammatic of potential relationship between ANP, VEGF, and ET-1.....	83
Figure 22. A diagrammatic representation of ANP and myocardial growth.	85
Figure 23. A diagrammatic representation of BNP, ADM and ECM formation.....	87
Figure 24. VEGF-A mRNA expression.....	93

List of Tables

Table 1. Overview of NPS gene-disrupted & transgenic animal models.	23
Table 2. Primer sequences used for quantitative PCR analysis.	37
Table 3. Heart, body, and heart-to-body weight values.	46
Table 4. Kidney, body, and kidney-to-body weight values.	47
Table 5. Lung, body, and lung-to-body weight values.	48

List of Abbreviations

ANP	atrial natriuretic peptide
A.U.	arbitrary units
BNP	B-type natriuretic peptide
cDNA	complementary deoxyribonucleic acid
cGMP	cyclic 3'-5'-guanosine monophosphate
CH	cardiac hypertrophy
CNP	C-type natriuretic peptide
CO	carbon monoxide
CV	cardiovascular
DEPC	diethylpyrocarbonate
DNA	deoxyribonucleic acid
DNP	dendroaspis natriuretic peptide
ECM	extracellular matrix
EDTA	ethylenediamine tetra acetic acid
eNOS	endothelial nitric oxide synthase
ET-1	endothelin-1
GC-A	guanylyl cyclase A
GD	gestational day
HW/BW	heart weight/body weight ratio
LM	light microscopy
LV	left ventricle or left ventricular
LVH	left ventricular hypertrophy
NE	norepinephrine

NEPneutral endopeptidase
NOnitric oxide
NPnatriuretic peptide
NPSnatriuretic peptide system
<i>Nppa</i> <i>natriuretic peptide precursor 1</i> gene
<i>Nppb</i> <i>natriuretic peptide precursor 2</i> gene
<i>Nppc</i> <i>natriuretic peptide precursor 3</i> gene
<i>Npr-1</i> <i>natriuretic peptide receptor 1</i> gene
<i>Npr-2</i> <i>natriuretic peptide receptor 2</i> gene
<i>Npr-3</i> <i>natriuretic peptide receptor 3</i> gene
NPR-Anatriuretic peptide receptor A
NPR-Bnatriuretic peptide receptor B
NPR-Cnatriuretic peptide receptor C
PCRpolymerase chain reaction
pGCparticulate guanylyl cyclase
PKGprotein kinase G
RTreverse transcription
sGCsoluble guanylyl cyclase
VEGFvascular endothelial growth factor

Chapter 1

Introduction

Organogenesis is commonly represented as occurring exclusively *in utero*. It is often forgotten that organs, specifically the heart, continue to develop and modify long after birth. During the earliest stages of postnatal development, the newly born is faced with an extreme physiological transition to *ex utero* life. Although functional, the postnatal heart must maintain a strict balance between short term physiological adaptations to postnatal life and structural modifications for long term survival in adulthood. There are many environmental, genetic, and physiological factors that influence the dynamic process of cardiac development, and consequently many potential pathological stimuli. Herein lies the concept that has given rise to recent widespread interest in postnatal programming: the reasoning that early postnatal adverse events may have repercussions in later life [1,2].

Cardiovascular disease, which encompasses cardiac pathologies, is the leading cause of morbidity and mortality in the developed world, and is becoming increasingly prevalent in the developing world [3]. It is, therefore, imperative for prevention, treatments, and therapies to be based on a sound understanding of normal cardiovascular processes, and mechanisms of disease establishment. The natriuretic peptide system (NPS) is known to be of central importance in adult cardiovascular homeostasis, and is expressed during critical developmental stages of prenatal development [4]; its altered expression has been implicated in the progression of various forms of cardiovascular disease. However, there has been limited work outlining the actions of the NPS during postnatal cardiac development. This study is designed to address this question. A detailed study of pathological consequences of postnatal cardiac development in the absence of atrial natriuretic peptide (ANP) will be done. The purpose of this study is to investigate the role of ANP during cardiac development by comparing morphologic, morphometric, and molecular

differences in ANP^{-/-} mice compared to ANP^{+/+} mice during a progression of postnatal time points. This work is therefore based on the hypothesis that an altered genetic profile during cardiac development will have a profound impact on final heart structure, and that gross physical characteristics, coronary vasculature volume and organization, and NPS expressional patterns will be altered in ANP^{-/-} mice as compared to postnatal development in ANP^{+/+} mice.

The ensuing background information will describe various aspects of cardiovascular disease; the cellular makeup of the developing and adult heart; the anatomy of developing and mature cardiac vasculature; the heart as an endocrine organ; the basic biochemistry of the NPs and their receptors; the NPS in cardiovascular function and disease, and during prenatal development; blood pressure establishment; and the NPS during postnatal cardiac development. This information will be put into context by the subsequent section outlining the hypothesis, experimental design and objectives, and specific aims of the current study.

Chapter 2

Literature Review

2.1 Burden of Cardiovascular Disease

Cardiovascular disease (CVD) encompasses coronary artery disease, heart disease, congestive heart failure, peripheral vascular disease, and cerebrovascular disease. CVD is the leading cause of both morbidity and mortality in developed countries, and rates are rapidly increasing in the developing world [3]. Here in Canada, heart disease is the leading cause of death in women, and the second leading cause of death in men [5]. Direct and indirect financial costs of CVD to the Canadian economy have been estimated to approach \$20 billion annually, and such a financial burden is expected to multiply in the next half century with our aging population [6].

In addition to established modifiable CVD risk factors, including tobacco, alcohol, blood pressure, physical inactivity, cholesterol levels, obesity, and unhealthy diet, there are non-modifiable CVD risk factors. These factors include age, sex, social and economic conditions, residential geography, and genetic composition [7]. The current investigation examines the underlying physiological and genetic mechanisms which contribute to varying CVD outcomes in mice. Knowledge gained from this study will further our understanding of the prevalence of CVD between and among human populations.

2.2 Cardiac Hypertrophy

Chronically sustained high blood pressure (hypertension) can result from many factors, including increased vascular resistance, or increased afterload [8]. Chronic hypertension will cause muscles of the heart to adapt to this pathological condition. Such adaptation results in structural changes including thickening of the ventricular wall [8]. The hypertrophic growth of

heart tissue is termed cardiac hypertrophy (CH). This growth is often attributed to increases in arterial blood pressure. However, hypertrophy can arise from a range of stimuli, including mechanical, hemodynamic, hormonal, and pathological changes [8].

CH is an important predictor of CVD, independent of increases in arterial blood pressure. CH arises from complex interactions among genetic, physiological, and environmental risk factors. There are physiological and pathological forms of CH, depending on the stimuli [9]. Although both forms result in increased cardiac mass, these differences are reflected in the structural changes observed in individual myocytes, and associated structural components such as vasculature and extracellular matrix [8,9].

Physiological hypertrophy results in an organized cellular arrangement, whereby sarcomeres are added in series and the left ventricular wall thickness to lumen ratio remains unchanged (eccentric hypertrophy). Conversely, pathological hypertrophy results in sarcomeres being added in parallel, resulting in an increased left ventricular wall thickness to lumen ratio (concentric hypertrophy) (Figure 1). While physiological hypertrophy is a non-permanent adaptive response, changes associated with pathological CH result in more permanent structural alterations, and reduced cardiac function leading to eventual heart failure. While both forms of CH are thought to be a functional change allowing the heart to meet systemic cardiovascular demands with the increased workload, it is apparent that cellular organization is critical to long-term cardiac function [9,10].

Factors active in the cardiovascular system mediate physical stimuli and changes to cardiac structure. The molecular pathways which lead to physical and functional changes are complex, necessitating a thorough appreciation of cardiac tissue constituents and morphological changes characteristic of this disease state.

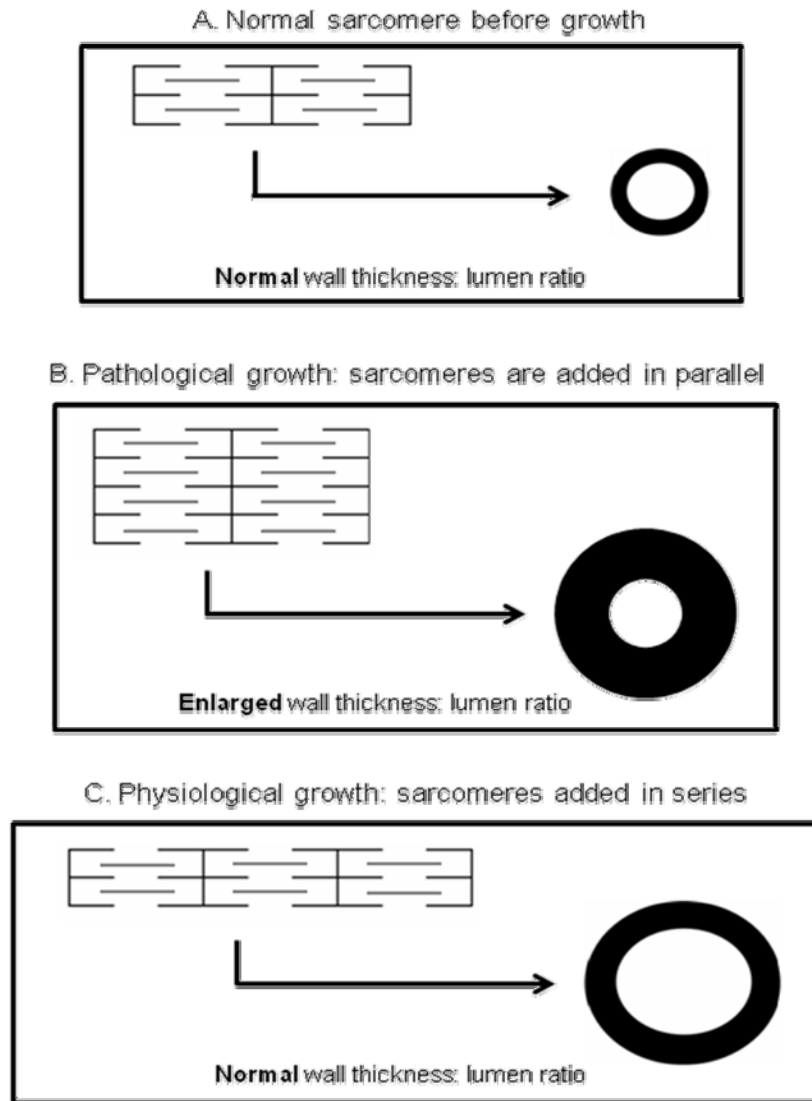


Figure 1. A schematic representation of structural changes to a myocyte during two types of hypertrophy. (A) Normal sarcomere organization (B) Sarcomeres are added in parallel (concentric hypertrophy). This leads to an increased wall thickness to lumen ratio. (C) Sarcomeres are added in series (eccentric hypertrophy). This results in a normal wall thickness to lumen ratio. Adapted from Garcia *et al.* [10]

2.3 Cellular Makeup of the Developing and Adult Heart

Various genetic, environmental, and physiological forces exert influence over the final architecture of the mature heart structure [9,10]. Previous studies have determined that cardiomyocytes rapidly proliferate during murine embryonic development, but exit the cell cycle during postnatal development soon after birth [11-16]. Some studies suggest that cardiomyocytes retain some proliferative capacity up until time of weaning [11-13]. Later postnatal enlargement of the heart is therefore primarily dependent on cellular hypertrophy, rather than hyperplasia. In fact, Soonpaa *et al.* demonstrated that cardiomyocyte DNA synthesis occurs in two temporally distinct stages; cardiomyocytes extensively proliferate during embryonic cardiac development, and then undergo binucleation in early neonatal life [12]. It has been suggested that since cardiomyocyte proliferation stops before birth, genetic factors critical to the regulation of this proliferation must be differentially expressed during fetal versus neonatal development [12, 17].

Thus, the development of the heart is an active perinatal process, comprised of organogenesis during prenatal development, and cardiomyocyte expansion and maturation during postnatal development [18]. Accordingly, the developmental expression of various cardiac constituents is a very complex and dynamic process responsive to both *in utero* and *ex utero* stimuli.

During normal cardiac development, cell components of the heart interact to dynamically respond to changing structure and physiology [17, 18]. In fact, the transition from fetal circulation to postnatal circulation marks a dramatic change in physiological demand. The developing cardiac tissue relies on various molecular mechanisms to sense developmental and homeostatic changes, thereby allowing it to keep up with increasingly elaborate structure and consequently higher functional demands. The early postnatal period is characterized by structural alterations to

the heart, as it adapts to adult blood pressure and volume with increased left ventricular size [19, 20].

The mature mammalian heart is a complex structural entity consisting of a variety of muscular, vascular and extracellular matrix cells. Accordingly, matured cardiac architecture and composition is the result of numerous regulatory processes during development [21]. While the mature heart is also very responsive to its physiological environment, it does so as a differentiated, fully-developed organ; stronger, more sustained stimuli are required to cause the same alterations observed in the less-malleable developed heart [19, 22].

Histologically, the matured heart can be organized into different layers: i) the innermost endocardium, which comprises a single cell layer endothelium, and a loose connective tissue subendothelial layer; ii) the myocardium, composed of cardiac muscle bundles and layers organized by separate cellular units joined by intercalated discs; and iii) an outermost epicardium, which surrounds the outside of the heart with loose connective tissue, and a single layer of epithelial cells, also called the visceral pericardium [23].

The cardiac skeleton is a fibrous base comprised of dense fibrous tissue, which provides a framework for these three layers, and is organized around the orifice of the aorta, pulmonary trunk, and the left and right atrioventricular canals (Figure 2). The cardiac connective tissue is mainly composed of collagen, of which 85% is collagen type I [23]. Such a tough collagenous extracellular matrix provides structural support; this matrix unites contracting myocytes for coordinated force, prevents chamber collapse during diastole, and provides stiffness during systole. In the myocardium, myocytes forms spirals of interweaving tissue bundles in an orientation that maximizes contractile efficiency [24, 25].

Alterations in cardiac collagen network, myocyte size and organization, and sarcomere protein expression can occur in response to pressure or volume overload resulting in interstitial

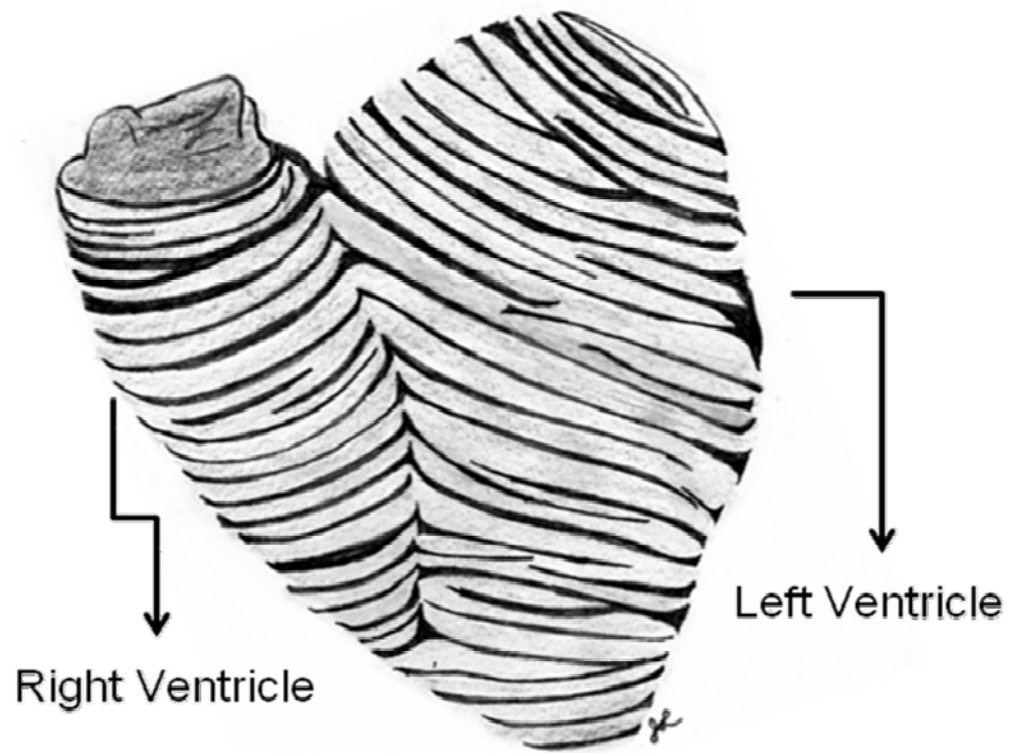


Figure 2. Myocardial fibres interweave to form specific spirals from the base to the apex. This organization allows for contractile precision within the organ, and is essential for proper and efficient ejection fraction. Disruption of the cellular balance has been linked to a series of cardiac pathophysiologies [24, 25].

fibrosis [26-30]. Mechanotransduction, a biological response to mechanical forces, explicates the hormonal response to chronic pathological physical stimuli in mature cardiac tissue. Such stimuli result in altered expression of proto-oncogenes (*c-fos*, *c-jun*, *c-myc*, etc.), which can in turn result in changes to the expression of downstream genes [30]. Overall, these changes can lead to widespread altered protein synthesis. Accordingly, recent advances in gene expression technology have proven that heart failure is accompanied by reversion to embryonic cardiac gene expression pattern [31].

Whether during development, or pathologically-induced post-development cardiac modification, it is apparent that the heart can undergo structural alterations in response to increasing physiological demands. Disruption in the amount or organization of any cardiac components limits the efficiency of cardiac function, and is deleterious to an organism's survival [25].

In essence, elaborate three-dimensional heart structures are made up of mainly cardiac fibroblasts, myocytes, endothelial cells, and vascular smooth muscle cells that have electrical, chemical, or biomechanical capacity. These constituents interact via autocrine, paracrine, and cell-to-cell interactions [24, 30]. As previously mentioned, the balanced proportion of these constituents (for example myocyte to blood vessel ratio) is fundamental to the normal developmental progression of the heart, as well as mature cardiovascular homeostasis [25, 32-34]. Interference or disruption of these interactions during cardiac development or remodeling has been shown to lead to distinct pathological conditions [35-37]. From a research perspective, the way in which these cellular populations alter during development and homeostasis allows insight into the mechanisms in diseased states.

2.4 Developing and Mature Cardiac Vasculature

Cardiac organogenesis ends in the formation of complex conduction and circulatory systems [38]. Although the heart contains blood, deep myocardial tissue that is not exposed to chamber blood requires an elaborate coronary vessel network to maintain its oxidative and nutritional requirements. The coronary circulation is comprised of coronary arteries which originate from the aortic sinuses. These branches, most commonly the right and left coronary arteries, lead away from the aorta to their respective sides of the heart. These arteries then branch into progressively smaller arteries, and deeper into the myocardium until they turn into a capillary network [38]. Post-capillary venules form progressively larger vessels until they drain into the coronary sinus – which is a main venous channel leading into the right atrium to complete the coronary circulation (Figure 3).

Coronary vessel formation is unique for each heart - there are dramatic variations observed throughout the entire network. While the patterning of the coronary system is predictable, there is even significant variation in the basic pathways taken by major vessels, including the first coronary arteries branching off the aorta [38].

Development of the coronary vessel network is fundamental to the efficiency of the heart, and such a process represents a complex interaction of various cell types and processes [25, 40] (Figure 4). The effect of subtle variation in the architectural arrangement of coronary vessels on myocardial structure and function has been thus far largely unexplored.

During embryonic development, the heart begins as an endothelial tube within a muscular tube. This tube then undergoes looping, compartmentalization, and valve formation. By gestational day (GD) 9.5, the heart has both endocardium and myocardium, but lacks the epicardium necessary to protect invading undifferentiated vessel forming cells [42]. In a concerted movement, the epithelial cells migrate to form a continuous epithelial sheet, providing

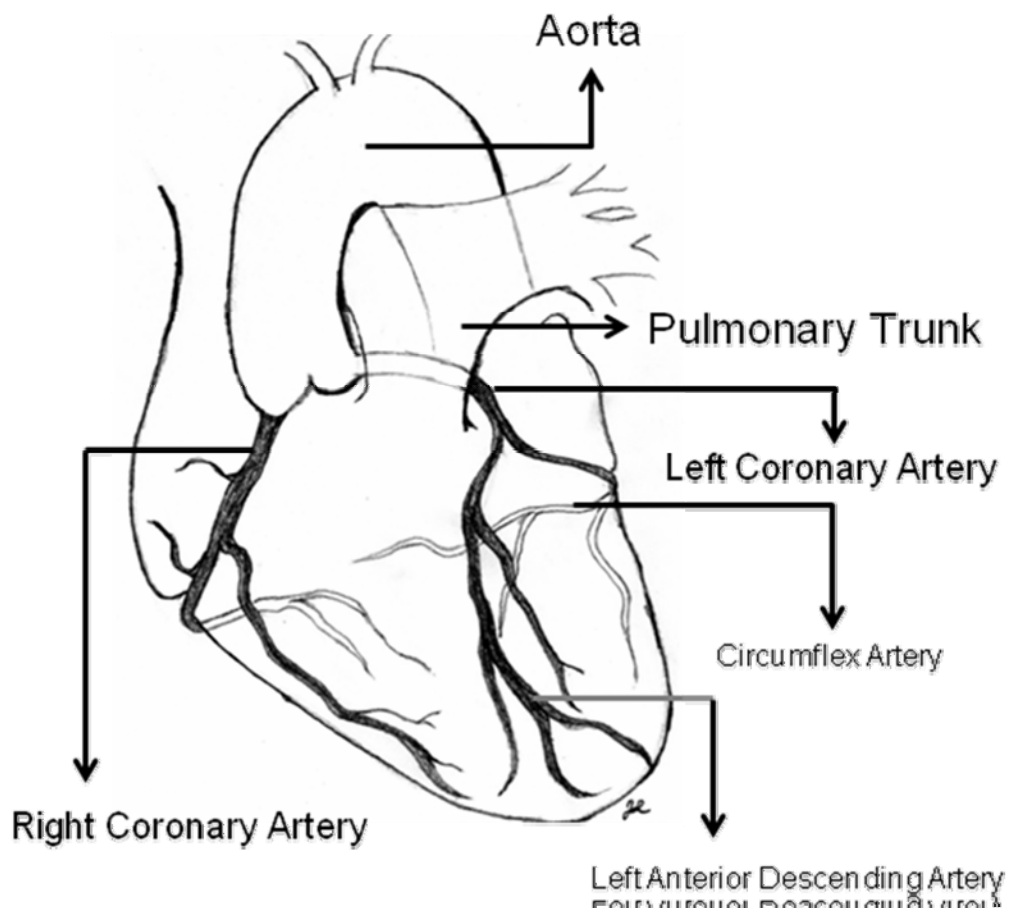


Figure 3. A depiction of the coronary vasculature of a mammalian heart. Major arteries are shown branching off the ascending aorta. Note that secondary branches travel perpendicularly to the apex of the heart. This system is optimized for regulated pressure and continuous blood flow during contraction/relaxation. Adapted from Gray's Anatomy Atlas [41].

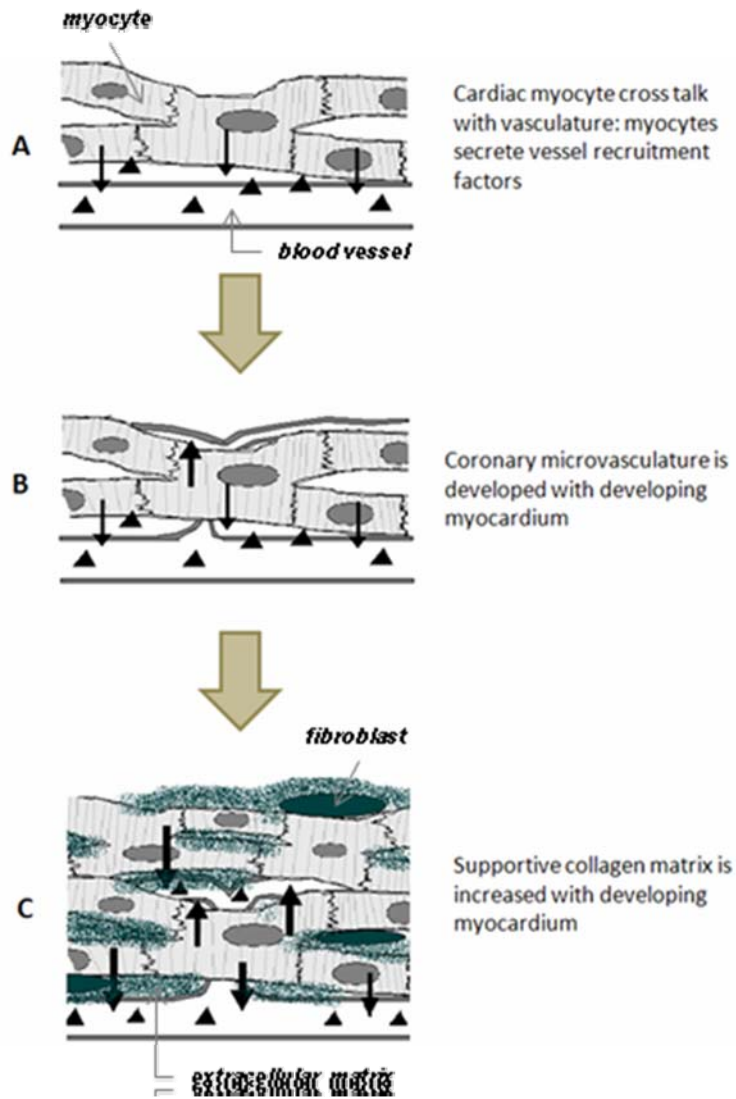


Figure 4. A diagrammatic representation of interactions between cardiomyocytes, microvessels, and extracellular matrix during cardiac development. A) Cardiomyocytes guide developing vasculature through mediating factors (black triangles). B) Coronary vasculature development is closely paired with myocardium development. C) Fibroblasts (darker ovals) secrete matrix fibres (dark speckles) to provide increasing architectural support for surrounding myocytes and coronary vessels. Dark arrows indicate the flow of factors.

a protective covering for the passage of nerves and blood vessels. This sheet also creates a contained environment, whereby factors and cellular signals are relayed to regulate cellular proliferation, migration, matrix remodeling, and the eventual formation of a complex three-dimensional coronary vasculature system [32, 38, 40]. The complexity of this process paired increases the potential for abnormalities to take place. Consequently, pathological coronary angiogenesis may result from miscommunication between vessels and cardiomyocytes [42-44], with resulting coronary abnormalities deleterious to proper cardiac architecture and long term heart function.

The development of the cardiac coronary vascular network is highly coordinated with the development of alternate cardiac structure, so as to ensure regulated flow with repetitive contraction [46]. Vascular structures of the coronary circulation vary with size and function [41]. Varied coronary circulation can result in altered branching of both major coronary vessels and the numerous capillaries of the coronary circulation between myocytes. These small and micro vessels, including arterioles, capillaries, and small venules, are highly organized and are extensive throughout cardiac tissue. These vessels are essential for meeting the high oxygen and nutrient demand of the contracting myocardium. The development of the coronary circulation in early cardiac development, and its developmental coordination with alternate cardiac tissue constituents reinforces the notion of inter-play between cardiac vasculature and other components of the heart [42-44].

Vascular smooth muscle cells contribute to and express various constituents of the blood vessel wall - elastic fibres, collagen, glycosaminoglycans, and other matrix components - as well as promote the addition of more smooth muscle cells [47]. Neighbouring myocytes also aid in the recruitment of factors which promote and contribute to increased vessel formation [47, 48]. This is relevant to the biological scenario of CH, as the prevention of hypoxic conditions requires the

enlarged myocardium be accompanied by an expanded coronary vasculature. Understanding the relationship between factors secreted by one heart constituent to exert influence over the development or post-developmental modification of another is pertinent to determining the disrupted molecular mechanisms underlying cardiac pathologies.

2.5 The Heart as an Endocrine Organ

In addition to extraordinary mechanical properties and intricate tissue composition, the mammalian heart is critically involved in molecular cardiac homeostasis. Although molecular cardiology is a pillar of current cardiovascular research, the unmasking of the heart as an endocrine organ only began in the latter half of the past century.

Dense granules in atrial tissues were first described by Kisch in 1956, however the function of these granules and the understanding of the heart as an endocrine organ was not investigated for another 25 years [49]. In 1981, de Bold *et al.* demonstrated the potent natriuretic, diuretic and anti-hypertensive effects of atrial extracts by infusing it into bioassayed rats [50]. Within a few years following its functional discovery, it was determined that specific atrial granules contain the pro-hormone form of atrial natriuretic peptide (*pro*ANP). ANP gives the heart an important endocrine role in blood pressure control, and water and electrolyte homeostasis [51].

The NPS is composed of at least three polypeptide entities and three different receptors; atrial natriuretic peptide (ANP), B-type natriuretic peptide (BNP), and C-type natriuretic peptide (CNP), and receptors natriuretic peptide receptor A (NPR-A), natriuretic peptide receptor B (NPR-B), and natriuretic peptide receptor C (NPR-C). ANP and BNP are mainly expressed and secreted by the atria and ventricles of the adult heart, respectively, and their natriuretic, diuretic

and vasorelaxant effects work to control blood pressure and fluid balance [51]. As well, both participate in the regulation of cardiovascular tissue development.

The NPS is highly conserved across mammalian species, and is essential for survival as it functions to maintain cardiovascular homeostasis and mediate healthy embryonic development [52-54].

2.6 ANP, BNP, CNP

While all three peptides share a common 17 amino acid ring structure in which most of the amino acids are conserved, a separate gene encodes each precursor pro-hormone (Figure 5). The tissue specific distribution and regulation of each peptide are unique, as NPs have unique physiological functions [52].

Atrial natriuretic peptide (ANP) is mainly produced by the cardiac ventricles in prenatal development, and in the atria of adult hearts. ANP is produced as pre-*pro*ANP, approximately 1kb in size, but is cleaved into the storage form of *pro*ANP, a 126 amino acid product which is stored in granules [55]. The prompt release of these granules into circulation is triggered by various stimuli, including increased atrial-wall tension (a reflection of increased intravascular volume), and the presence of various hormones and neurotransmitters. Upon release, *pro*ANP₁₋₁₂₆ is cleaved into *pro*ANP₁₋₉₈ (amino-terminal fragment), and the biologically active peptide carboxy-terminal portion, ANP₉₉₋₁₂₆ by the enzyme corin [56]. Despite the short half life of ANP, this peptide has potent direct and indirect physiological effects, including natriuresis, diuresis, vasodilation, vasorelaxation, and negative inotropy. Specifically, ANP increases venous capacity, reduces sympathetic tone in peripheral vasculature, and suppresses the renin-angiotensin-aldosterone system [52]. ANP has also been shown to inhibit the growth of cardiac fibroblasts [57, 58] - possibly by limiting collagen deposition - thus having the potential to minimize cardiac

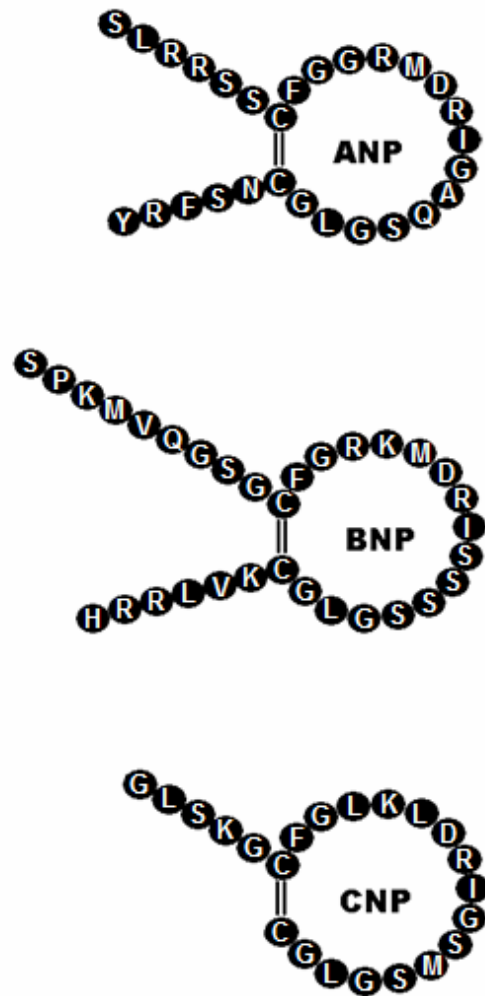


Figure 5. Secondary protein structure of Atrial, B-type and C-type natriuretic peptides (ANP, BNP, and CNP, respectively). All three NPs share considerable conserved homology in amino acid sequence, with ANP and BNP being the most similar. ANP, BNP and CNP also share a 17-amino acid ring which is considered characteristic of this group of hormones. Adapted from Levin *et al.* [52].

remodeling. ANP can also induce cardiac myocyte cell cycle arrest [59, 60], likely limiting myocardial proliferation during development, or hypertrophic response to injury or ischemia in later life.

B-type natriuretic peptide, or BNP, was initially isolated from porcine brain tissue [61], however it is now known that BNP is expressed in highest concentration by the cardiac ventricles [62]. Human pro-BNP is 108 amino acids, and like ANP, it is cleaved before secretion. In humans BNP is comprised of a biologically active carboxy terminal fragment of 32 amino acids, and a biologically silent 76 amino-terminal fragment (commonly used as a diagnostic screen for cardiac dysfunction) [63]. In mice the mature BNP is 45 amino acids long. BNP is stored differently in each compartment of the heart [62]. In the atria, BNP is expressed and stored in granules. In the ventricle, BNP is produced and constitutively released. BNP mRNA levels are constitutively increased with chronic blood volume overload, and causes hemodynamic effects similar to ANP [52, 53]. In addition, BNP has been shown to have inhibitory effects on fibroblasts, reducing collagen secretion and thereby moderating fibrotic deposition [64].

C-type natriuretic peptide, or CNP, was also initially discovered in porcine brain, however, was later determined to be mainly produced in vascular endothelium [65, 66]. Depending on the species, CNP is cleaved into either a 22- (mice) or 53- (human) amino acid biologically active fragment.

Similar to ANP and BNP, CNP is a powerful vasorelaxant of vascular smooth muscle, however it causes only mild diuresis and natriuresis. Despite low levels in circulation, CNP acts to control fluid movement across capillaries. Such local regulation has been shown to be essential in the blood vessels of the brain [67]. CNP also plays a critical role in normal skeletal development, as it serves to regulate the growth of bone and cartilage [68]. More recently, CNP has been implicated as an antifibrotic and antihypertrophic agent in the fibrosis of cardiac

dysfunction [69, 70]. Horio *et al* reported that CNP attenuated left ventricular enlargement in post-myocardial infarction (MI), attenuated collagen deposition in cardiomyocytes, and suppressed MI-induced gene expression [69].

It should be noted that additional NPs, sharing structural and biological properties characteristic of the aforementioned NPs, have been identified in various species. Dendroaspis natriuretic peptide, or DNP, was isolated from the venom of green mamba [71], and various natriuretic peptides have been associated with related physiological systems in nature [72].

2.7 NPR-A, NPR-B, NPR-C

Physiological response to circulating NPs is initiated by NP interactions with three characteristically different NP receptors; NPR-A, NPR-B and NPR-C (Figure 6). NPR-A and NPR-B are 44% homologous in the ligand-binding extracellular domain, and are members of the cell-surface family of guanylyl cyclase (GC) receptors [73]. GC is an enzyme which catalyzes the synthesis of the intracellular second messenger, cyclic 3'-5'-guanosine monophosphate (cGMP). cGMP in turn activates cGMP-dependent protein kinase (PKG), which results in the GTP-dependent phosphorylation of various cellular proteins. This phosphorylation leads to an intracellular signalling cascade catalyzing a range of cardioprotective activities throughout the body, including vascular smooth muscle relaxation subsequent to vasodilation and increased blood flow (Figure 7) [74, 75].

NPR-A is activated by physiologic concentrations of ANP and BNP, but not CNP. NPR-A is most abundant in large blood vessels, and upon activation, multiple domains located on the

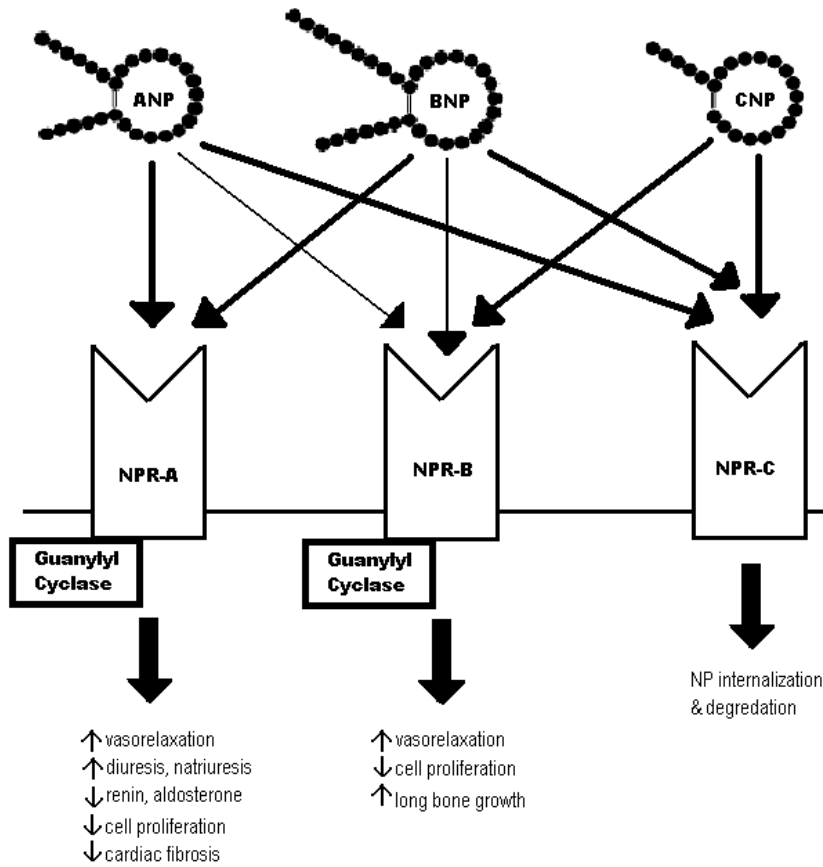


Figure 6. Natriuretic peptide receptor A, natriuretic peptide receptor B and natriuretic peptide receptor C (NPR-A, NPR-B, NPR-C). NPR-A and NPR-B share similar structural properties, however bind to NPs with different affinities. NPR-A binds ANP and BNP with almost the same affinity, but has no affinity for CNP. NPR-B has weaker (but almost equal) affinities for ANP and BNP, as it mainly acts as a receptor for CNP. NPR-A and NPR-B contain a transmembrane domain linked to an intracellular kinase-like domain linked to particulate guanylyl cyclase. Binding of NPs causes a conformational change to the guanylyl cyclase domain, allowing GTP to be dephosphorylated to cGMP. cGMP is the secondary messenger responsible for catalyzing the phosphorylation of alternate intracellular molecules, and thus mediating the overall physiologic response of ANP and BNP. NPR-C is not cGMP-linked, binds to all NPs with equal affinity, and functions as a clearance receptor [77].

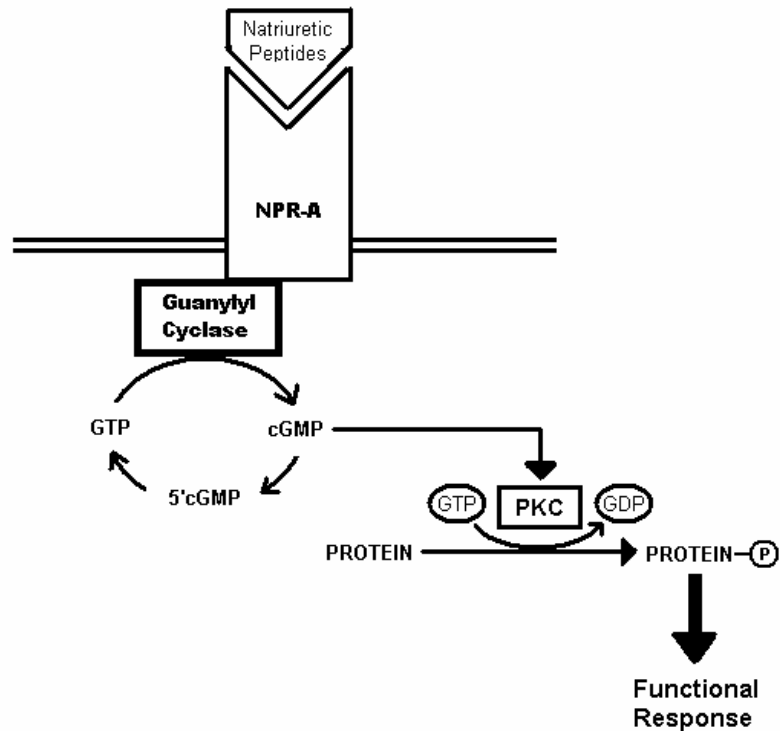


Figure 7. Intracellular signaling cascade upon natriuretic peptide receptorA/B activation by NP ligands (ANP, BNP, CNP). Upon activation by natriuretic peptides, NPR-A and NPR-B activate guanylyl cyclase to convert GTP (guanosine triphosphate) into cGMP (cyclic-guanosine monophosphate). cGMP is considered the intracellular second messenger, and activates cGMP dependent protein kinase (PKC). In the presence of GTP, PKC phosphorylates a variety of proteins (□ = added phosphate group). These phosphorylated proteins further instigate intracellular activities which transmit into the overall physiological response [74, 75].

inside and outside of the plasma membrane mediate the oligomerization of NPR-A into a homodimer [76].

While NPR-B mediates most of the biological effects of CNP, it has low affinity for ANP and BNP. Similar to NPR-A, upon activation NPR-B dimerizes to become a homodimer complex. NPR-B predominates in brain tissue, however is also found in adrenal gland and kidney tissue [77].

NPR-C is not GC-linked, as it functions as a clearance receptor regulating circulating levels of NPs [78]. NPR-C bind ANP, BNP and CNP with relatively similar affinities. NPR-C binds the NP and internalizes this receptor-ligand complex for ligand degradation and receptor recycling. NPR-C is the most abundantly expressed receptor, and is normally found within close proximity to NPR-A and NPR-B [79]. Neutral endopeptidase (NEP) present on the plasma membrane also inactivates NPs through cleavage of the peptides into biologically inactive fragments [80].

2.8 The Natriuretic Peptide System in Cardiovascular Function and Disease

In order to reduce preload, NPs cause extravasation of fluid into the extravascular compartment, promote renal salt and water excretion, promote vascular relaxation, inhibit production and activity of vasoconstrictive peptides, and inhibit sympathetic tone [81, 82]. During pre- and postnatal development, the NPS may function to restrict cardiac growth and regulate cardiac function [83, 84]. Recent work has demonstrated that NPRs also have a role in cardioprotection [81]. NPR-A mediates the well-known effects of ANP and BNP [85], and although the cardiac functions of NP signaling through NPR-B are not widely evaluated or discussed, the cardioprotective function of NPR-B is gaining increasing attention [86].

In accordance with the importance of the NPS in cardiovascular function and disease, various animal models have been created in order to more fully elucidate various aspects of the functional NPS.

There are various strategies used for researching complex, interacting physiological systems; selectively mutating genes, and creating excessive or deleted gene expression. Each of these strategies has been used within the context of the NPS, and has greatly contributed to the understanding of the physiological and pathological functioning of the NPS. Specifically, elimination of a single genetic influence, as in the case of homologous recombination in embryonic stem cells, is commonly used to create knockout animal models. Such knockout animal models exist for ANP, BNP, CNP and NPR-A (Table 1). These animal lines permit the evaluation of the significance of that specific gene product, as reflected by the progression of CVD pathology in their absence.

Previously published work from our lab reported that ANP^{-/-} mice demonstrate cardiac enlargement and salt sensitive cardiac hypertrophy. The cardiac enlargement in these animals is drastic: 40% increase in heart weight to body weight ratio (HW/BW) compared to wildtype littermates [51].

NPR-A knockout mice exhibit hypertension, BP-independent eccentric LVH with interstitial fibrosis and sudden death, increased responsiveness to pressure overload by transverse aortic constriction, and demonstrate reduced litter sizes [87, 88]. Few NPR-A^{-/-} males survive to 6 months, mainly due to cardiovascular events.

BNP knockout mice demonstrate ventricular interstitial fibrosis without CH or systemic hypertension [64]. CNP knockout mice exhibit dwarfism due to impaired endochondral ossification. Additional physiologic properties have been reported for CNP: inhibition of cardiac fibroblast proliferation, vasodilatory effects, promotion of endothelial cell differentiation and

Table 1. Overview of effects of NPS gene disrupted, and NPS transgenic animal models on circulatory and cardiac phenotypes. KO= knockout; OE = overexpression.

Animal	Adult circulatory phenotype	Adult heart phenotype
ANPKO	salt-sensitive hypertension	cardiac enlargement
BNPKO	normotension	cardiac fibrosis
CNPKO	not described	not described
NPRAKO	salt-independent hypertension	cardiac hypertrophy, cardiac fibrosis
NPRCKO	hypotension	not described
ANPOE	hypotension	not described
BNPOE	hypotension	reduced cardiac weight
NPRAOE	normotension	reduced cardiac weight

vasculogenesis [64]. CNP gene-disruption is not embryologically lethal, however less than half of $CNP^{-/-}$ mice survive past postnatal development [68].

Aside from physiologic and gross morphologic changes, animal models with genetically disrupted NP systems also provide insight into resulting altered molecular interactions. More specifically, a disrupted NPS has been a means of uncovering its inherent compensatory flexibility. A deficiency or absence of ANP, as in the $ANP^{+/-}$ heterozygous and $ANP^{-/-}$ homozygous mutant mice, respectively, leads to subsequent up-regulation of ventricular BNP mRNA transcripts [89]. $NPR-C^{-/-}$ mice are hypotensive [90], and conversely, $NPR-A^{-/-}$ mice are hypertensive and exhibit increased circulating ANP and BNP [88].

Although the NPS has been shown to have compensatory properties, these mouse models demonstrate that, despite similar structure and properties, the NPs are not redundant. Furthermore, these mouse models demonstrate that although NPRs share binding chemistry, they mediate unique physiologic responses.

Whether alteration in the expression of natriuretic peptides is induced experimentally or as a clinical manifestation of disease, any NPS dysregulation has proven to be a sensitive indicator of cardiac pathogenesis in both the developing and the mature heart.

2.9 The Natriuretic Peptide System during Prenatal Development

While a functional NP system is critical in both the embryo and adult, NPs are expressed differently in the developing and mature heart. In contrast to the normal adult heart, ANP and BNP are mostly expressed and secreted in the embryonic ventricles [91].

Of apparent relevance, the NPS appears to be fully functional by midgestation – thus allowing the developing embryo to respond to volume changes and mediate body fluid homeostasis [4]. The early expression of the NPS during embryonic and fetal development, and

its modulation during critical periods of heart maturation, suggest an important role in normal cardiac ontogeny. Major peak ANP and BNP mRNA expression levels occur at GD 9, 12 and 15, all correlating with major progressions in cardiovascular organ development; regular heart beat, septal formation, and alteration of heart axis, respectively [83]. Such a large energy investment into the production of NPs and the establishment of the NPS during the primary stages of embryonic development signifies the critical role of the NPS during this time [83]. In addition, previous studies have reported the fetal NPS to be an autonomous hormonal system, as fetal plasma NP concentration differs from that of maternal or placental circulation [54].

Although NPs respond to similar stimuli and perform similar cardiovascular functions during development as they do in adults, during development the physiological roles of the NPS extend beyond that of blood pressure and body fluid homeostasis (Figure 8). During organogenesis and postnatal cardiac maturation, the NPs work to regulate growth and development of CV tissue and bone [92]. Although there is apparent interplay between NPs, these peptides are differentially expressed and demonstrate independent functions: ANP has potent antihypertrophic effects on cardiac myocytes [59]; BNP has antiproliferative effects on fibroblasts [64]; and CNP regulates the growth of bone [68].

2.10 Cardiovascular Fluid Homeostasis during Postnatal development

The transition from *in utero* to *ex utero* represents a phase of extreme physiological demand which requires the orchestration of numerous signaling cascades, and results in a massive fluid expulsion from the lungs. This rapid fluid adjustment requires the extravasation of sodium and water from the lungs, to allow immediate, independent pulmonary gas exchange. ANP is involved in both prenatal and adult sodium/fluid homeostasis [93, 94], thus making it likely that ANP plays a central role in the massive water riddance in early postnatal development.

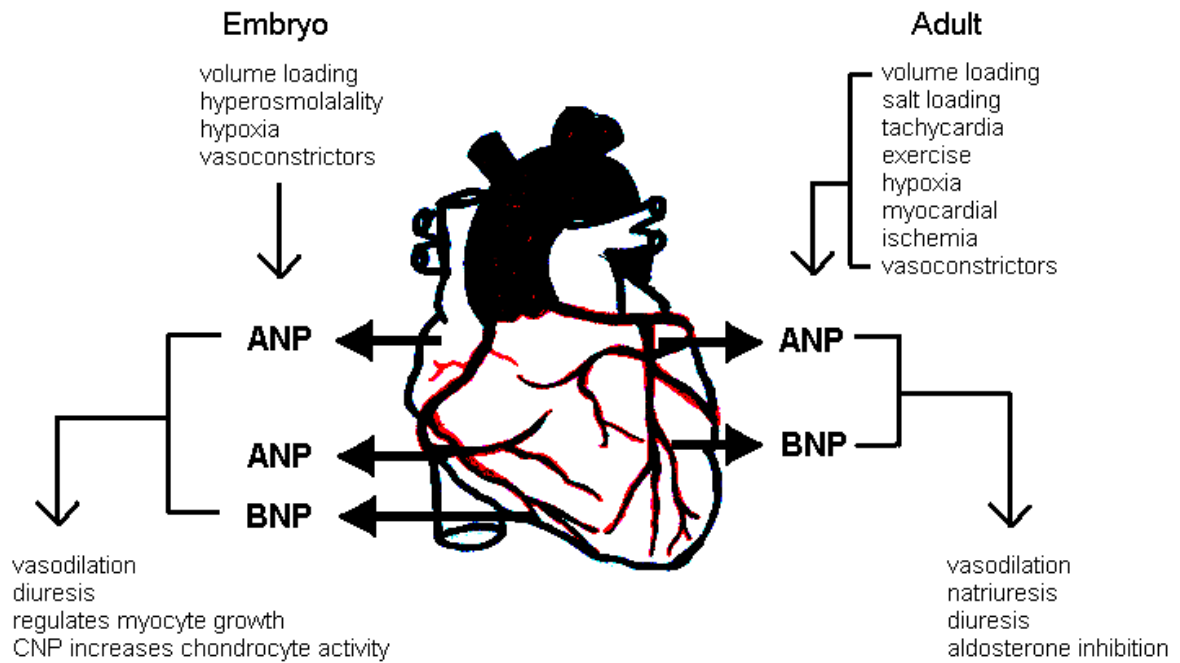


Figure 8. A diagrammatic comparison of the functional properties in embryonic and adult NPS. NP release is triggered differentially in developing embryonic hearts (left) and mature adult hearts (right). NPs are differentially expressed, and secreted from different cardiac chambers during embryonic development compared to a mature heart. NPs similarly share vasodilatory and natriuretic properties in embryonic and adult cardiovascular systems, however, elicit different physiological responses in embryonic and adult organs. Adapted from Cameron *et al.* [54].

2.11 Blood Pressure Establishment

Blood pressure is a sensitive indicator of both short-term and long-term cardiovascular homeostasis, and as previously outlined, sustained high blood pressure is strongly correlated with deleterious cardiovascular outcomes [6, 7]. Advances in biotechnology have permitted timecourse measurements of blood pressure in animal models. Reliable blood pressure values give insight into the physiological responsiveness of an organism under normal circumstances, in the case of genetic disruption, and during/after pharmacological and physiological insults. In rodent models, arterial blood pressure has been traditionally measured in the tail using a device which uses either LED (photoplethysmography), ceramic crystal (piezoplethysmography), or differential pressure transducers (volume pressure recording) to non-invasively record blood pressure [95]. These technologies have had varying degrees of success in adult animals, and have not been developed or standardized for neonatal mice [95]. More recently, great technological advances in the field of bio-radiotelemetry has allowed the more common use of subcutaneously implanted devices to continuously collect blood pressure measurements in freely moving lab animals [95]. This technique has proven to be exceptionally reliable, as it allows the evaluation of a blood pressure profile, and reflects a somewhat physiologically normal scenario. However, because radiotelemetry is a highly invasive procedure, and involves surgical anesthesia, its use in a neonatal cohort is extremely implausible. Anesthesia has been proven to cause decreased body temperature which leads to fluctuating blood pressure [96]. The procedures surrounding implantation, as well as the physical, physiological, and psychological stress (for example, maternal rejection) involved once the animal heals makes radiotelemetry impossible for neonatal animals with current technology. As such, only inferences can be made on the establishment of blood pressure during postnatal development. However a culmination of studies has shown that

blood pressure is gradually established during the cardiac modulatory phase of postnatal cardiac development [97, 98].

2.12 The Natriuretic Peptide System during Postnatal development

Despite the intensively investigated diverse roles of the NPS during prenatal cardiac development and mature CV homeostasis, there is limited understanding of the role of the NPS during normal postnatal cardiac development. Understanding the NPS in postnatal cardiac development and its potential implication in various neonatal cardiomyopathies is of sufficient importance, however, it is probable that potential pathological cardiac structure/function in *proANP* gene disrupted mice during development is linked to adverse cardiac phenotypes observed in adult mice. It is currently unknown when CH is established in *ANP^{-/-}* adult mice; this phenotype is believed to be initiated in the mature heart, however the earliest time course of this manifestation has never been established, leaving the potential for CH presenting in adulthood to actually begin during postnatal development. In order to fully understand the properties of the NPS in development and disease, it is imperative for the specific actions of ANP during postnatal cardiac development to be determined.

Chapter 3

Objectives, Hypothesis, Specific Aims

3.1 Experimental Design and Objectives

A strong body of literature indicates that ANP is critical to normal prenatal cardiac development and normal cardiovascular homeostasis in adults. The absence of ANP leads to adverse cardiovascular outcomes in adults, however, there is limited understanding of the expressional pattern or role of the NPS during postnatal development. Accordingly, the objective of the present study is to elucidate some of the mechanisms of developmental abnormality underlying cardiac hypertrophy observed in adult ANP^{-/-} mouse populations.

3.2 Hypothesis

The absence of ANP during early postnatal development will be evident in gross physical characteristics, coronary vasculature volume and organization, and NPS mRNA expression as compared to postnatal development in ANP^{+/+} mice.

3.3 Specific Aims

- i) Compare gross physical characteristics in male and female ANP^{+/+} and ANP^{-/-} mice during postnatal development.
- ii) Using a vascular casting experimental approach, qualitatively evaluate whether morphological differences in coronary vasculature exist in the hearts of ANP^{-/-} mice as compared to ANP^{+/+} mice during postnatal development.

- iii) Using a stereological method, quantitatively confirm morphometric vascular volume differences in the hearts of ANP^{-/-} mice as compared to ANP^{+/+} mice during postnatal development.
- iv) Using real-time RT-PCR, quantitatively evaluate molecular expressional changes in natriuretic peptides and receptors in the hearts of ANP^{-/-} mice as compared to ANP^{+/+} mice during early postnatal development.

Chapter 4

Materials & Methods

4.1 Animals

Experimental protocols pertaining to the use of mice in this study have been approved by the Animal Care Committee of Queen's University in accordance with the guidelines of the Canadian Council on Animal Care. ANP gene disrupted mice, initially established by John *et al.* [51] were bred and maintained in the Animal Care Facility at Queen's University. Breeding pairs of ANP^{+/+} and ANP^{-/-} mice were established and housed in plastic cages (1:1 male/female ratio) and kept at a room temperature of 21±1°C with a 12:12-hr light-dark schedule. All animals were fed a normal mouse chow diet containing 0.8% NaCl (Lab Diet®, Brentwood, MO), and tap water was provided *ad libitum*.

Multiple litters were collected at 1 day, 1 week, 2 weeks, 3 weeks ± 1 day, 4 weeks ± 1 day and 5 weeks ± 1 day. Day 1 litters were harvested on the day of birth, and 3 week old litters were collected at 21 days, before weaning. Day 1 was selected as the first time point to capture immediate postnatal physiology. Expecting moms were checked twice a day – in the morning and in late afternoon – to ensure that harvesting occurred within 24 hours after birth for the day 1 mice.

4.2 Genotyping

Tail samples were taken from each animal at the time of weaning to perform genetic analysis and to confirm their identified genotype of ANP^{+/+} or ANP^{-/-}. All chemicals used for genotyping purposes were purchased from Bioshop (Burlington, Ontario) unless otherwise stated. Tail samples (2-3mm pieces) were digested with Proteinase K in tail lysis buffer (50mM TRIS

pH 7.5; 100 mM EDTA pH 8.0; 100 mM NaCl; 1% SDS) at 56°C overnight. After the tissue was dissolved, DNAzol (Molecular Research Center. Inc, Burlington, ON) was added and the samples were centrifuged. Ethanol was then added to precipitate the DNA. The purified DNA was re-suspended in water and stored at 4°C until use.

Multiplex PCR was used to amplify the genomic DNA in order to detect the presence of the neomycin resistance gene in ANP^{-/-} mice. A core mixture of sense and anti-sense primers for ANP and neomycin-resistance genes (Cortec DNA Service Laboratories Inc., Kingston ON) were combined with HP TAQ DNA Polymerase (UBI Life Sciences, Saskatoon, SK), TAQ polymerase buffer and MgSO₄. Samples were left on ice until loaded into a thermocycler (Eppendorf MasterCycler EP-S, 22331, Hamburg).

The thermocycler was programmed to begin at a temperature of 95°C for 5 mins. The program ensued with 45 cycles of repeated temperature fluctuations (95°C for 15s; 62°C for 20s; 72°C for 45s). After the thermocycler program was completed, DNA loading buffer was added to each sample. DNA samples were then loaded onto a 2% agarose gel containing 0.1 µg/ml ethidium bromide and size separated by electrophoresis. The gel was visualized with a UV transilluminator to ensure single amplicon expression of ANP and neomycin-resistance gene.

4.3 Plasma and Tissue Collection

The weights of all animals were recorded. 1 day, 1 week and 2 week old mice were sacrificed by decapitation. Older animals were euthanized with an intraperitoneal injection overdose of Somnotol® (100 mg/kg body weight). Blood was collected in EDTA-lined capillary tubes from neck stumps in 1 day, 1 week and 2 week old mice, and by cardiac puncture in 3 week, 4 week and 5 week old mice. Capillary tubes were then placed in a hematocrit centrifuge and spun at maximum speed for ten minutes. Plasma to red blood cell ratio (hematocrit) was

measured for each animal using a digital caliper. The blood was then drained from the left ventricle, and the entire heart was removed from the thoracic cavity. The heart was dissected free of adherent tissue, blotted, weighed, snap-frozen as a whole in liquid nitrogen, and stored at -80°C until further use (Figure 9). Kidneys and lungs were similarly collected. Lungs from a small cohort of animals were weighed fresh (wet), then weighed after being dehydrated in an air-compressed centrifuge for 12-24 hours.

4.4 RNA Isolation and Preparation

Total RNA was isolated from frozen heart tissue samples by a modification of the acid-guanidinium-phenol-chloroform method (Tri Reagent, Sigma, Oakville, ON) combined with a High Pure RNA Isolation Kit (Roche, Montreal, QU). Glass and metal equipment used in RNA isolation was baked in a lab oven at 200°C for 12-24 hours to inactivate RNAses. All disposal plasticware were certified to be nuclease-activity-free by the manufacturer. Chemicals used for the preparation of wash buffers were purchased as nuclease-activity-free when possible and are maintained RNase free. All aqueous solutions and buffers without secondary and tertiary amines were DEPC (diethyl pyrocarbonate) treated and autoclaved. Gloves were worn, benches were cleaned, and samples were kept on ice as much as possible during the entire process of RNA isolation.

Tissue samples were frozen and stored at -80°C and were placed in liquid nitrogen, weighed frozen, and immediately placed in TriReagent (RNA/DNA/Protein isolation reagent, Tr-118, Molecular Research Centre, Burlington, ON), and homogenized (Polytron PT-10 Homogenizer, Luzern-Schweiz, Germany). Chloroform was added, the mixture was vortexed and allowed to stand for 10 min. The sample was then centrifuged and the top aqueous phase was collected. Ethanol was added and the sample was loaded onto a silica spin cup. The column was

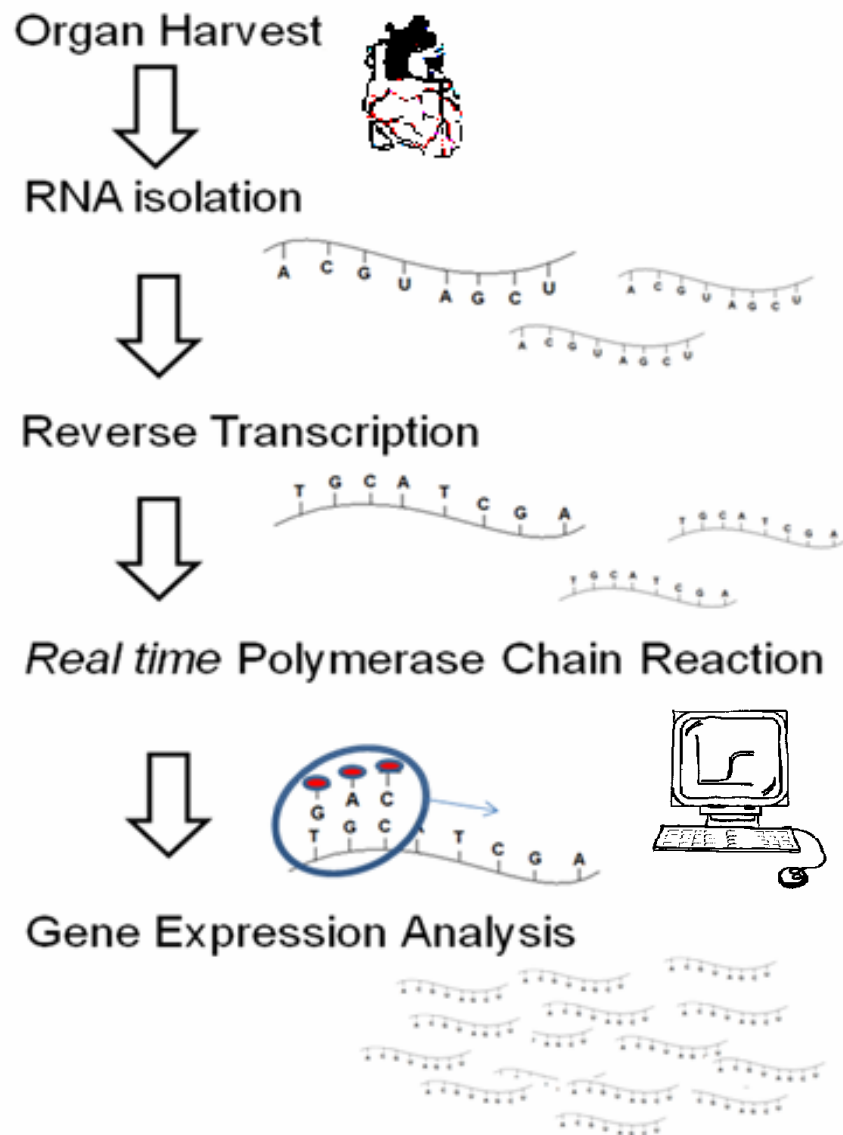


Figure 9. Diagram of the progression of molecular biology techniques utilized in the current study.

spun at 12,000rpm for 30s. The flow-through fraction was discarded and 10 units of DNA I in DNase Incubation Buffer (Roche High Pure RNA isolation Kit, Roche, Montreal, PQ) was added to the RNA retained in the cup. Samples were then purified in a High Pure Filter Tube with various wash buffers, according to the High Pure RNA Isolation Kit (Table A.1, Appendix A). RNA was collected from this phase and was then resuspended in RNase free water.

Two μL of RNA/200 μL of nanopure water was subsequently added to a UV plate, and RNA concentration was determined using spectrophotometric analysis at 260nm (SpectraMax Plus UV-VIS plate reader, Molecular Devices, Sunvale CA).

The quality of RNA was subsequently evaluated. Each RNA sample was combined with formaldehyde gel loading buffer (50% sterile glycerol, 1mM EDTA pH 8.0, 0.25% bromophenol blue, 0.25% xylene cyanol FF) to track RNA migration during electrophoresis. Samples were denatured by heating at 65°C for 10 min, were loaded onto an RNA agarose-formaldehyde gel, and run at 50V for 45 min. A gel documentation system (Kodak Gel Logic 2200 Digital Imaging System, New Haven, Connecticut) was used to ensure the presence and quality as determined by strong 18s and 28s bands.

4.5 Reverse Transcription of mRNA

In order to create a complimentary DNA template necessary for Polymerase Chain Reaction (PCR), RNA must be reverse transcribed into cDNA. This was done using M-MLV reverse transcriptase, oligo-dt primers, dNTP bases, and random nonamers.

After RNA concentration was quantified using UV spectroscopy, 1 $\mu\text{g}/\mu\text{L}$ was measured, diluted to 0.2 $\mu\text{g}/\mu\text{L}$ and made up to 10 μL with nuclease free water. This concentration of RNA was optimized to reduce the amount of housekeeping gene expression in RT-PCR. Diluted RNA samples were placed in the thermocycler and heated to 95°C for 10 mins to denature the

secondary structure of RNA strands, and then 5°C to minimize refolding. A core mix of RNase inhibitor, Reverse Transcriptase, RNase-free water, oligonucleotides and dNTP was added to each sample from a Transcriptor Reverse Transcriptase Kit (Roche, Montreal, QC).

The thermocycler was programmed to run for 25 mins at 25°C, then 60 mins at 37°C. This allows the oligo anchored primer to bind to the polyadenylate (poly-A) tail of the 3' end of the mRNA strands. Random nonamers (Cortec DNA Laboratories Inc., Kingston ON) were then added to each sample, after which the samples were incubated for an additional 60 min at 37°C. The resultant cDNA samples were stored at 4°C until further use.

4.6 Production of Primers

DNA primers for atrial natriuretic peptide (ANP), B-type natriuretic peptide system (BNP), C-type natriuretic peptide (CNP), Natriuretic Peptide Receptor A (NPR-A), Natriuretic Peptide Receptor B (NPR-B) and Natriuretic Peptide Receptor-C (NPR-C), were designed according to published sequence (GenBank, <http://www.ncbi.nlm.nih.gov/>) using Geneblast. Gene sequences were inputted into Primer Design 2.01 software (National Center for Biotechnical Information, Bethesda), to select appropriate primer pairs based on size, annealing temperatures, primer dimer propensity and G:C content. Sequences of sense and antisense primers used in real-time RT-PCR are listed in Table 2.

4.7 Testing of Sequenced PCR products

Sense and anti-sense primers were tested using conventional PCR to screen for secondary products. Each pair of diluted primers was combined with a core mix of TAQ Polymerase and

Table 2. Primer sequences used for quantitative PCR analysis. Sense and Antisense primers are represented by (S) and (AS), respectively.

Gene	Sequence (5' to 3')
ribosomal 18s	(S)-TCGATGCTCTTAGCTGAGTG (AS)-TGATCGTCTTCGAACCTCC
ANP	(S)-CAAGAACCTGCTAGACCACC (AS)-AGCTGTTGCAGCCTAGTCC
BNP	(S)-CCAGAGACAGCTCTTGAAGG (AS)-TCCGATCCGGTCTATCTTG
NPR _A	(S)-GGTTCGTTCTATTGGCTC (AS)-CCACCATCTCCATCCTCTC
NPR _B	(S)-GCTGGCTGCTTCTATGAT (AS)-ATGAGCGAGCCGTA ACT
NPR _C	(S)-CAGCAGACTTGGAACAGGA (AS)-CCATTAGCAAGCCAGCAC

pooled cDNA from ANP^{+/+} mouse hearts. Each sample was loaded into the thermocycler which was programmed to cycle between 95°C (15s), 62°C (20s), and 72°C (45s). Amplified products were loaded onto a 2% agarose gel. A 100bp ladder was run on the gel simultaneously. Gels were run at 45V for 30 min and then imaged on the gel documentation system to confirm single product amplification as represented by a single band.

4.8 Real-time RT-PCR

Real-time RT-PCR is used to amplify a specific gene on the cDNA to allow comparison between biological samples. Due to the high sensitivity of the real-time RT-PCR technique, core mixtures of TAQ Polymerase were used whenever possible in order to minimize pipetting errors.

SYBR Green I master mix (Roche, Montreal, QU) was combined with sense and anti-sense primers of each gene of interest to form a core mix. Upon the addition of duplicate cDNA samples, this core mix was equally added to each well of a Roche 96-well plate to a volume of 10µL. The plate was sealed with transparent plate sealing foil, and centrifuged at room temperature for 2 minutes at 2,000 rpm. The plate was then placed into the real-time RT-PCR machine (LightCycler 480, Roche, Montreal, QC) for the duration of the run. A typical temperature program consists of 10 minutes activation at 95°C followed by a cycling step which consisted of 95°C (15s), 62°C (15s) and 72°C (15s). At the end of the 72°C step the fluorescence signal of the amplicons was electronically collected. Up to 60 cycles were completed, depending on the gene studied.

A standard curve was generated for each primer set, which allowed the determination of relative concentrations of each biological sample. ANP^{+/+} cDNA samples were pooled and added to nuclease free H₂O to generate serial dilutions for a standard curve and internal experimental controls (used as a standard). In addition to using a standard dilution as an internal calibrator, an

internal non template control (NTC) was also included. Ribosomal 18s was used as reference gene which normalizes each sample for loading errors (Figures B1, B2, Appendix B).

Logistically, overall molecular analysis of each gene was impossible to do on a single PCR plate without compromising the number of biological replicates. In order to compare expressional differences between genotypes, samples were analyzed in two groups: day 1/week 1/week 2, and week 3/week 4/week 5. Accordingly, additional assays were performed to compare expressional differences between week 2 and week 3, in order to normalize run efficiencies between plates of the same gene. This split-assay technique allowed the complete analysis of both genotypes and ages without compromising accuracy with lower n values. Data was analyzed for each genotype and timepoint, and expressional profiles were obtained for each gene.

4.9 Gene Expression Analysis

To minimize error, only standard curves of primer sets with efficiencies of 2.0 ± 0.2 were accepted (an efficiency of 2.0 indicates a theoretical doubling of cDNA in a single PCR cycle). Expression profiles of each gene of interest, plus ribosomal 18s were generated. Target gene expression profiles were then converted into concentration by fitting the values to a non-linear curve fitting algorithm – Roche LC-480 software Release 1.51, and compared to reference (ribosomal 18s) gene expression (Appendix B). Data were compiled in Microsoft Excel, and then plotted with GraphPad Prism 4.0 (GraphPad Software Inc., La Jolla, California), and analyzed using one-way ANOVA with a Tukey *post hoc* test. Statistical significance was accepted at $p \leq 0.05$. All graphs are presented as mean \pm standard error of the mean (SEM).

4.10 Vascular Casting

Each animal used for vascular casting experiments was euthanized by an overdose of gaseous Isoflurane (Baxter Corporation, Mississauga ON), upon which the abdomen/thorax was dissected, exposing the beating heart. A butterfly needle (21G-1inch from Becton Dickinson & Co., Franklin Lakes NJ) connected to a gravitational perfusion unit (set at a height exerting 60 mm Hg pressure) containing perfusion fluid (Appendix C) was inserted into the apex of the left ventricle.

The inferior vena cava was exposed and clipped just below the renal vein. Perfusion was closely monitored for 5 minutes, after which the animal was placed under a dissecting microscope (WILD M3Z, Heerbrugg Switzerland) where the thoracic aorta was dissected. Two sutures were loosely threaded around the vessel, to eventually be tied around the inserted needle (Figure 10).

At this time, Batson's No 17 Plastic Replica polymer (Polysciences Inc, Warrington, PA) was prepared by mixing dye, catalyst and reagent according to manufacturer's instructions. The polymer was placed in a syringe and expelled with constant pressure through a needle inserted into the aorta. After visualizing perfusion into coronary arteries, sutures were tied off around the aorta, and the polymer was left to cure. After 48 hours, hearts were carefully excised and placed in 0.1M NaOH for 12 hours, and then 5% Contrad *70 detergent (Baxter Corporation, Mississauga ON) water solution for 12 hours, leaving the polymer casting of the heart vessels (Appendix C). The casts were then suspended in water until imaging and analysis.

4.11 Vascular Imaging

Vascular casts were submerged in a water filled petri dish, over a white background to be imaged with a Wild M3Z dissecting microscope (Heerbrugg, Switzerland).

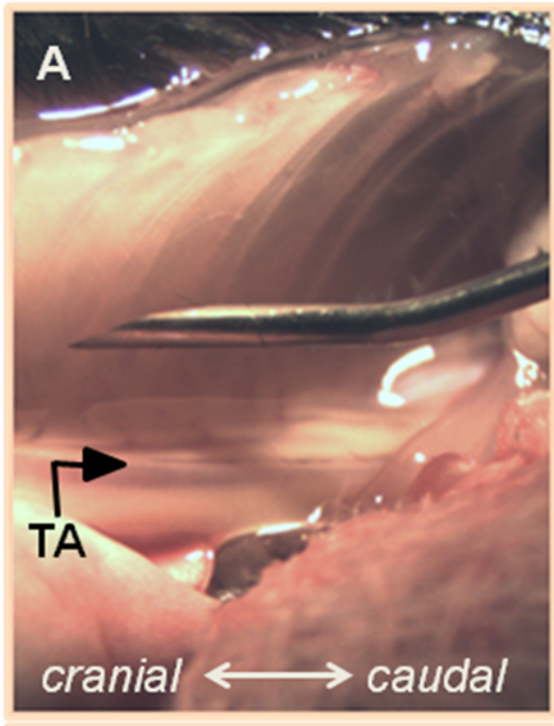


Figure 10. Methodological images of polymer injection into the posterior thoracic cavity of 5 week old ANP^{+/+} mouse. (A) Size comparison of needle and thoracic aorta (labelled TA). (B) Demonstration of cannulation technique with 5-0 silk suture thread support. Direction indicated as cranial/caudal.

4.12 Histology

Each animal used for histological purposes was euthanized by an overdose of gaseous Isoflurane, upon which the abdomen/thorax was dissected, exposing the beating heart. Perfusion was performed as described in the vascular cast section (Appendix C). Using identical apparatus and technique, each animal was perfused with 4% paraformaldehyde (PFA) in 0.1M PBS. Flow was closely monitored for 5 minutes, after which individual organs were carefully excised, and immersed in 4% PFA for 18-24 hours. Finally, tissues were placed in 70% ethanol and stored at 4°C until processing.

Tissues were carefully cleaned of surrounding connective tissue and cut transversely at the mid-point of the heart. The lower half, including the heart apex, was placed in a labelled tissue cassette. Tissues were processed in a series of graded ethanol (70%, 90%, 100%, 100%), and toluene. The cassettes were placed in paraffin wax inside a vacuum oven, to allow for complete wax infiltration. Tissues were embedded as a paraffin block.

Paraffin blocks were trimmed, and cut into 5µm thick sections. These sections were lifted on positively charged glass slides, and allowed to dry overnight. Slides were baked at 60°C for 20-24 hours. Slides were cleared with toluene, rehydrated through a series of graded alcohols, and then stained using Weigart's Iron Hematoxylin and alcoholic eosin. Stained slides were coverslipped and allowed to set for 20-24 hours. Slides were stored until analysis.

4.13 Histological Imaging and Analysis

Slides were imaged using a Nikon Eclipse E800 light microscope (Nikon, Japan) with Q capture (Surrey, BC). Image areas were selected based on cross section of myofibres. At least four animals were processed per time point and genotype, and seven images were taken per slide (Figures D1-D2, Appendix D).

Images were formatted to be a consistent size and orientation, and were then coded and organized in random sequence to allow for blind analysis. A stereological grid transparency was placed over the computer screen (Figure D3, Appendix D), and constituents of each slide were counted and recorded. Data were de-coded, inputted into GraphPad Prism 4.0, and analyzed using a one-way ANOVA with a Tukey *post hoc* test.

Chapter 5

Results

5.1 Physical Data

*pro*ANP gene-disrupted mice (ANP^{-/-}) exhibit cardiac hypertrophy throughout postnatal development. ANP^{-/-} mice showed a significant increase in heart-to-body weight (HW/BW) ratio compared to ANP^{+/+} mice at all time points studied. Most notably, these differences are evident even at day 1, where ANP^{-/-} mice have a HW/BW ratio of 9.95±1.50mg/g, whereas the ANP^{+/+} mice have a HW/BW ratio of 7.01±1.07mg/g. ANP^{-/-} mice exhibit 42% increased HW/BW ratios compared to ANP^{+/+} at day 1, and this difference was maintained throughout development, however narrowed to be 31% by week 5. The effects of the absence of ANP on cardiac size in relation to body weight are shown in Figure 11. All animals demonstrated increased heart weight and increased body weight with increasing age, independent of genotype (Table 3). There were no significant differences in either the heart weights or the body weights between male and female neonates of either genotype at all time points studied (Table 4).

Ratios of tissue weights to body weights of other organs including kidney to body weight, lung to body weight and liver to body weight demonstrated no significant differences in ANP^{-/-} compared to aged matched ANP^{+/+} postnatal male mice (Table 5). Wet lung weight to dry lung weight ratios demonstrated no significant differences in ANP^{-/-} compared to age matched ANP^{+/+} postnatal male mice (Table E.1, Appendix E).

Hematocrit was also measured for each animal. A significant decrease in hematocrit was noted in the ANP^{-/-} mice at the 2 week time point. Similar profiles were observed between genotypes at all other aged matched groups (Figure 12).

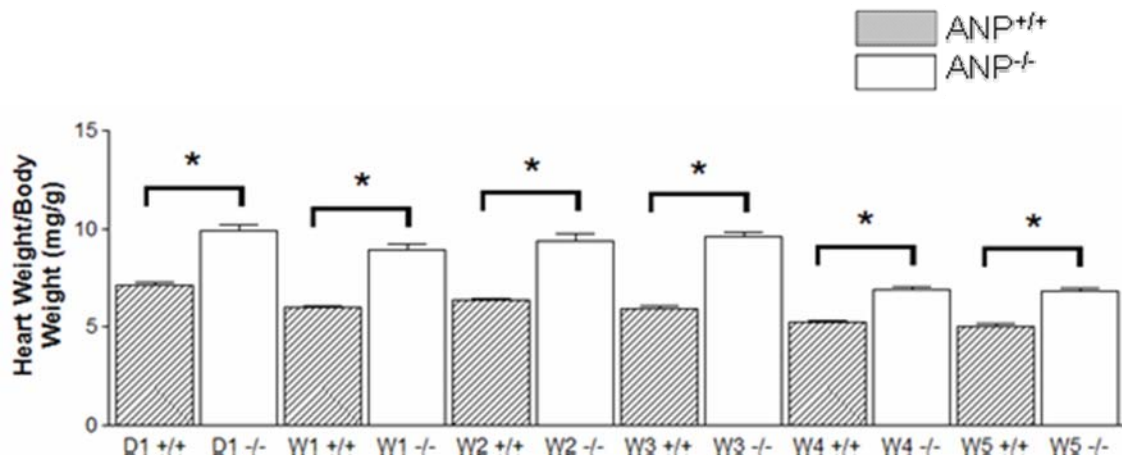


Figure 11. Effect of *proANP* gene-disruption on cardiac development as represented by heart weight to body weight ratios of mice at indicated postnatal timepoints. Day 1 = D1, and weeks 1 to 5 = W1, W2, W3, W4, and W5. Data are represented as the mean \pm S.E.M. * denotes $P < 0.05$ as determined by one way ANOVA followed by Tukey *post hoc* test; $n = 12-30$ /group.

Table 3. Heart, body, and heart-to-body weight values for ANP^{+/+} and ANP^{-/-} male (A) and female (B) mice throughout postnatal development (day 1, weeks 1 to 5).

A

postnatal timepoint	ANP wildtype neonates (males)				ANP knockout neonates (males)			
	n	Heart weight (mg)	Body weight (g)	Heart-to-body weight (mg/g)	n	Heart weight (mg)	Body weight (g)	Heart-to-body weight (mg/g)
day 1	14	9.58 ± 1.23	1.38 ± 0.12	7.01 ± 1.07	13	14.82 ± 2.43	1.49 ± 0.16	9.95 ± 1.50
week 1	32	28.94 ± 5.85	4.77 ± 0.75	6.05 ± 0.70	14	39.39 ± 9.49	4.92 ± 0.94	8.47 ± 1.96
week 2	14	60.51 ± 7.96	9.33 ± 0.92	6.47 ± 0.46	9	92.49 ± 17.83	9.86 ± 0.56	9.37 ± 1.70
week 3	10	65.10 ± 2.76	11.25 ± 1.56	5.89 ± 0.89	7	99.53 ± 8.59	9.95 ± 1.14	10.08 ± 1.15
week 4	17	92.35 ± 11.43	18.09 ± 2.00	5.11 ± 0.40	19	118.20 ± 19.14	17.92 ± 2.30	6.60 ± 0.65
week 5	19	105.79 ± 14.99	21.25 ± 2.28	4.97 ± 0.46	12	140.75 ± 14.48	21.81 ± 2.77	6.50 ± 0.70

B

postnatal timepoint	ANP wildtype neonates (females)				ANP knockout neonates (females)			
	n	Heart weight (mg)	Body weight (g)	Heart-to-body weight (mg/g)	n	Heart weight (mg)	Body weight (g)	Heart-to-body weight (mg/g)
day 1	17	9.66±1.75	1.34±0.13	7.20±1.03	6	15.90±3.89	1.61±0.23	9.81±1.30
week 1	12	28.34±5.87	4.54±0.86	6.25±0.61	13	42.58±9.24	5.02±1.24	9.21±1.26
week 2	12	53.08±5.90	8.46±0.92	6.28±0.20	14	99.59±20.87	10.19±1.11	9.83±2.13
week 3	23	64.32±7.55	10.83±1.30	5.99±0.73	8	99.10±7.60	10.86±0.82	9.14±0.49
week 4	14	85.96±8.41	15.97±1.12	5.39±0.47	12	121.58±23.78	15.65±1.62	7.77±1.30
week 5	15	92.18±11.70	18.07±2.75	5.15±0.60	5	140.73±18.14	19.88±2.30	7.13±0.98

Table 4. Kidney, body, and kidney-to-body weight values for ANP^{+/+} and ANP^{-/-} male (A) and female (B) mice throughout postnatal development (day 1, weeks 1 to 5).

A

postnatal timepoint	ANP wildtype neonates (males)				ANP knockout neonates (males)			
	n	Kidney weight (mg/g)	Body weight (g)	Kidney-to-body weight (mg/g)	n	Kidney weight (mg/g)	Body weight (g)	Kidney-to-body weight (mg/g)
	day 1	6	14.82 ± 2.27	1.38 ± 0.12	10.05 ± 1.19	10	13.89 ± 2.55	1.49 ± 0.16
week 1	23	48.08 ± 8.62	4.77 ± 0.75	10.51 ± 1.44	16	49.20 ± 10.23	4.92 ± 0.94	10.05 ± 0.68
week 2	9	102.23 ± 13.49	9.33 ± 0.92	11.40 ± 5.67	8	131.89 ± 23.48	9.86 ± 0.56	12.96 ± 1.91
week 3	9	128.86 ± 13.75	11.25 ± 1.56	10.99 ± 0.42	6	113.98 ± 4.54	9.95 ± 1.14	11.94 ± 0.16
week 4	12	213.65 ± 38.51	18.09 ± 2.00	11.57 ± 0.90	16	297.23 ± 37.67	17.92 ± 2.30	11.67 ± 0.84
week 5	15	264 ± 22.09	21.25 ± 2.28	12.19 ± 0.87	8	270.09 ± 49.59	21.81 ± 2.77	12.34 ± 1.92

B

postnatal timepoint	ANP wildtype neonates (females)				ANP knockout neonates (females)			
	n	Kidney weight (mg)	Body weight (g)	Kidney-to-body weight (mg/g)	n	Kidney weight (mg)	Body weight (g)	Kidney-to-body weight (mg/g)
day 1	5	12.80±1.50	1.34±0.13	9.26±0.99	3	15.70±2.43	1.61±0.23	10.69±0.70
week 1	7	43.83±8.32	4.54±0.86	10.31±0.78	14	51.70±1.49	5.02±1.24	10.25±0.70
week 2	8	94.09±5.48	8.46±0.92	11.58±0.46	7	115.63±26.60	10.19±1.11	11.18±2.44
week 3	16	139.11±12.37	10.83±1.30	12.18±0.72	5	139.06±24.98	10.86±0.82	12.89±1.05
week 4	11	188.32±14.93	15.97±1.12	11.71±0.73	7	183.81±21.08	15.65±1.62	12.04±0.77
week 5	9	206.91±17.84	18.07±2.75	11.33±1.24	4	225.18±26.15	19.88±2.30	10.67±1.20

Table 5. Lung, body, and lung-to-body weight values for ANP^{+/+} and ANP^{-/-} male (A) and female (B) mice throughout postnatal development (day 1, weeks 1 to 5).

A

postnatal timepoint	ANP wildtype neonates (males)				ANP knockout neonates (males)			
	n	Lung weight (mg)	Body weight (g)	Lung-to-body weight (mg/g)	n	Lung weight (mg)	Body weight (g)	Lung-to-body weight (mg/g)
day 1	16	31.03 ± 3.77	1.38 ± 0.12	22.61 ± 2.57	15	34.44 ± 7.97	1.49 ± 0.16	22.89 ± 3.44
week 1	32	90.95 ± 20.31	4.77 ± 0.75	19.11 ± 3.23	16	93.12 ± 14.45	4.92 ± 0.94	19.12 ± 1.91
week 2	8	110.70 ± 4.32	9.33 ± 0.92	12.46 ± 1.19	7	146.84 ± 19.74	9.86 ± 0.56	14.89 ± 1.35
week 3	8	102.00 ± 8.42	11.25 ± 1.56	8.72 ± 0.50	5	116.08 ± 6.44	9.95 ± 1.14	12.16 ± 0.61
week 4	12	135.73 ± 14.98	18.09 ± 2.00	7.43 ± 0.76	16	133.86 ± 18.18	17.92 ± 2.30	7.62 ± 0.94
week 5	15	140.29 ± 11.22	21.25 ± 2.28	6.46 ± 0.34	8	146.63 ± 8.51	21.81 ± 2.77	6.75 ± 0.72

B

postnatal timepoint	ANP wildtype neonates (females)				ANP knockout neonates (females)			
	n	Lung weight (mg)	Body weight (g)	Lung-to-body weight (mg/g)	n	Lung weight (mg)	Body weight (g)	Lung-to-body weight (mg/g)
day 1	17	33.82±6.34	1.34±0.13	25.16±3.57	6	40.70±9.65	1.61±0.23	25.16±3.17
week 1	10	85.4±17.36	4.54±0.86	18.89±2.31	14	92.32±18.84	5.02±1.24	18.60±1.74
week 2	8	106.94±7.10	8.46±0.92	13.19±1.10	6	164.6±30.35	10.19±1.11	16.01±2.39
week 3	16	106.20±13.38	10.83±1.30	9.38±0.76	5	130.72±11.34	10.86±0.82	12.19±0.19
week 4	11	124.07±11.16	15.97±1.12	7.72±0.66	7	124.23±11.05	15.65±1.62	8.19±0.91
week 5	9	130.70±20.37	18.07±2.75	7.07±4.28	4	152.93±6.18	19.88±2.30	7.26±3.42

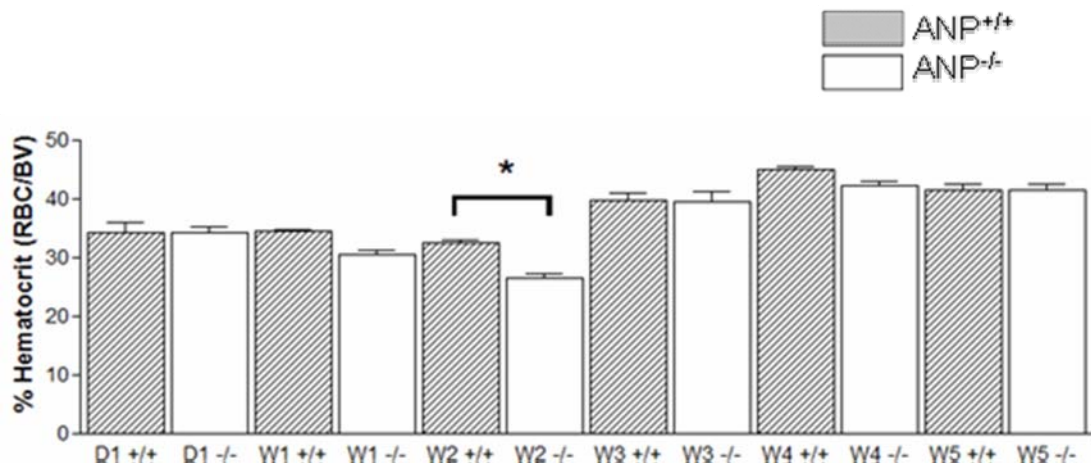


Figure 12. Effect of *proANP* gene-disruption on hematocrit during postnatal development of ANP^{+/+} and ANP^{-/-} mice. Time points include day 1 (D1), and weeks 1 to 5 (W1, W2, W3, W4, W5). Data are represented as the mean \pm S.E.M. * denotes $P < 0.05$ as determined by one way ANOVA followed by Tukey *post hoc* test; $n = 12-30/\text{group}$.

5.2 Vascular Organization and Composition

5.2.1 Morphological Analysis

A comparison of the coronary vasculature between ANP^{+/+} and ANP^{-/-} mice was made possible using a corrosion casting technique. Retrograde injection of this polymer into the thoracic aorta allowed the coronary arteries and not the cardiac chambers to be filled with polymer. After the polymer was set, chemical digestion of the surrounding tissues rendered a negative imprint of the coronary vessels (Figure 13). A visual comparison of LM images (of similar major vessels) gave a clear depiction of the disorganized branching patterns, and overall denseness of arterial vessels in the ANP^{-/-} mice. While the vessel arrangement observed in ANP^{+/+} mice follow a normal progression of vessel size (large vessels branching into progressively smaller vessels), the vessel arrangement of ANP^{-/-} appeared to be much less ordered. The coronary arterial casts in the ANP^{-/-} mice exhibit small vessels branching off directly from major vessels, and an overall cobweb-like appearance.

5.2.2 Morphometric (Stereological) Analysis

The qualitative results obtained from the vascular cast are well complemented with quantitative analysis. As such, the method of quantifying vessel volume using stereological analysis provides a more discrete method of examining the vascularity of the coronary vessels. As demonstrated in Figure 13, *proANP* gene-disrupted mice showed increased cardiac vessel volume at all developmental time points studied. In order to confirm that this difference was not influenced by histological sampling, or alternate heart constituents (and artifacts), difference in vessel volume was confirmed for both absolute and relative (Figure 14) cardiac vessel density.

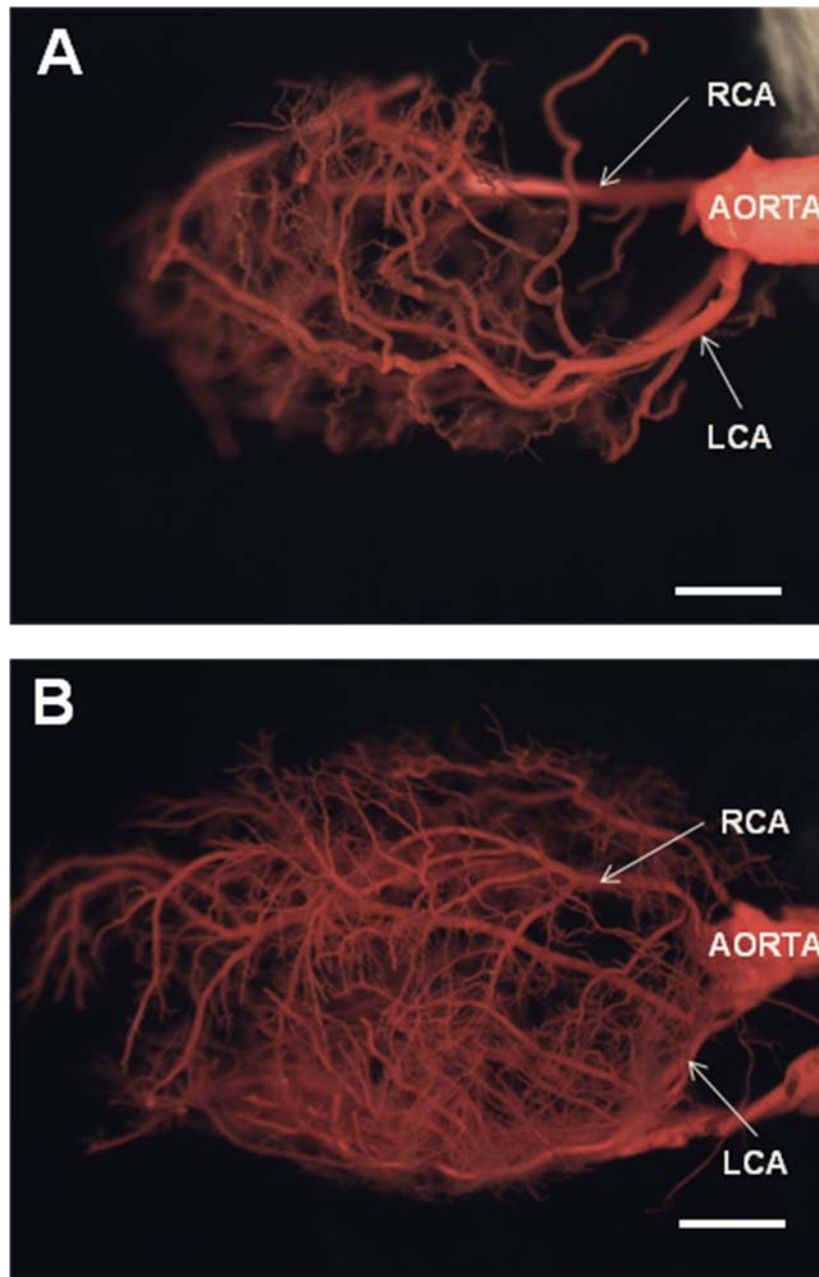


Figure 13. Representative light microscopy images of coronary vascular casts of ANP^{+/+} (A) and ANP^{-/-} (B) neonatal mice at 4 weeks of age. RCA = right coronary artery; LCA = left coronary artery. Scale bar = 1mm.

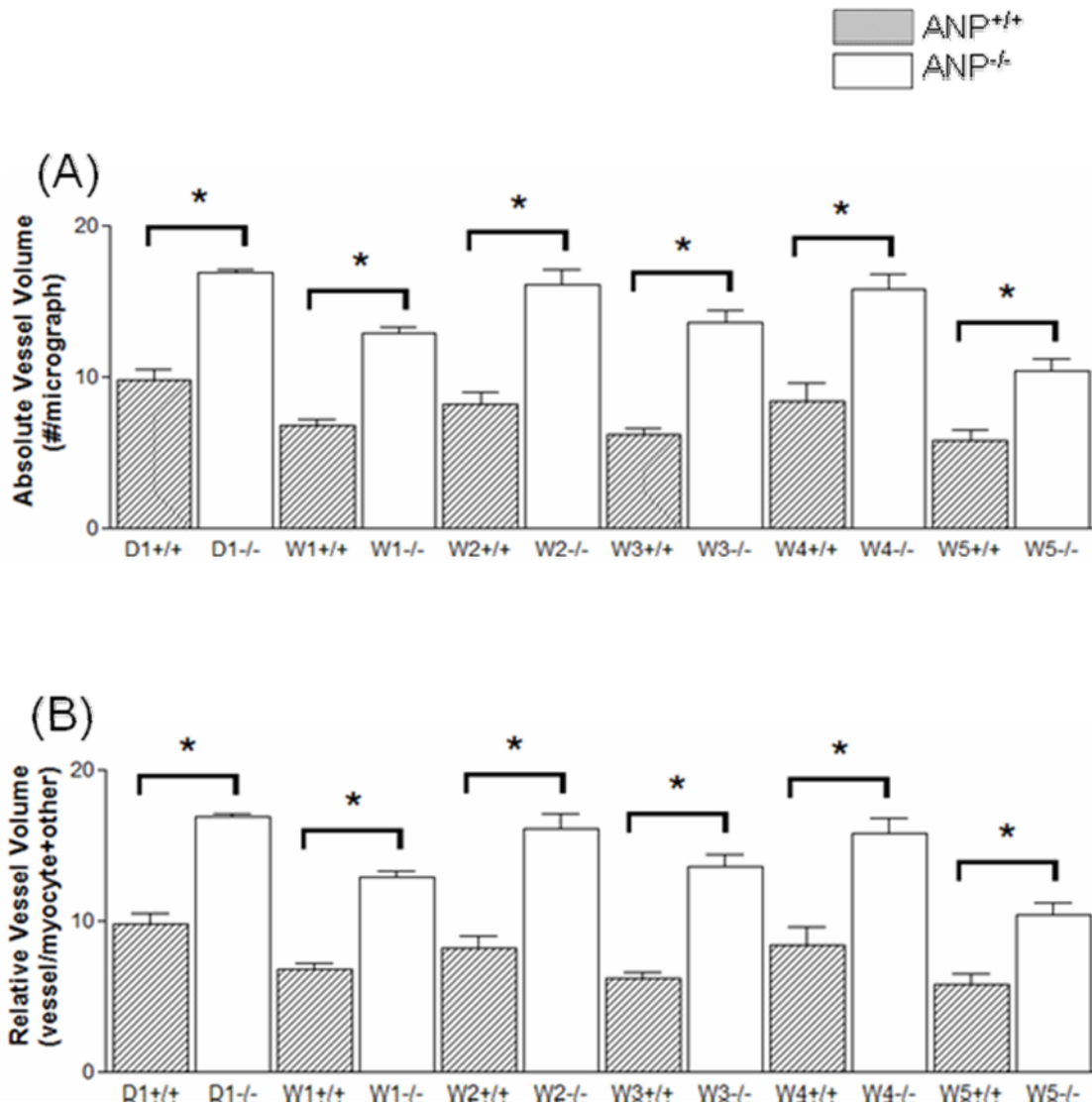


Figure 14. Analysis of absolute (A) and relative (B) vessel volume in ANP^{+/+} and ANP^{-/-} mouse hearts during early postnatal development. Relative vessel volume values are relative to myocyte and “other” volume (“other” includes fibroblasts, collagen and elastic fibres, histological artifacts, and space). Day 1 = D1, and weeks 1 to 5 = W1, W2, W3, W4, and W5. Data are represented as the mean \pm S.E.M. * denotes $p < 0.05$ by one way ANOVA followed by Tukey *post hoc* test; $n = 4-5$ per group of averaged values of seven micrographs per sample.

Representative images of ANP^{+/+} and ANP^{-/-} mice are shown in Figure 15. It appeared that space occupied by the coronary arterial vessels was greater for the ANP^{-/-} mice as compared to ANP^{+/+} mice.

Quantification of either absolute (Figure 16) or relative myocyte volume yielded no significant differences in ANP^{-/-} compared to ANP^{+/+} postnatal mice. Similarly, “other” volume (includes fibroblasts, collagen fibres, elastic fibres, histological artifacts, space) also remained unchanged throughout development (Figure 16).

In summary, ANP^{-/-} mice demonstrate increased cardiac vessel volume throughout all timepoints studied.

5.3 Molecular Analysis

5.3.1 Expression of ANP during postnatal development

In order to characterize the developmental profile of cardiac ANP expression during postnatal cardiac development of ANP^{+/+} mice, mRNA levels of ANP were quantified by real-time RT-PCR. Consistent with previous literature, the current experiment confirmed a significant drop in ANP mRNA expression at 1 week postnatally (Figure 17). This expression profile demonstrates relatively higher expression at day 1, and an upwards trend in timepoints subsequent to week 1. ANP^{-/-} mice were not analyzed for ANP expression with the exception of two random samples to confirm complete absence of ANP in the proANP gene-disrupted heart samples.

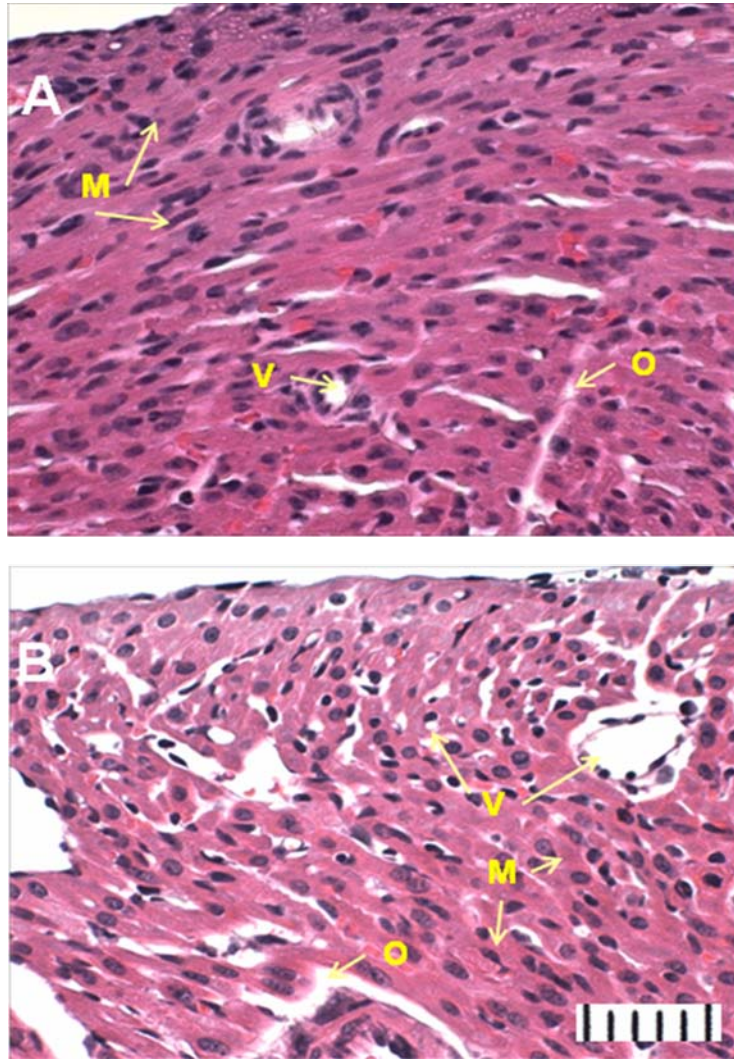


Figure 15. Representative light microscopy images of 5 week ANP^{+/+} (A) and 5 week ANP^{-/-} (B) used for stereological analysis of vessel volume, myocyte volume, and “other” (includes fibroblasts, collagen and elastic fibres, histological artifacts, and space) volume. Example vessel is indicated with V; myocyte with M; and “other” with O. A collection of 7 images from each of the four heart samples from ANP^{+/+} and ANP^{-/-} early postnatal mice used for stereological analyses. Time points include day 1 (D1), and weeks 1 to 5 (W1, W2, W3, W4, W5). The bottom reference measurement was photographed using the same magnification as all images analyzed (5 bars represent 50µm).

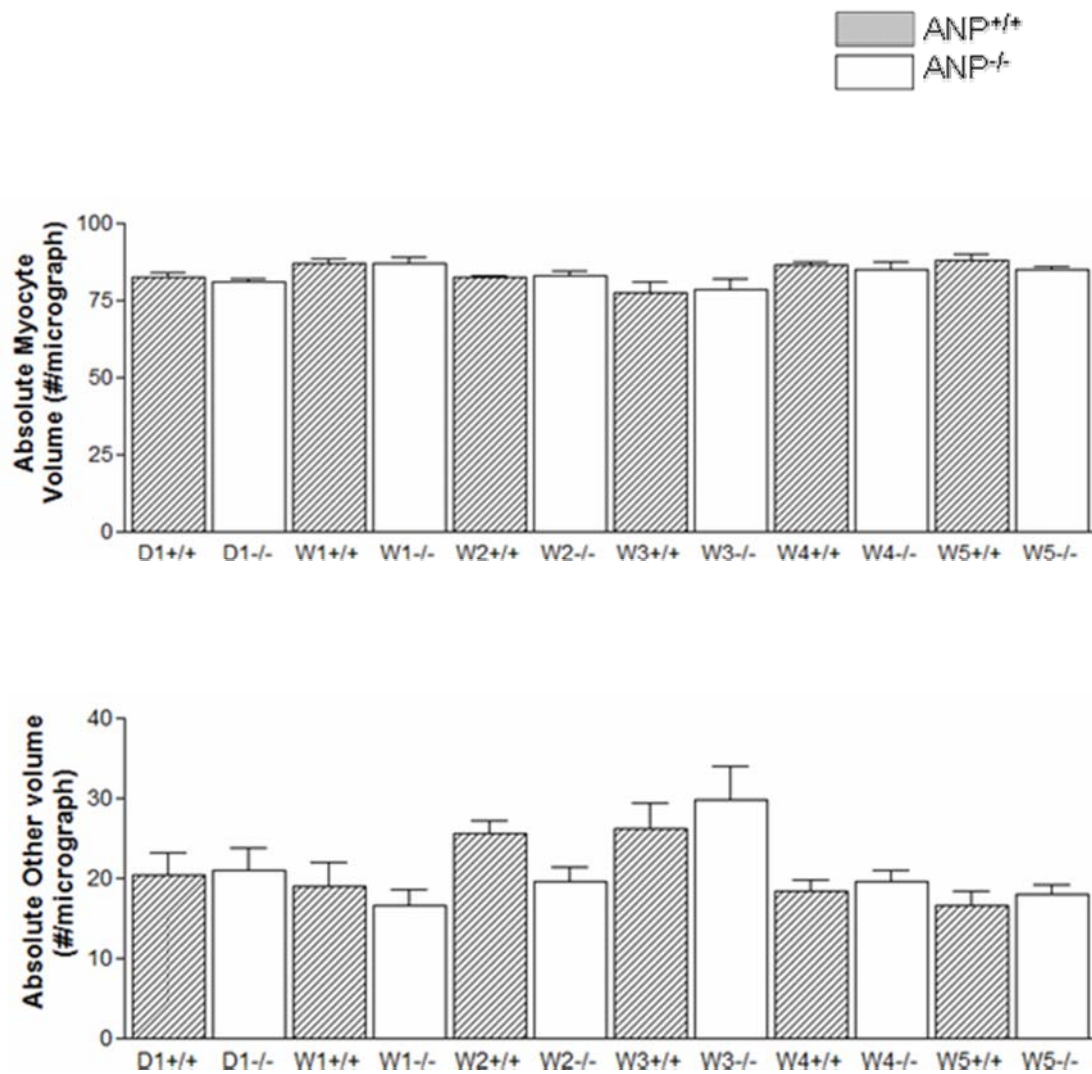


Figure 16. Analysis of absolute myocyte volume (A) and absolute “other” volume (B) in ANP^{+/+} and ANP^{-/-} mouse hearts during early postnatal development. “Other” volume includes fibroblasts, collagen and elastic fibres, histological artifacts, and space. Day 1 = D1, weeks 1 to 5 = w1, w2, w3, w4, and w5. w=week. Data are represented as the mean \pm S.E.M. * denotes $P < 0.05$ as determined by one way ANOVA followed by Tukey *post hoc* test; n=4-5 per group of averaged values of seven micrographs per sample.

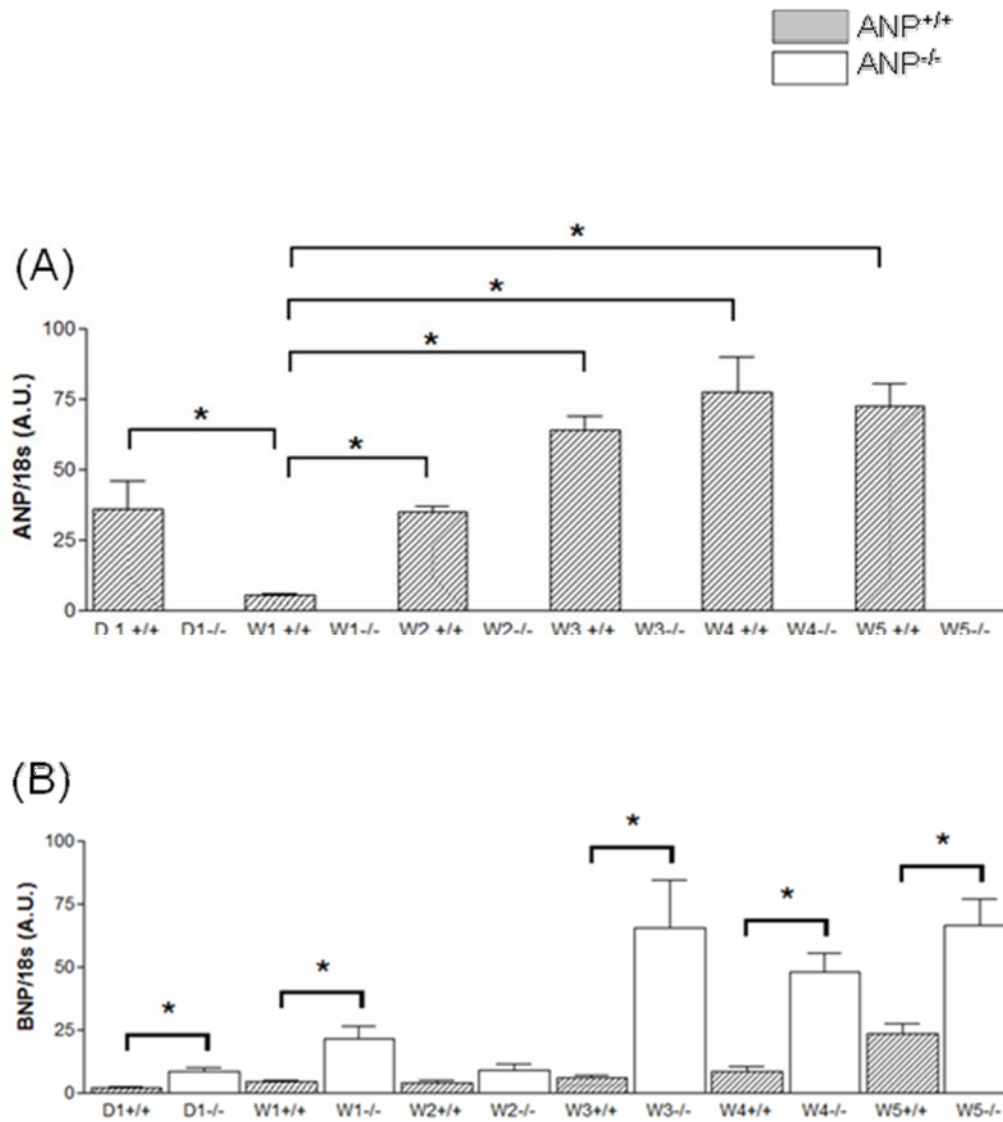


Figure 17. ANP (A) and BNP (B) mRNA expression in ANP^{+/+} postnatal mice at day 1, and weeks 1 to 5. The vertical axis is the ratio of target gene expression (ANP or BNP) to reference gene expression (m18s). ANP^{-/-} mice have no ANP mRNA expression, and are thus not represented in (A) data analysis. Day 1 = D1, weeks 1 to 5 = w1, w2, w3, w4, and w5. w=week. Data are represented as the mean \pm S.E.M. * denotes $P < 0.05$ as determined by one way ANOVA followed by Tukey *post hoc* test; $n = 6-8$ per age, per genotype.

5.3.2 Expression of BNP during postnatal development

BNP mRNA levels were measured in the heart of the neonatal mice in order to determine whether this hormone, credited as being central to the compensatory nature of the NPS, was altered in the absence of ANP. BNP expression analysis demonstrated an overall increased expression in ANP^{-/-} mice as compared to age-matched ANP^{+/+} mice. As measured by real-time RT-PCR expression of BNP mRNA in ANP^{-/-} mice was significantly higher at all time points studied with the exception of week 2 (Figure 17). While ANP^{+/+} and ANP^{-/-} mice both demonstrate varied BNP mRNA expression during development, there appears to be a gradually increasing trend in ANP^{+/+} mice, while ANP^{-/-} mice demonstrate an immediate and drastic expressional increase throughout development.

5.3.3 Expression of NPR-A during postnatal development

Analysis of NPR-A expression provides insight into the NP receptor population during postnatal development. Specifically, it appears as though NPR-A mRNA is consistently expressed during normal postnatal development. However, in the absence of ANP there is a significant decrease in NPR-A mRNA expression at week 1, and although not significant, expression appears to be decreasing in subsequent timepoints (Figure 18).

5.3.4 Expression of NPR-B during postnatal development

Although a secondary receptor for ANP, analysis of NPR-B mRNA expression was necessary for a more comprehensive understanding of the compensatory actions of the NPS in the absence of ANP. Figure 18 demonstrates an overall increasing NPR-B mRNA expression throughout development. In ANP^{+/+} animals, a significant increase in NPR-B mRNA expression

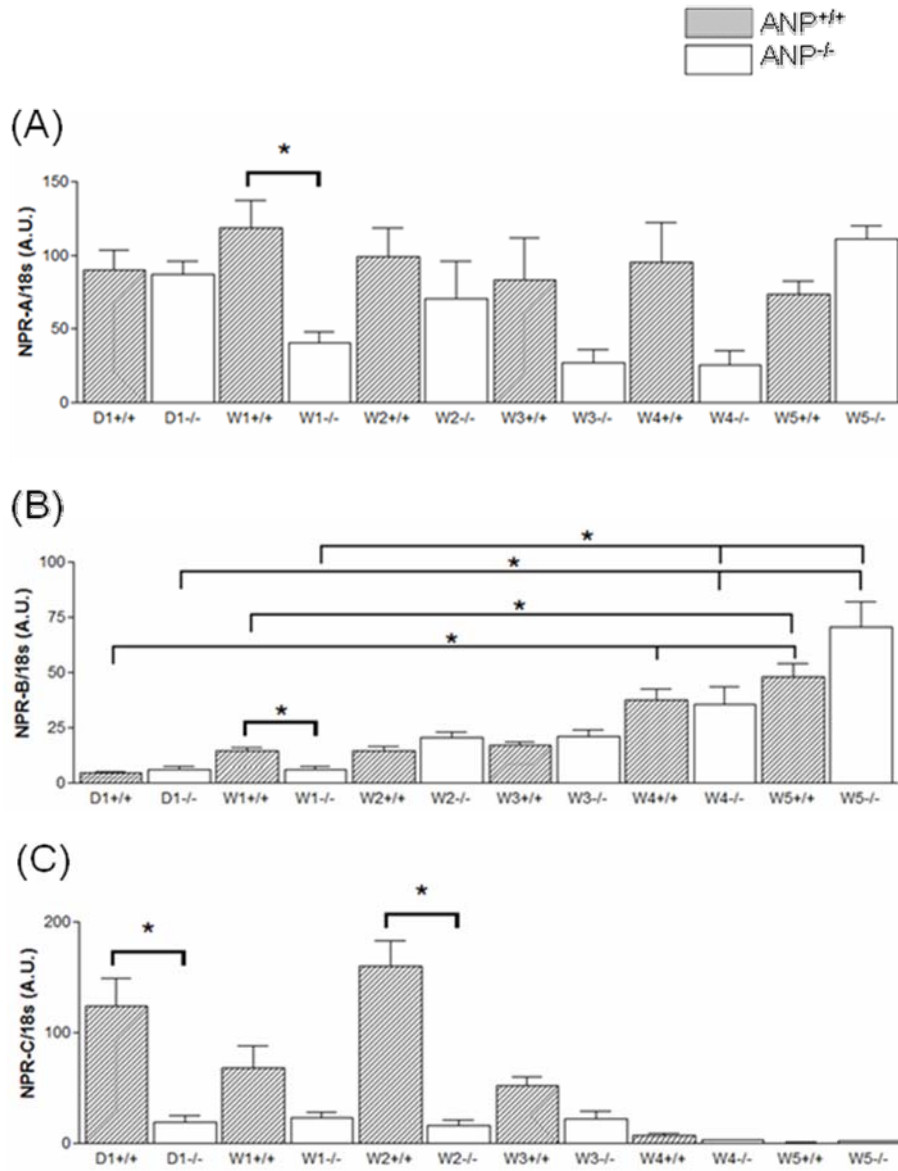


Figure 18. NPR-A (A), NPR-B (B), and NPR-C (C) mRNA expression in ANP^{+/+} and ANP^{-/-} postnatal mice at day 1, and weeks 1 to 5. The vertical axis is the ratio of target gene expression (NPR-A) to reference gene expression (m18s). Day 1 = D1, weeks 1 to 5 = w1, w2, w3, w4, and w5. w=week. Data are represented as the mean \pm S.E.M. * denotes P < 0.05 as determined by one way ANOVA followed by Tukey *post hoc* test; n=6-8 per age, per genotype.

was evident from day 1 and week 1, to weeks 4 and 5. ANP^{-/-} mice exhibit a similar overall expressional profile of gradual increase, however, without consistent rates of expressional increases between timepoints. Differences in expression between ANP^{+/+} and ANP^{-/-} reaches significance at 1 week.

5.3.5 Expression of NPR-C during postnatal development

Examination of NPR-C mRNA expression in ANP^{+/+} mice during postnatal cardiac development renders a physiologically normal expressional profile. As quantified by real-time RT-PCR, a trend seemed to emerge whereby expressional levels of NPR-C mRNA in earlier development were initially high, but waned by week 4. This later expressional reduction is evident in week 4 and 5 ANP^{-/-} or ANP^{+/+} mice (Figure 18). Such a high initial expression level of NPR-C mRNA followed by immediate down-regulation in subsequent weeks indicates a time point for postnatal establishment of this receptor population. Notably, there is a slight depression in NPR-C mRNA expression in ANP^{+/+} mice week 1 mice which is not observed in ANP^{-/-} week 1 mice. Overall, NPR-C mRNA levels are down-regulated in ANP^{-/-} mice, as NPR-C mRNA expression levels are consistently lower in ANP^{-/-} mice as compared to age-matched ANP^{+/+} mice. These differences reach significance at day 1, and week 2 (P<0.05).

Chapter 6

Discussion & Conclusion

6.1 Rationale for Examining Postnatal Age, ANP^{-/-} Mouse Model, and Whole Heart

Disruption and deterioration of the structure and function of the myocardium is the basis for cardiomyopathy, and the presentation of such disorders during neonatal development is particularly associated with poor prognosis [99, 100]. While the underlying pathophysiology of cardiomyopathy in neonates and adults are fundamentally similar, by virtue of the stimuli, onset, and outcomes, they are intrinsically different [100, 101]. Thus the developing heart should not be thought of as a smaller version of the adult heart, but as a malleable composition of tissues heavily influenced by the progression of maturation. Disruption or alteration of any of the processes entailing cardiac maturation can induce permanent pathological adaptations [8, 11].

During development, cardiac tissues rely on various molecular mechanisms to sense developmental and homeostatic changes, and to respond to increasing physiological demands with structural growth. The fact that the heart instigates this endocrine control with the production and secretion of the cardiac NPS [52] – and that this hormonal system is fully functional by midgestation [4] – infers that the processes involved in cardiac development and maturation are largely self-regulated.

In order to understand the scope of the physiological role of the NPS, the gene expression profiles and cardiac phenotypes of NPS gene-disrupted animal models have been scrutinized. Research groups have honed experimental procedures to investigate the differences in hypoxic/myocardial infarction conditions [102, 103], under nutritional deprivation and excess [104], and with salt-induced hypertension [105]. Expressional profiles of the embryonic NPS

have also been investigated [4, 106, 107, 108], along with NPS expression profiles of maternal organs and circulation, and placenta [109]. However, there has been very limited work investigating the role of the NPS during postnatal cardiac development. This developmental period is the *ex utero* progression of perinatal cardiac establishment [110], however limited literature even refers to the NPS during neonatal life. Although there exist potential chamber specific expressional patterns during prenatal development [111], the benefits, feasibility, and accuracy of evaluating the postnatal heart as a whole outweighed the benefits of separately analyzing the physical and molecular characteristics of each chamber. The small size of early postnatal hearts would have made gross chamber dissections inefficient and potentially inaccurate, and exclude the possibility of combined cardiac NPS expression.

The premise of the current study is three-fold; the NPS is involved in normal cardiac development [4]; the murine heart undergoes dramatic growth and differentiation during the first weeks of life [98, 112, 113]; and it is unclear when adverse cardiac phenotypes are established in adult ANP gene-disrupted mice [51]. For these reasons, we decided to use the ANP^{-/-} mouse model to better understand the role of the NPS (and specifically ANP) during postnatal cardiac development.

6.2 Results Interpretation

6.2.1 Physical data

Heart weight to body weight ratio (HW/BW) is a strong indicator of cardiac enlargement. The size of the heart increases in proportion to the size of the body, and an enlarged heart can be indicative of dysfunction. HW/BW ratios are conserved among mammalian species, and serves as

a simple but reliable measure of cardiac hypertrophy [114]. This is the first controlled, detailed study documenting HW/BW ratios in ANP^{-/-} mice during the first five weeks of development. The results from this study show that ANP^{-/-} mice have significantly increased HW/BW ratios as compared to ANP^{+/+} mice starting at day 1 and at all subsequent timepoints examined. Accordingly, the early establishment of cardiac enlargement is a permanent phenotype of ANP^{-/-} mice, as increased HW/BW ratios are observed in adult ANP^{-/-} mice, as compared to ANP^{+/+} mice.

Examining the HW/BW ratios in the current study also permits the investigation of the differential cardiac growth rates between timepoints in ANP^{+/+} mice. In addition to demonstrating the progression of normal cardiac enlargement, these comparative growth rates reveal gross physical changes to the heart during the earliest stages of life. Modulatory *post partum* processes which contribute to the transition from prenatal to postnatal to mature cardiac structure are forecasted in the decreasing HW/BW ratios at day 1 ($7.01 \pm 1.07 \text{mg/g}$), 5 weeks after birth ($4.97 \pm 0.46 \text{mg/g}$), and in ANP^{+/+} adult mice ($4.04 \pm 0.30 \text{mg/g}$). Compared to the normal progression of heart growth exhibited by ANP^{+/+} mice, the cardiac growth profile exhibited by ANP^{-/-} mice clearly indicates an altered trajectory. With the exception of a slightly stunted growth in ANP^{-/-} mice at 3 weeks, ANP^{+/+} and ANP^{-/-} mice have very similar body weights throughout postnatal development. Accordingly, HW/BW ratios of ANP^{-/-} mice remain elevated well beyond that of normal cardiac development. Similar body weights between ANP^{+/+} and ANP^{-/-} during postnatal development confirms that greater HW/BW ratios exhibited by ANP^{-/-} are predominantly a direct result of cardiac enlargement and not from altered body growth between the two groups of mice. The slight developmental delay observed at 3 weeks can potentially be attributed to a resource conservation mechanism just before weaning. This time marks an important transition, when neonatal mice switch from a largely liquid diet to a solid diet. This

metabolic progression of food processing may have great implications in the developmental profile of overall body mass.

ANP is known to improve gas exchange and fluid clearance in the lung [94, 115], and fluid homeostasis is known to be a critical process in the development of the lung [93]. In order to quantify gross pathological lung adaptations in ANP^{-/-} mice, compared to ANP^{+/+} mice during development, lungs were collected, weighed, and dehydrated. These values were converted to dry lung weight/wet lung weight and compared among ANP^{+/+} and ANP^{-/-} mice to determine whether the absence of ANP was detrimental to the maturation of the lung. When analyzed, these values revealed no significant differences between genotypes. Although wet lung/dry lung ratios provide interesting growth profiles for normal lung development, these findings did not show any significant changes. However, this finding does not exclude the necessity of ANP in the lung during development, as the measure of dry lung weight/wet lung weight may be ineffective at measuring such physiological differences in ANP^{+/+} and ANP^{-/-} animals. Organ to body weight ratios for lung, liver, and kidney were also measured. However these ratios revealed no differences between ANP^{+/+} and ANP^{-/-} mice. The importance of the NPS in prenatal cardiac development and adult cardiovascular homeostasis warranted the initial investigation of kidney, liver and lung, as these organs are involved in various aspects of cardiovascular-related endocrine control. However, upon the discovery of the drastic heart size differences in ANP^{-/-} mice, and the lack of size differences in the lungs, liver and kidneys, the research effort was narrowed to exclusively focus on the heart.

Similarly, data were analyzed separately, according to gender. There were no significant differences in the weights of either the heart or the body between male and female mice of either genotypes at any postnatal age evaluated. The absence of dramatic trends between genders of the same genotype led to the exclusive use of male tissues for subsequent experimental analysis.

Both ANP^{+/+} and ANP^{-/-} genotypes exhibited similar hematocrit across all age groups with the exception of week 2, when the hematocrit value was significantly decreased in ANP^{-/-} mice. This drop could be pre-emptive of developmental increases in blood pressure, and increased blood pressure demands in the circulation of ANP^{-/-} mice.

6.2.2 Vascular organization and composition

Work previously performed in our laboratory revealed stark differences in the coronary vasculature of adult ANP^{-/-} compared to ANP^{+/+} mice (Tse, Davies & Pang, unpublished data). This finding involved the use of an experimental polymer injection technique. Scanning electron microscopy of the polymer casts demonstrated dramatic increases in vascular density, branching patterns, and overall vessel organization in ANP^{-/-} adult mice.

In normal cardiac vasculature, larger coronary arteries branch into progressively smaller arteries. The natural logic of this progression is two-fold, i) the gradually decreasing diameter of vessels which branch into vessels of similar diameter conserves coronary blood pressure, and ii) as structural properties of vessels of different diameters vary (larger vessels are more resilient, with greater tensile strength), vessels require proper organization in order to protect the smaller vessels from the pressures experienced by the larger vessels [38, 39].

While the regulated, progressively smaller coronary vessels of the ANP^{+/+} animal appear to follow this principle, it is qualitatively evident that such a progression is not present in ANP^{-/-} mice. Instead, some small vessels branch directly off larger vessels. Similarly, coronary vessels of ANP^{+/+} mice are organized in a very ordered network, as the vasculature radiates outward from primary to secondary to tertiary coronary branches. This organization is lost in ANP^{-/-} mice - large and small vessels appear to be clustered into cobweb-like masses.

These findings in the fully differentiated mature adult heart led to the supposition that such changes could actually be a manifestation of pathological adaptations during cardiac development. Although the mature heart is responsive to various stimuli and has the capacity for considerable modification, fundamental differences in coronary vessel architecture point to pathological developmental origin.

Although anatomical research reports considerable variability in cardiac structure, for simplicity these unique qualities are often underrepresented by the typical heart in textbooks [40, 41]. Consequently, an appreciation for the immense variability in the coronary vasculature is lost. While the patterning of the coronary system is predictable, there are dramatic differences in the overall architecture of the coronary vasculature. There is even significant variation in the pathways taken by major vessels [40].

The complex molecular signaling mechanisms involved in the establishment of the coronary circulation [40, 42-44] makes studying this system in the ANP gene-disrupted animal model relevant to the overall understanding of pathological cardiac development in the absence of ANP.

6.2.3 Morphological analysis

Vascular corrosion casting has been shown to be effective in the investigation of normal and abnormal vascular anatomy [116, 117, 118]. Although it was challenging to modify the polymer injection procedure to conserve the delicate cardiovascular structures of postnatal mice, this experimental procedure gave great insight into the overall direction of the current study. Corrosion casting renders accurate 3-dimensional visualization of blood spaces, and depending on the quality of the injected polymer and precision of the catheterization of such delicate vessels, provides important information of small vessel and capillary structures [116]. Light microscopy

images of postnatal coronary casts revealed apparent morphological differences in coronary vasculature between ANP^{+/+} and ANP^{-/-} mice. In the earliest stages of development, ANP^{-/-} mice exhibit irregular branching and coronary vessel patterning as compared to ANP^{+/+} mice.

While the development and patterning of the coronary vascular system is largely unexplored in this mouse model, resulting qualitative analysis revealed an interesting pathological, as well as normal progression of coronary vessel development. After confirming morphological differences in the coronary vasculature between ANP^{+/+} and ANP^{-/-} mice during postnatal development, the experimental focus then shifted to quantifying these differences. Such quantification was not performed in adult tissue, but was a logical experimental progression considering i) the gross physical changes (HW/BW) evident so early in development, ii) the morphological coronary vasculature changes evident so early in development, and iii) the consistent vascular phenotypes in both postnatal and adult ANP^{-/-} mice.

6.2.4 Stereological analysis

In essence, the rationale for using stereological analysis is to interpret a series of two-dimensional images – using a stereological grid, pre-determined counting method, and stereological equation – to convert findings into a three-dimensional quality. This method has been proven, both theoretically and practically, to predict the space (volume) a specified vascular structure occupies [120].

Stereological analysis of vessel volume in ANP^{-/-} compared to ANP^{+/+} mice during postnatal cardiac development revealed stark differences in vessel volume profiles throughout development. Cardiac organogenesis studies have demonstrated that complex circulatory systems are in place before birth [38, 44]. As determined by the developmental progression of vessel volume in ANP^{+/+} mice, these complex circulatory systems continued to develop and expand

throughout postnatal development. This expansion mirrored the expansion of the heart. In addition to vessels, myocyte and “other” (other structures includes fibroblasts, collagen and elastic fibres, histological artifacts, and space) volumes were also quantified using this method. The analysis of myocytes and other volumes revealed no trends or volume profiles of interest, and thus are not further discussed. However, it should be clarified that lack of changes in myocyte volume cannot be interpreted as lack of difference in myocyte organization, cell size or cell number, as total myocyte volume was not differentiated into the above listed characteristics.

Comparing vessel volume differences between ANP^{+/+} and ANP^{-/-} mice at each timepoint gives additional insight into potential mechanisms underlying pathological vascular development. ANP^{-/-} mice exhibit dramatically increased coronary vessel volume at all timepoints evaluated, as compared to age matched ANP^{+/+} mice. Consistent with the morphological analysis, the discussed altered vascular volume in ANP^{-/-} mice as compared to ANP^{+/+} mice implicates ANP as being critical to the normal development of cardiac vasculature.

The early postnatal period is characterized by structural alterations to the heart, as it adapts to adult blood pressure and volume, and left ventricular size. Development of coronary vessels is fundamental to the efficiency of the heart, and such a process represents the complex interaction between various cell types and processes [17, 18, 113]. The observed differences in vessel volume may be attributable to dysregulated myocyte proliferation. Although this study did not conclusively attribute the quantified cardiac hypertrophy to uncontrolled myocyte proliferation, it is likely that this is the case. ANP is well known to inhibit cardiac myocyte proliferation [120, 121], and cell culture studies using neonatal cardiomyocytes demonstrate that ANP has this effect in this population of cells [59]. Uncoordinated myocardial overgrowth likely interferes with the regular patterning and branching of the developing vasculature network [22]. The hyper-vascularity and variation in architectural arrangement of coronary vessels in the

context of myocyte hyper-proliferation has been largely unexplored, however may be of relevance to research surrounding the mechanisms underlying cardiac tissue adaptation.

Interestingly, examination of the differences in fluctuations between developmental profiles of ANP^{+/+} compared to ANP^{-/-} mice reveals a conserved progression. Although ANP^{-/-} mice exhibit increased vessel volume, the overall profile created is maintained. The conserved fluctuations within timepoints may be reflective of postnatal specific developmental stages tightly controlled by hormonal compensation in the absence of ANP.

6.2.5 Molecular Analysis

In order to better understand the molecular events during the pathological cardiac development of ANP^{-/-} mice during postnatal development as demonstrated by gross physical, morphological, and morphometric changes observed thus far, the current study sought to evaluate expressional differences of the NPS in ANP^{-/-} as compared to ANP^{+/+} mice at the timepoints previously described. As outlined, cardiac development begins with the formation and patterning of the primitive heart tube during ontogenesis, and is followed by complex morphological events throughout perinatal development [19, 20]. Although each stage is characterized by distinct patterns of gene expression [11, 12, 17], gene expression analysis should be interpreted as a collection of snapshots of cardiac development rather than a prolonged state of expression.

Admittedly, analysis involving an averaging of gene expression profiles can be misleading; because developmental stages can differ within litters (possibly due to the differences in timing of fertilization), and between litters (varying intrauterine physiology, unequal maternal care) even biological replicates (of the same age and genotype) experience a unique developmental profile. However, the large sample number, accurate tissue harvesting times, and large litter variations have limited inter- and intra-litter variability within each genotype.

Recent advances in biotechnology, and specifically the increased sensitivity of PCR equipment and quality of SYBR green TAQ polymerase, has led to effective and efficient means of determining even minor shifts in NPS expression. Quantitative real-time RT-PCR analysis of mRNA expression of ANP, BNP, NPR-A, NPR-B, and NPR-C in ANP^{+/+} and ANP^{-/-} mice during postnatal cardiac development proved to be beneficial in understanding the normal and pathological expressional profiles in these respective animal groups.

Studies have shown that measurement of ANP mRNA levels mirror the expression of ANP [122]. Correlating this finding to postnatal ages makes it relevant to examine mRNA expression levels, as peptide expression profiles give an accurate representation of true ligand activity.

6.2.5.1 Exclusion of CNP from Analysis

The mRNA expression of CNP, as determined in this study, is at extremely low levels in the neonatal mouse hearts. CNP is expressed in various tissues throughout the body: vascular endothelium, brain, kidney, and female reproductive tract [123, 124]. CNP is also reported to circulate in low concentrations, and accordingly, this can be attributed to its vast distribution, and diverse biological actions. Pertinent to ANP mRNA gene expression, CNP has previously been described to negatively regulate ANP secretion through the NPR-B pathway, and this regulation changes during postnatal development [125]. Although cardiac mRNA expression of CNP was not included in the current study, the interactions CNP has with alternate components of the NPS make it relevant to discuss potential explanations for its low cardiac expression during development.

Although barely detectable, even slight cardiac CNP mRNA expression changes may contribute to the altered physical, morphological and molecular profiles in the hearts of ANP^{-/-}

mice observed throughout postnatal development. Such a conclusion is plausible by virtue of the relational physiological actions of CNP with both ANP and BNP, as well as the expressional control CNP exerts over ANP during postnatal development. Kim *et al.* demonstrated that the inhibitory effect of CNP on atrial ANP secretion varied with age (absent at weeks 2 and 4, but observed at week 8), suggesting that this effect is developmentally regulated [125].

The diverse properties and unique physiologic actions of CNP in various organs throughout the body may also partially explain the low cardiac levels. Logically, CNP expressed by vascular endothelium may be secreted directly into circulation, whereby effects are mediated – and regulated – by the up-and-down regulation of NPR-B, which is differentially expressed in organs throughout the body.

6.2.5.2 Expression of ANP

Perinatal ANP gene expression gives an important reference profile for times of highest cardiac demand [126-128]. Prenatal ANP expression is correlated with times of peak cardiac development [4, 83], and molecular analysis in the current study revealed high ANP expression immediately after birth followed by a drastic reduction. Specifically, ANP mRNA expression is high at day 1, then significantly drops at week 1, subsequently increases back to day 1 levels by week 2, and these levels are sustained throughout the remaining postnatal period. The immediate reduction in ANP mRNA expression at approximately 1 week postnatally has been previously reported, however Wu *et al.* did not examine subsequent developmental times [108], and accordingly, the mechanisms involved in such an intricately regulated process continue to be unresolved. The subsequent re-expression of ANP mRNA after week 1 indicates the importance of ANP in the regulation of cardiac development. This new information, combined with prenatal ANP mRNA expression, reveals that ANP expression is developmentally regulated during normal

perinatal cardiac development. The antihypertrophic effect ANP has on cardiomyocytes is most likely the basis for this differential expression.

Analysis of ANP mRNA gene regulation has provided important insights into the molecular mechanisms underlying cardiac chamber formation and differentiation. It is apparent that the expressional patterns exhibited in the developing and mature heart are relevant to understanding CVD in adults, and more specifically the mechanisms underlying reactivation of embryonic expressional patterns in the diseased adult heart. The postnatal down regulation of ANP mRNA expression is particularly a marker for maturing cardiac myocardium, and represents a transitional time for alternate NPS expressional changes. It is apparent that NPS expression is tightly regulated in response to developmental, hormonal and hemodynamic stimuli, and disruptions in normal physiology can result in varied expression in alternate NPS components [129, 130]. The fact that ANP mRNA expression undergoes such drastic decrease at week 1 indicates a strict developmental change at this timepoint.

6.2.5.3 Expression of BNP

The profile of BNP gene expression has never been described in the hearts of postnatal ANP^{-/-} mice, and has not been comprehensively described in the hearts of postnatal ANP^{+/+} mice. Analysis of BNP mRNA expression revealed significant differences between ANP^{+/+} and ANP^{-/-} mice at all postnatal timepoints examined, with the exception of week 2. This reduction in BNP mRNA expression may be delayed from week 1, consistent with the downregulation of ANP at the week 1 timepoint in ANP^{+/+} mice.

Greatest BNP expression in the hearts of ANP^{+/+} mice is observed at week 1 which coincides with the timepoint where ANP expression is drastically reduced in ANP^{+/+} mice. Although this correlation does not lead to any overt conclusions, examining BNP mRNA

expression in the context of ANP mRNA expression in normal cardiac development reveals potential interplay between – and unique, individual roles of – ANP and BNP during development.

BNP expressional levels were increased throughout postnatal development in ANP^{-/-} mice as compared to ANP^{+/+} mice. Differences were most pronounced at 1 and 3 weeks of age. ANP^{+/+} expressional profile reveals a continuous but gradual increase in BNP expression during normal cardiac development. This increasing trend is not apparent in the ANP^{-/-} mice, however, as expressional levels are increased after day 1, and are sustained during subsequent timepoints.

The compensatory nature of the NPS has been established in alternate NP gene-disrupted animal models, and specifically in adult ANP^{-/-} mice [89]. However the compensatory interactions within the NPS have not previously been described during postnatal development. If BNP were compensating for the absence of ANP it would be logical for its expression to somewhat mirror the expressional patterns of ANP in ANP^{+/+} mice. However examining the overall BNP mRNA expressional profile in ANP^{-/-} mice reveals that BNP was overexpressed at all timepoints, and is seemingly maximally expressed or dysregulated.

The overall reduced expression of BNP mRNA in both genotypes before week 3 may be attributed to the anti-proliferative effects BNP has on fibroblasts. The lack of BNP during this time period would allow for the proliferation and establishment of the resident cardiac fibroblast population. Such a conclusion is well supported in relevant literature [57, 131]. Increases in BNP expression in both genotypes at later timepoints may reflect greater blood pressure demands [98].

6.2.6 Total NP Ligand Effect

Although ANP and BNP share biochemical properties and primarily mediate their effects through the same receptor, they are differentially expressed in various physiological and

pathological conditions; ANP is highly expressed during long term cardiac overload without changes in BNP mRNA expression in adult circulation, whereas BNP is significantly increased in response to short-term volume overload [52, 53, 132]. A similar parallel may be relevant in the understanding of perinatal development; perhaps ANP and BNP are differentially expressed according to long term and short term volume changes.

Of relevance, previous studies have demonstrated that sustained increases in plasma BNP concentrations are correlated with cardiac enlargement, decreased contractility, and increased wall stiffness [64]. While developmental ANP mRNA expression is integral for regulated growth of cardiomyocytes, it is likely that developmental BNP mRNA expression exerts anti-fibrotic effects during ECM establishment. Thus, although BNP expression is seemingly increased to compensate for the lack of ANP in ANP^{-/-} mice during postnatal development, it is apparent from functional NP studies that since these peptides are autonomous in their physiological properties [52, 53]. By virtue of the relationship between molecular signal transduction and physiological responses, such a compensation can never be without consequence. Since the overexpression of BNP mRNA in the hearts of ANP^{-/-} postnatal mice does not exaggerate the ANP mRNA expressional profile in the hearts of ANP^{+/+} mice during this same period, it is apparent that BNP mRNA overexpression is most likely the result of complex interactions between alternate cardiac molecular factors.

The specific stages of cellular proliferation and growth of the heart have been examined in both rats and mice (Figure 19). The progression of cardiomyocyte proliferation to differentiation takes place approximately 1 week after birth, although the myocytes of the left ventricle continue to divide into the second week [12, 13]. This growth difference between left and right ventricular myocytes contributes to the increased weight and myocyte count in left compared to right ventricles, which is characteristic of final adult cardiac structure [12]. By the

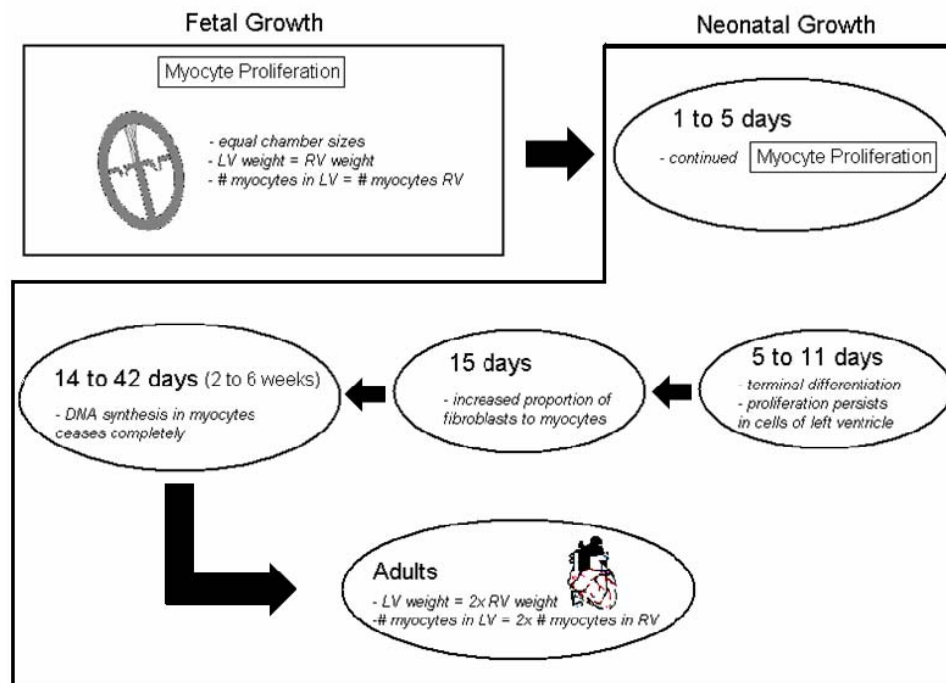


Figure 19. A diagrammatic representation of myocyte proliferation and differentiation during perinatal development. During fetal growth cardiomyocytes (CMCs) undergo extensive proliferation. At this stage all cardiac chambers are of equal size, and composed of similar cell populations. After 1 to 5 days after birth, myocyte proliferation is dramatically reduced. Left ventricular myocytes retain some proliferative capacity in order to gain size in proportion to the right ventricle (to become twice as heavy, with twice as many myocytes in the adult heart). After 15 days, there are dramatic increases in non-CMC cell populations, and previous studies have determined there to be an increased proportion of fibroblasts to myocytes. Between 2 to 6 weeks, it has been documented that DNA synthesis completely subsides in CMCs, in order to be completely differentiated by the time of weaning. This developmental transition of the CMC into a differentiated, non-dividing cell during postnatal development results in cardiac structural and functional properties of the heart structure in adults (increases in size are hypertrophic instead of hyperplastic due to this differentiation).

2nd week after birth, there are proportionally more fibroblasts to myocytes, a proportion that is characteristic of a differentiating myocardium [16]. Although significant hyperplasia ceases after the first week, developing cardiomyocytes retain some proliferative capacity until approximately the time of weaning (3 weeks) [12, 14]. Consistently, an alternate study has demonstrated that DNA synthesis ceases completely between 2 and 6 weeks after birth [15].

These stages of cellular proliferation and growth of the heart correlate well with ANP expression in ANP^{+/+} mice during postnatal development. ANP has been shown to inhibit cultured neonatal cardiomyocyte proliferation through increased apoptosis [60], and ANP/NPR-A signaling cascade has been recognized as an important regulator of cardiac growth of expansion [58]. The current study observed a marked decrease in ANP mRNA expression in ANP^{+/+} mice at the 1 week timepoint; it is possible for the regulator of cardiac hyperplasia to be down-regulated at a developmental stage to allow the heart to undergo rapid expansion. In the ANP^{-/-} mice at the same time point, it is apparent that alternate components of the NPS (BNP, NPR-A, NPR-B) are differentially expressed. These expressional changes, paired with previous knowledge of cardiac expansion at roughly this timepoint all indicate that major cardiac changes are occurring at week 1.

6.2.6.1 Expression of NPR-A

Analysis of receptor levels can also give insight into the molecular mechanisms underlying a physiological response. As previously outlined, the physiological effects of both ANP and BNP are mediated through NPR-A. ANP and BNP both participate in the extravasation of excess intravascular fluid across vascular endothelial cells. Previous studies have correlated NPR-A expression to embryonic endothelial cells, implicating this receptor with such diuretic properties of ANP and BNP [72, 115]. Fluid balance is critical to cardiovascular homeostasis, and

is absolutely crucial to perinatal survival [93]. Intravascular fluid balance changes with differing and increasing solute concentrations, increasing surges in blood pressure, and physiological stimuli (for example, weaning).

During normal cardiac development, NPR-A expressional levels are similar throughout all timepoints. Interestingly, NPR-A receptor expression was reduced in ANP^{-/-} mice between weeks 1 to 4, and these differences reached significance at the 1 week timepoint. This result may be explained by a receptor-ligand feedback mechanism; the expression initially mirrors that of the ANP^{+/+} mouse, however is reduced in the absence of total ligand (ANP) during subsequent timepoints until week 5. Conversely, the significantly decreased NPR-A expression at week 1 may be a reactive compensation to the increased BNP mRNA overexpression also observed at this timepoint.

Whereby NPR-A mRNA expression gradually increased during postnatal cardiac development, fluctuations observed in the overall NPR-A mRNA expression profile in ANP^{-/-} mice throughout development are most likely reflective of underlying homeostatic fluid imbalance immediately after birth, and higher-than-normal blood pressure demands at later timepoints.

6.2.6.2 Expression of NPR-B

Although increases in NPR-B mRNA expression in ANP^{-/-} mice consistently lag behind NPR-B mRNA expression in ANP^{+/+} mice throughout development, both ANP^{+/+} and ANP^{-/-} mice demonstrate an upward trajectory of increasing expression of NPR-B. This trend was interrupted in ANP^{-/-} mice at 1 week, when levels significantly drop at this timepoint exclusively. Such a decrease is consistent with the mRNA expressional decreases in ANP and NPR-A. Again, the interacting nature of the NPS is seemingly responsible for this decrease.

Perhaps similar to NPR-A, the significant decrease in mRNA expression of NPR-B at week 1 may be a reactive compensation to the drastic increase in BNP mRNA expression at this timepoint. Conversely, NPR-B may be decreased due to decreased ligand (ANP, BNP) expression at this timepoint. Although CNP is the primary ligand for NPR-B, ANP and BNP share similarly weak binding affinities for this receptor, potentially underlying its differential gene expression.

NPR-B has been localized to the cell membrane of fetal smooth muscle cells, implicating this receptor in mediating the vasodilatory actions of ligand NPs [72, 86]. Although transient, sustained vasodilation needs can be logically correlated to changes in blood pressure and intravascular volume changes. Accordingly, blood pressure has been shown to increase throughout development [97, 98], which would warrant the need for vasodilation to maintain intravascular blood volume and flow homeostasis, especially at later timepoints.

6.2.6.3 Expression of NPR-C

mRNA expression levels of NPR-C, the receptor responsible for the clearance of peptides from circulation, also pointed to the compensatory nature of the NPS. In normal cardiac development, expression of NPR-C was consistently high until 3 weeks, after which it drops off. This trend was not evident in the ANP^{-/-} mouse; NPR-C expression is significantly decreased at day 1, and this decrease is apparent throughout development.

Similarities between ANP^{+/+} and ANP^{-/-} mice include the reduction of NPR-C mRNA expression after the 3rd week. Examining such overall NPR-C mRNA expression profiles in both ANP^{+/+} and ANP^{-/-} mice, it is apparent that NPR-C populations were gradually established throughout development, whereby negligible changes were made after week 3. This effect can be partially explained by the greater blood pressure demands during later postnatal timepoints, and thus the need for NPs to remain in circulation.

Specifically in ANP^{-/-} mice, levels were reduced immediately at day 1, and remained reduced throughout development. The drastic changes observed after week 3 in ANP^{+/+} mice were not nearly as prominent in the overall expressional profile of ANP^{-/-} mice, which may be indicative of NP conservation throughout development in the absence of ANP.

When this trend is compared with the established plateau of ANP mRNA expression, it seems plausible that this timepoint marks the age when the NPS is primarily established and the neonate has adapted to the *ex utero* hemodynamic load. It is probable that minor adjustments in NP and NPR expression are made to match subsequent demand for BP homeostasis. Examination of NP receptors support the notion that BNP is not the only molecule with the capacity to compensate for the absence of ANP, and that ANP gene-disruption results in vast molecular changes; at week 1 the receptors responsible for mediating the physiological effects of all NPs, NPR-A and NPR-B were both significantly down-regulated.

6.2.7 Total NP Ligand-Receptor Effect

Just as genetically disrupted mouse models have demonstrated that NP mRNA expression is controlled by different factors, the current study proves postnatal cardiac development to be differentially regulated in the absence of ANP. NPR mRNA expression has been previously reported to be up-or-down regulated according to physiological need [122]. NPR internalization/recycling is an intrinsic measure of control over NP actions, thus making it probable for NPR populations to become established during early postnatal development.

General observations of NPR trends in both ANP^{+/+} and ANP^{-/-} mice suggest interesting differences between the expression of each NPR; NPR-A expression appears to be somewhat constitutively expressed throughout development, NPR-B is gradually increased, and NPR-C is gradually decreased. Comparing these differences with the less specific trends of NPs (besides the

drop in ANP expression at week 1 in ANP^{+/+} mice), suggests postnatal ligand control happens at the NPR mRNA expression level instead of the NP mRNA expression level.

6.2.8 Interpretation of Current Results with Overall Implication in the Literature

As demonstrated in the above outlined physical, morphological, morphometric, and molecular analysis, it is clear that the absence of ANP during development leads to cardiac enlargement, and dysregulated vessel organization and volume. By virtue of the intricate organ-level processes involved in prenatal development (cardiac looping, myocardial differentiation, septation, trabeculation, and valve formation) [112, 113] and in postnatal development (regulated growth of the myocardium, continued vasculogenesis, and extracellular matrix deposition) [19] comprising normal cardiac development, the overall perinatal processes of cardiac ontogenesis and maturation involve a complex integration of molecular signals into physiological adaptations. Although there is overlap among these factors, each maintains unique signalling qualities. While such overlap allows for immediate survival, in any case of cardiac gene disruption there is obvious detriment to the final cardiac structure. The pathological severity of a gene-disrupted phenotype can be directly correlated to the position of the gene product within its signalling cascade; if a molecule is a higher order effector it is less likely to share redundant properties with alternate factors, and likewise, if a molecule is a lower order effector it is more likely that alternate molecules can better compensate for its absence.

Because proANP gene disruption does not result in embryonic lethality, it is clear that ANP is not critical for survival. In this model, BNP is able to compensate for some of the functions of ANP. This rationale is supported by examining the outcome of the NPR-A^{-/-} mouse model [87]. NPR-A^{-/-} exhibit reduced survival and a more severe phenotype compared to ANP^{-/-}

mice; NPR-A^{-/-} mice show that even with severely restricted ANP plus BNP actions (NPR-B was shown to be upregulated), at least short term survival is likely. Up-regulation of the NPR-B receptor demonstrates the cross reactivity of the ligands and receptors in this system. Although survival does not depend on the regulated expression of NP during development, the current study outlines how *proANP* gene disruption results in immediate structural changes which likely contribute to the compromised cardiac phenotype observed in adult animals of the same genotype. The role of ANP in the regulation of cardiomyocyte development is linked to proper coronary vasculature development, and similarly proper structural architecture contributed by the extracellular matrix (Figure 20).

The increasing cardiac phenotype severity of *corin*^{-/-}, *ANP*^{-/-}, and *NPR-A*^{-/-} mice, combined with the findings of the current study plausibly point to a strong link between pathological cardiac development and the compromised cardiac structure and function observed in all three mouse models. This gradient is apparent in adult outcomes: *corin*^{-/-} mice demonstrate cardiac hypertrophy, spontaneous hypertension, and mildly declined cardiac dysfunction later in life (which is exacerbated by pregnancy) [133]; *ANP*^{-/-} mice demonstrate cardiac hypertrophy, and salt sensitive and chronic hypertension [51]; and *NPR-A*^{-/-} mice demonstrate hypertension, marked cardiac fibrosis, cardiac hypertrophy, and proves to be lethal in male mice before the age of 6 months [87, 88]. The severity of cardiac hypertrophy, as measured by HW/BW, also mirrored this gradient of phenotype severity; *corin*^{-/-} mice demonstrate a 25% increase in LVW/BW over wildtype littermates [133]; *ANP*^{-/-} mice demonstrate a 40% increase in HW/BW [51]; and *NPR-A*^{-/-} demonstrate between a 33% (females) and an 85% (males) increase in HW/BW over wildtype littermates [87].

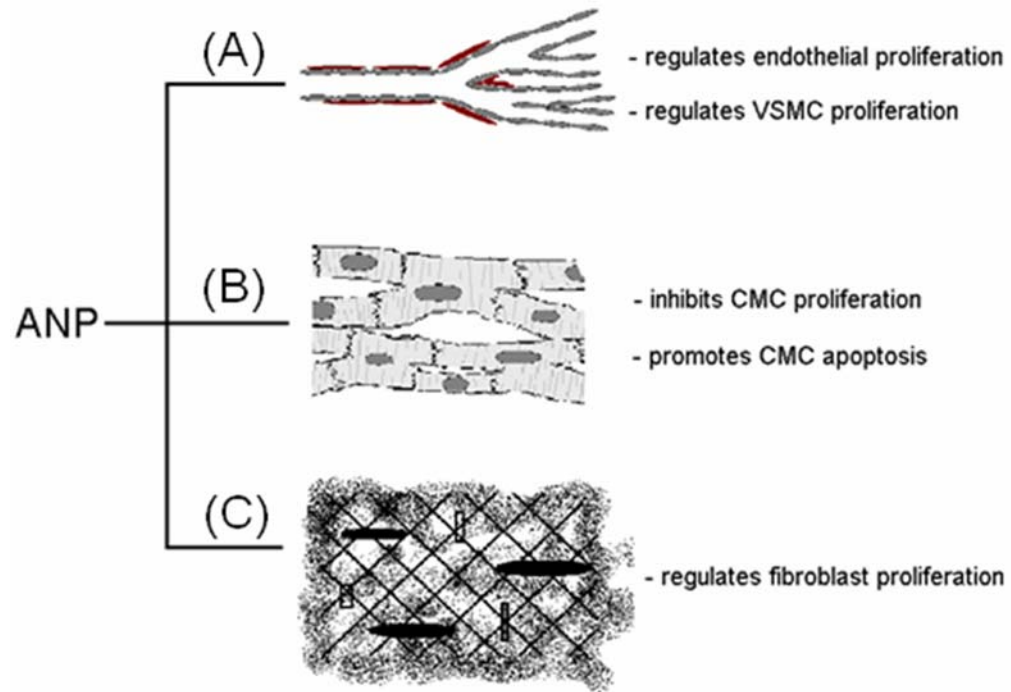


Figure 20. A schematic of the diverse properties of ANP on various components of cardiac development. A) ANP regulates endothelial cell proliferation and vascular smooth muscle cell (VSMC) proliferation which contributes to overall regulation of coronary angiogenesis. B) ANP inhibits cardiomyocyte (CMC) proliferation, and has been shown to promote apoptosis in cultured CMCs. C) ANP has been shown to participate in the regulation of fibroblast proliferation, thus contributing to the regulation of extracellular matrix.

The cardiac hypertrophy observed in NPR-A^{-/-} mice is disproportionately greater than the observed increases in blood pressure. In fact, when blood pressure was therapeutically corrected, NPR-A^{-/-} mice maintained significantly greater cardiac hypertrophy as compared to NPR-A^{+/+} mice [87]. Conclusively, NPR-A mediates an anti-hypertrophic, as well as an anti-hypertensive physiological response. The physical data of the current study reveal drastic cardiac remodelling during early postnatal development, which may be the result of the prolific capacity of cardiomyocytes in the absence of ANP.

It is of relevance to note that all morbidities in NPR-A^{-/-} mice were reported to be of circulatory, and more specifically congenital heart failure. Echocardiographic and hemodynamic data were analyzed to reveal a drastically increased stroke volume and basal stroke work, suggesting severe cardiac cardiomyopathy [87]. Because postnatal cardiac development has not been described in any NP gene-disrupted mouse model, it is possible that the adverse cardiac phenotypes observed in the outlined mouse models are a resultant of pathological perinatal cardiac development. The exacerbated hypertension and hypertrophy, plus cardiac-derived lethality observed in NPR-A^{-/-} mice strongly support this conclusion, as the complete lack of NPs during the growth and modulatory stages of development likely lead to the deleterious cardiac outcomes in adulthood.

Previous studies have also outlined the interactions of ANP with alternate cardiac hormonal systems (Figure 21). Of these, the expression of nitric oxide (NO), or the enzyme responsible for its production, endothelial nitric oxide synthase (eNOS), appears to also be closely linked to the regulation of myocardial development [134, 135, 136]. Studies involving the use of eNOS^{-/-} mice have revealed a likely role of NO in perinatal cardiac development; eNOS^{-/-} mice exhibit septal defects, congenital heart failure, and interestingly, sustained ANP expression at 1 week postnatally [134]. The latter finding suggests a possible inter-regulatory role of ANP

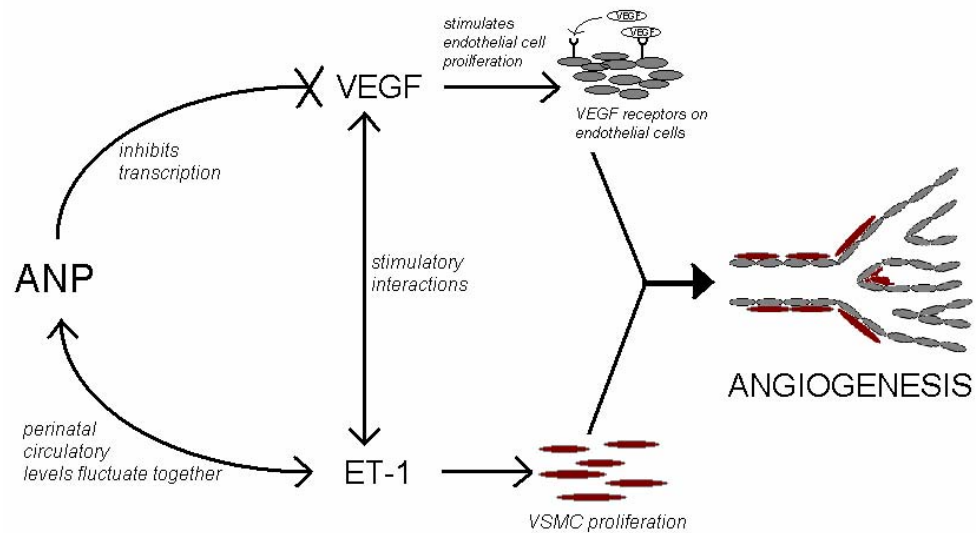


Figure 21. A diagrammatic representation of potential relationship between ANP, vascular endothelial growth factor (VEGF), and endothelin-1 (ET-1) during coronary vasculogenesis. ANP inhibits the transcription of VEGF, which stimulates the proliferation of endothelial cells. The intravascular levels of ANP and ET-1 have been shown to fluctuate together, suggesting co-regulation between ANP and ET-1. ET-1 stimulates vascular smooth muscle cell (VSMC) proliferation. Both VEGF and ET-1 contribute to increased vasculature in the absence of ANP.

over eNOS expression, as well as a compensatory capacity of NO in the absence of ANP. Similar to ANP, NO mediates its intracellular effects through the second messenger, cGMP [135]. Increased intracellular concentrations of cGMP lead to the nuclear accumulation of Akt and zyxin [137].

Nuclear accumulation of Akt and zyxin permit these molecules to interact, leading to altered transcriptional activities, which results in reduced myocyte proliferation [138]. Norepinephrine (NE) causes increased intracellular concentration of cAMP, which leads to reduced cGMP, thus counteracting the physiological effects of ANP. Accordingly, NE has been implicated in the stimulation of myocardial angiogenesis [135].

As such, rapid myocardial growth is accompanied with the expansion of capillary vasculature through various communicatory mechanisms (Figure 22). The increased/disorganized vasculogenesis observed in ANP^{-/-} mice throughout postnatal development can be correlated to the regulatory capacity ANP has over vascular endothelial growth factor (VEGF) [139], and this interactive relationship endothelin-1 (ET-1) [140, 141, 142].

Previous studies have linked VEGF with increased angiogenesis, specifically stimulating the proliferation of endothelial cells [143, 144]. Similarly, previous studies have linked ET-1 with the proliferation of vascular smooth muscle cells (VSMC) [145-147].

As previously outlined, the pathological severity of a gene-disrupted phenotype can be directly correlated to the position of the gene product within its signaling cascade. The promoter regions of ANP and BNP are regulated by a number of GATA factors and diverse transcription factors. The interaction of GATA transcription factors, with co-factor FOG-2, has been shown to be essential for normal coronary system development [44]. Accordingly, previous studies have demonstrated that various GATA factors are critical for embryonic cardiogenesis, and specifically cell migration, cell differentiation and matrix remodeling [142, 148, 149]. These actions are

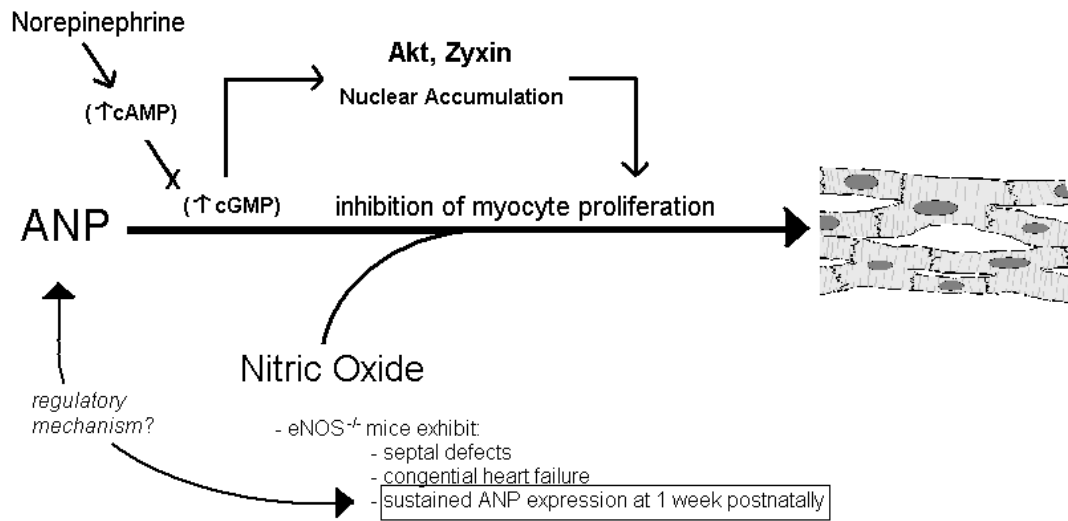


Figure 22. A diagrammatic representation of the potential relationships between ANP and the regulation of myocardial growth. ANP signaling leads to increased intracellular concentrations of cyclic guanosine monophosphate (cGMP), which causes nuclear accumulation of Akt and zyxin. These transcription factors in turn regulate the proliferative capacity of CMCs. Norepinephrine (NE) has been shown to inhibit the accumulation of intracellular cGMP through the accumulation of cAMP. Nitric oxide (NO), the enzymatic product of eNOS (endothelial nitric oxide synthase), has been shown to mediate similar physiological effects as ANP. The investigation of this relationship in eNOS^{-/-} mice during perinatal cardiac development have demonstrated a co-regulatory/stimulatory relationship with ANP.

consistent with the actions of the NPS. A clear understanding of the beginning of the NPS cascade will inevitably shed light on alternate consequences of NPS gene disruption. As such, a dysregulated myocardial growth, paired with abnormal coronary vasculature development, likely bear consequence on the closely linked extracellular matrix support.

The postnatal timeframe is a critical time in the transition of ECM composition and arrangement to that seen in the adult. The NPs have also been shown to have a role in ECM establishment, and overall architecture of coronary collagen [150]. ANP, BNP and CNP have all been shown to suppress cardiac fibroblast proliferation or growth in culture [57, 113]. In particular, BNP and adrenomedullin have been shown to limit extracellular matrix expansion [151-155]. In total, these properties are critical in the regulation of myocardial development, as well as modifications to final adult cardiac architecture in the scenario of cardiac hypertrophy and fibrosis (Figure 23). Overall, these findings and postulations point to the conclusion that a single gene disruption leads to a myriad of altered expressional profiles.

6.3 Relationship to Disease in Human Populations

The current study demonstrates how adverse conditions during early development can manifest into altered cardiac structure. Specifically, the lack of ANP during postnatal development results in cardiac hypertrophy, and abnormal coronary vasculature organization and volume. This work is in support of the notion that independent of blood pressure, gross physical and morphological changes in cardiac mass and composition are preceded by altered genetic profiles of endogenous systems responsible for cardiovascular tissue development and physiological homeostasis. Molecular work revealed that NPR-A, NPR-B paired with ANP and BNP are differentially expressed through normal postnatal cardiac development, suggesting that

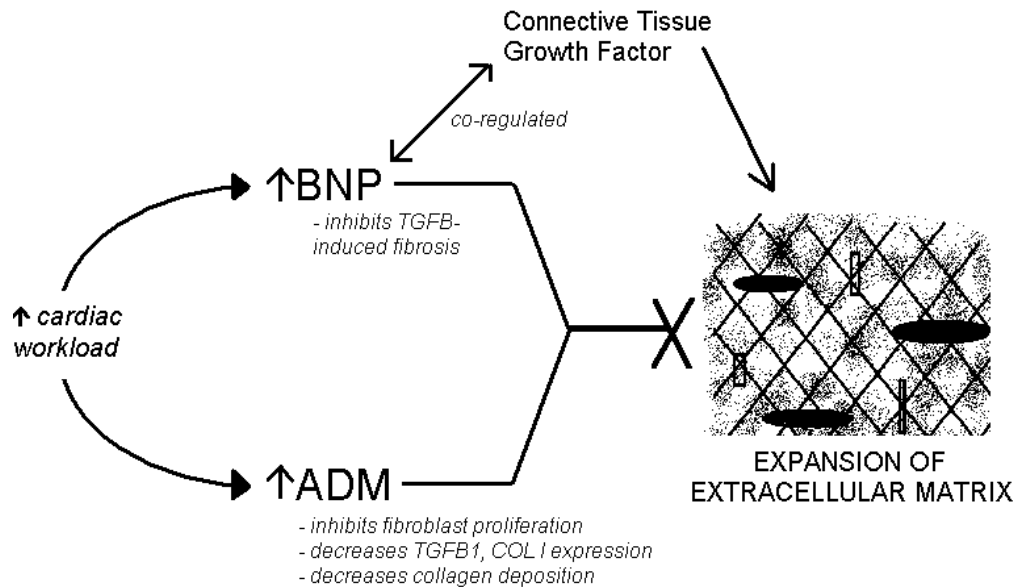


Figure 23. A diagrammatic representation of potential relationship between BNP, adrenomedullin (ADM), and extracellular matrix (ECM) formation. Increased cardiac workload constitutes increased blood pressure, or reduced cardiac efficiency (in the case of structural abnormalities). BNP and ADM have both been shown to be upregulated with such stimuli. BNP is co-regulated with connective tissue growth factor (CTGF), and disruption in the expressional ratio of these two factors results in dysregulated ECM formation. Both BNP and ADM act to inhibit fibroblast proliferation, and regulate expansion capacity of the ECM.

these factors are involved in the critical processes of growth modulation and postnatal blood pressure establishment. Examining the expression of these same hormones/receptors in ANP^{-/-} mice during postnatal cardiac development revealed NPR-B, NPR-C and BNP to be differentially regulated (or dysregulated) in the absence of ANP. The differential expression in ANP^{-/-} mice, plus the high survival rate of ANP^{-/-} offspring suggest the expressional adjustments of NPR-B, NPR-C and BNP. Alternate NPS factors may in fact somewhat compensate for ANP, assuming a shared role in the growth modulation and increasing blood pressure demands in ANP^{-/-} mice.

The NPS has been fully implicated in the modification of cardiac tissue; during development the NPS regulates cardiac development and allows the cardiovascular system to adapt to increasing and changing physiological conditions [83]; in the mature heart, the NPS maintains cardiovascular homeostasis [52, 53]; and in the diseased heart, the NPS is involved in the cardiac remodeling, and consequential adaptive genetic reprogramming [156]. It is inarguable that a complete understanding of the NPS in cardiovascular development, function and disease is critical to advancing the field of CVD prevention, treatment and therapies in human populations. The relationship between the NPS expression and normal neonatal development is also of importance in establishing diagnostic and prognostic therapeutic options in neonatal cardiomyopathies.

Already, it has been established that neonatal heart weight is extremely sensitive to nutritional status, cardiovascular and metabolic abnormalities, as well as adverse intra uterine conditions (for example, maternal diabetes and pre-eclampsia) [157, 158]. Currently, plasma BNP levels are clinically assayed to indicate severity of heart failure symptoms [159], administered (as Nesiritide) to treat heart failure [160], and to gauge the extent of cardiac dysfunction in children with congestive heart failure [161-167]. Thus the actions of the NPS in various physiological and pathological contexts are diverse and complex. However, the vast potential for advances with

NPS in the field of molecular cardiology warrants further investigation into the developmental properties of the NPS.

6.4 Conclusion

The absence of ANP during early postnatal development is evident in gross physical characteristics, coronary vasculature volume and organization, and NPS expressional patterns as compared to postnatal development in ANP^{+/+} mice. Although the small size and vulnerable physiology of the postnatal age cohort limits the use of blood pressure measurement, the physical, morphological, morphometric and molecular observations obtained in the current study have helped create a developmental profile during normal and pathological postnatal cardiac development in ANP^{+/+} and ANP^{-/-} mice, respectively. Such findings implicate the role of ANP during cardiac organogenesis and early development; it is clear that early molecular events have a profound impact on final heart structure and function.

Chapter 7

Future Directions

This thesis outlines some of the mechanisms of cardiac developmental abnormality underlying hypertrophy and salt-sensitive hypertension observed in adult ANP^{-/-} mouse populations. This work investigated morphologic, morphometric, and molecular changes in the developing hearts of ANP^{+/+} and ANP^{-/-} mice during a progression of early postnatal timepoints. The findings demonstrate that ANP plays an important role in early postnatal development, and that the pathological cardiac phenotype observed in mature animals is at least partially established during postnatal cardiac development.

A number of studies contribute the cardiac pathology observed in various heart failure animal models to a physical manifestation of chronic hypertension and other physiological disturbances. The current study revealed cardiac pathology as a result of ANP gene-disruption to be present on the first day of birth – long before blood pressure is thought to increase to mature levels. This thesis has laid a foundation for the role of ANP during early postnatal development, and opens up several avenues for future work in the structural and functional characterization of pathological cardiac development in the absence of ANP.

Of these avenues, it would be fruitful to analyze the expression of alternate factors known to be involved in adult cardiovascular homeostasis – including the renin-angiotensin system (RAS) [168], the adrenomedullin system [154], the nitric oxide system [10], the endothelin system [141], and intracellular molecules such as Akt [169-171] - as the ANP^{-/-} animal model provides unique forum for the investigation of underlying mechanisms of cardiac pathology in the absence of a single critical factor.

Extracellular matrix is composed of proteoglycans, non-proteoglycan polysaccharides, and fibres (mainly collagen), and in the heart provides structural integrity for coronary

vasculature and contracting myocytes [23]. The structural integrity of the ECM is critical for survival, and collagen modification is an indication of changing architecture – whether developmentally or pathologically induced. The pathological disruption of factors involved in ECM homeostasis has been shown to be deleterious to both micro-and-macroscopic structures. The current work outlines how ANP gene-disruption leads to early molecular events during cardiac development which in turn have profound impact on final heart structure. The gross structural changes in cardiac size observed could be attributed to altered ECM formation with the use of histological special staining techniques (to determine differential collagen deposition, arrangement).

Although alternate NPS factors are differentially expressed in the absence of ANP, it is apparent by previous and current work that these factors cannot fully compensate for the normal developmental or physiological actions of ANP. Consequently, it would be beneficial to differentially express ANP; ANP could be reintroduced into circulation in order to confirm the critical role of ANP during development. The subsequent lessening or reversal of the pathological cardiac phenotype would confirm the centrality of ANP in cardiac development. Similarly, the actions of ANP could be blocked in the circulation of prenatal, postnatal, and adult ANP^{+/+} mice.

The comparison of cardiac phenotypes would delineate the role of ANP during these very different developmental stages (organogenesis versus postnatal cardiac modification versus cardiac maturation).

Along a similar line of thought, it would also be interesting to investigate the postnatal cardiac phenotype of ANP transgenic animals; again, the central role of ANP would be confirmed if this overexpression led to an improved cardiovascular outcome compared to ANP^{+/+} animals.

Reduced heart size and hypotension are observed in adult ANP transgenic mice [51], making it plausible that excess ANP production would cause a similar result during postnatal development.

ANP^{+/+} and ANP^{-/-} neonatal mice exhibit drastic differences in vasculogenesis. While the focus of the current study was to document this process, other differences were also observed. Of particular interest were the severe HW/BW differences at all timepoints examined. Although morphometric analysis used to quantify differences in blood vessel volume, no difference in myocyte volume was observed. As outlined in the discussion section, cardiac size difference between ANP^{+/+} and ANP^{-/-} neonatal mice is likely attributable to the anti-proliferative effects of ANP on myocytes. However, it would be very interesting to verify this finding/conclusion through the determination of cell size and number. This analysis could involve the use of electron microscopy with a nucleus counting procedure, or cell/nucleus ratio determination procedure [172, 173].

An additional future direction has been pursued following up on the hyper-vascularization observed in the hearts of ANP^{-/-} mice during early postnatal development, as outlined in the current study. Numerous studies have shown VEGF-A, a signaling molecule in the angiogenic cascade responsible for the recruitment and differentiation of endothelial cells [147], to be upregulated in pathological angiogenic states. Since VEGF-A is such a potent angiogenic factor, it was logical to examine its expression in the hearts of ANP^{-/-} mice during early vascular establishment (Figure 21). Molecular biology techniques used to examine VEGF-A expression were identical to that previously described, however insufficient samples were available from the day 1 age cohort to include in this additional experiment. As anticipated, VEGF-A mRNA expression was shown to be significantly upregulated in the hearts of ANP^{-/-} mice between weeks 2 to 5 (Figure 24). In order to better understand the role of VEGF during the establishment of

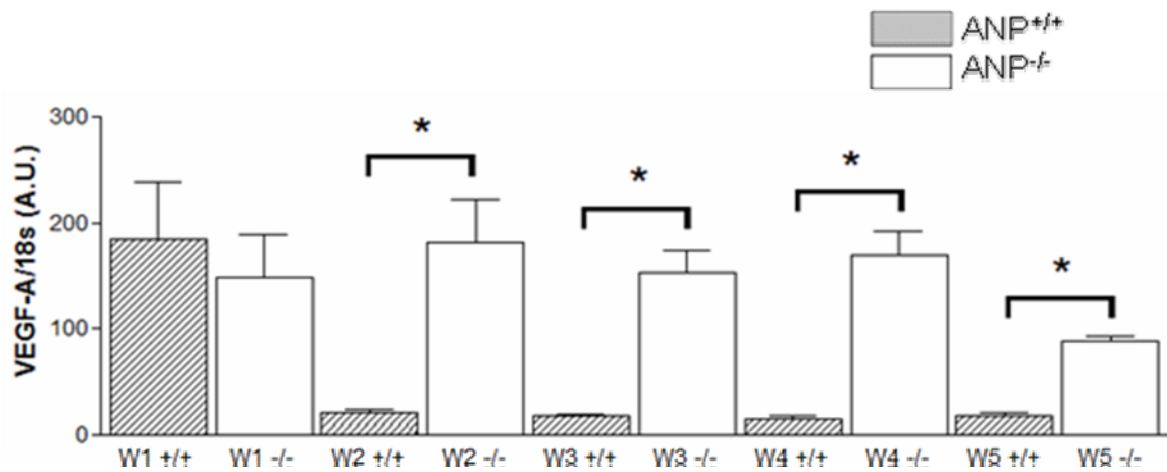


Figure 24. VEGF-A mRNA expression in ANP^{+/+} and ANP^{-/-} postnatal mice at weeks 1 to 5. The vertical axis is the ratio of target gene expression (VEGF-A) to reference gene expression (m18s). Weeks 1 to 5 = w1, w2, w3, w4, and w5. Data are represented as the mean ± S.E.M. * denotes P<0.05 as determined by one way ANOVA followed by Tukey *post hoc* test; n=4-6 per age, per genotype.

coronary vasculature in both normal and pathological cardiac development, it is important to consider this signaling molecule in the context of its receptors and cofactors. Although ANP has been reported to inhibit general VEGF expression, additional work examining alternate types of VEGF (VEGF-B, VEGF-C, VEGF-D, PlGF) and VEGF receptor (VEGFR-1, VEGFR-2, VEGFR-3) [147] expression is required for the eventual elucidation of the definitive relationship of VEGF and ANP during early cardiac coronary angiogenesis.

Bibliography

1. Soukhava-O'hare GK, Ortines RV, Gu Y, Nozdrachev AD, Prabhu SD, and Gozal D. Postnatal intermittent hypoxia and developmental programming of hypertension in spontaneously hypertensive rats: the role of reactive oxygen species and L-Ca²⁺ channels. *Hypertens* 52(1):156-162, 2008.
2. Porrello ER, Bell JR, Schertzer JD, Curl CL, McMullen JR, Mellor KM, Ritchie RH, Lynch GS, Harrap SB, Thomas WG, and Delbridge LM. Heritable pathologic cardiac hypertrophy in adulthood is preceded by neonatal cardiac growth restriction. *Am J Physiol Regul Integr Comp Physiol* 296:672-680, 2009.
3. World Health Organization. (2009, Dec 15). *Cardiovascular disease: prevention and control*. Retrieved from <http://www.who.int/dietphysicalactivity/publications/facts/cvd/en/>
4. Cameron VA, Aitken GD, Ellmers LJ, Kennedy MA, and Espiner EA. The sites of gene expression of atrial, brain, and c-type natriuretic peptide in mouse fetal development: temporal changes in embryos and placenta. *Endocrinol* 137:817-824, 1996.
5. Tu JV, Nardi L, Fang J, Liu J, Khalid L, Johansen H, for the Canadian Cardiovascular Outcomes Research Team. National trends in rates of death and hospital admissions related to acute myocardial infarction, heart failure and stroke, 1994-2004. *CMAJ* 180(13):113-125, 2009.
6. Heart and Stroke Foundation, Health Canada, Statistics Canada, *The Changing Face of Heart Disease and Stroke in Canada 2000*, pages 61-62: "Cost of Cardiovascular Disease", Heart and Stroke Foundation, Ottawa, 1999.

7. **Public Health Agency of Canada. (2009, Dec 15). *Chronic Disease Risk Factors*. Retrieved from http://www.phac-aspc.gc.ca/cd-mc/risk_factors-facteurs_risque-eng.php.**
8. **Hunter JJ, and Chien KR. Signaling pathways for cardiac hypertrophy and failure. *New Eng J Med* 341(17):1276-1283, 1999.**
9. **Rossi MA, and Carrillo SV. Cardiac hypertrophy due to pressure and volume overload: distinctly different biological phenomena? *Int J Cardiol* 2:133:41, 1991.**
10. **Garcia JDA, and Incerpi EK. Factors and mechanisms involved in left ventricular hypertrophy and the anti-hypertrophic role of nitric oxide. *Arq Bras Cardiol* 90(6):443-450, 2008.**
11. **Ahuja P, Sdek P, and Maclellan WR. Cardiac myocyte cell cycle control in development, disease, and regeneration. *Physiol Rev* 87:521-544, 2007.**
12. **Soonpaa MH, Kim KK, Pajak L, Franklin M, and Field LJ. Cardiomyocyte DNA synthesis and binucleation during murine development. *Am J Physiol* 271:2183-2189, 1996.**
13. **Clubb FJ, and Bishop SP. Formation of binucleated myocardial cells in the neonatal rat. An index for growth hypertrophy. *Lab Invest* 50:571-577, 1984.**
14. **Li F, Wang X, Capasso JM, and Gerdes AM. Rapid transition of cardiac myocytes from hyperplasia to hypertrophy during postnatal development. *J Mol Cell Cardiol* 28:1737-1746, 1996.**
15. **Anversa P, Olivetti G, and Loud AV. Morphometric study of early postnatal development in the left and right ventricular myocardium of the rat:**

hypertrophy, hyperplasia, and binucleation of myocytes. *Circ Res* 46(4):495-502, 1980.

16. Banerjee I, Fuseler JW, Price RL, Borg TK, and Baudino TA. Determination of cell types and numbers during cardiac development in the neonatal and adult rat and mouse. *Am J Physiol Heart Circ Physiol* 293:1883-1891, 2007.
17. Chien KR, Knowlton KU, Zhu H, and Chien S. Regulation of cardiac gene expression during myocardial growth and hypertrophy: molecular studies of an adaptive physiologic response. *FASEB J* 5:3037-3046, 1991.
18. Moorman AFM, and Christoffels VM. Cardiac chamber formation: development, genes, and evolution. *Physiol Rev* 83:1223-1267, 2003.
19. Penney DG. Postnatal modification of cardiac development (a review). *J App Cardiol* 5(5):325-337, 1990.
20. Nemer G, and Nemer M. Regulation of heart development and function through combinatorial interactions of transcription factors. *Ann Med* 33:604-610, 2001.
21. Hirschy A, Schatzmann F, Ehler E, and Perriard J-C. Establishment of cardiac cytoarchitecture in the developing mouse heart. *Dev Biol* 289:430-441, 2006.
22. Rumyantsev PP. Interrelations of the proliferation and differentiation processes during cardiac myogenesis and regeneration. *Int Rev Cytol* 51:187-273, 1977.

23. Young B, Lowe J, Stevens A, Heath J, and Deakin P (2000). **Wheater's Functional Histology (Fourth Edition)**. Churchill Livingstone Elsevier, Elsevier LTD, Philadelphia PA.
24. Sanchez-Quintana D, Climent V, Garcia-Martinez V, Rojo M, and Hurle JM. **Spatial arrangement of the heart muscle fascicles and intramyocardial connective tissue in the Spanish fighting bull (*Bos taurus*)**. *J Anat* 184(2): 273-283, 1994.
25. Buckberg G, Hoffman JIE, Mahajan A, Saleh S, and Coghlan C. **Cardiac mechanics revisited: the relationship of cardiac architecture to ventricular function**. *Circ* 118:2571-2587, 2008.
26. Wolf CM, Moskowitz IPG, Arno S, Branco DM, Semsarian C, Bernstein SA, Peterson M, Maida M, Morley GE, Fishman G, Berul CI, Seidman CE, and Seidman JG. **Somatic events modify hypertrophic cardiomyopathy pathology and link hypertrophy to arrhythmia**. *PNAS* 102(50):18123-18128, 2005.
27. Medugorac I, and Jacob R. **Characterization of left ventricular collagen in the rat**. *Cardiovasc Res* 17:15-21, 1983.
28. Weber KT. **Cardiac interstitium in health and disease: the fibrillar collagen network**. *J Am Coll Cardiol* 13:1636-1652, 1989.
29. Mukherjee D, and Sen S. **Collagen phenotypes during development and regression of myocardial hypertrophy in spontaneously hypertensive rats**. *Circ Res* 67:1474-1480, 1990.
30. Schunkert H, Jahn L, Izumo S, Apstein CS, and Lorell BH. **Localization and regulation of c-fos and c-jun protooncogene induction by systolic wall stress**

in normal and hypertrophied rat hearts. *Proc Natl Acad Sci* 88(24):11480-11484, 1991.

31. Bovill E, Westaby S, Reji S, Sayeed R, Crisp A, and Shaw T. Induction by left ventricular overload and left ventricular failure by the human Jumonji gene (JARID2) encoding a protein that regulates transcription and reexpression of a protective fetal program. *J Thoracic Cardiovasc Surg* 136:709-716, 2008.
32. Westerhof N, Boer C, Lamberts RR, and Sipkema P. Cross-talk between cardiac muscle and coronary vasculature. *Physiol Rev* 86:1263-1308, 2006.
33. Boheler KR, Carrier L, Chassagne C, de la Bastie D, Mercadier JJ, and Schwartz K. Regulation of myosin heavy chain and actin isogenes expression during cardiac growth. *Mol Cell Biochem* 104(1-2):101-107, 1991.
34. Chen HW, Yu S-L, Chen W-J, Yang P-C, Chien C-T, Chou H-Y, Li H-N, Peck K, Huang C-H, Lin F-Y, Chen JJW, and Lee Y-T. Dynamic changes of gene expression profiles during postnatal development of the heart in mice. *Heart* 90:927-934, 2004.
35. Gopinath B, Trent R, and Yu B. The unique expression profile of the androgen receptor gene in a rat model of neonatal cardiac hypertrophy. *Pathol* 38(2):142-144, 2006.
36. Schwartz K, Boheler KR, De La Bastie D, Lompre AM, and Mercadier JJ. Switches in cardiac muscle gene overexpression as a result of pressure and volume overload. *Am J Physiol Regul Integr Comp Physiol* 262:364-369, 1992.
37. Vikstrom KL, Bohlmeier T, Factor SM and Leinwand LA. Hypertrophy, pathology, and molecular markers of cardiac pathogenesis. *Circ Res* 82:773-778, 1998.

38. Reese DE, Mikawa T, and Bader DM. Development of the coronary vessel system. *Circ Res* 91:761-768, 2002.
39. Tanaka N, Takazawa K, Takeda K, Aikawa M, Shindo N, Amaya K, Kobori Y, and Tamashina A. Coronary flow-pressure relationship distal to epicardial stenosis. *Circ J* 67:525-529, 2003.
40. Sweeney LJ. A molecular view of cardiogenesis. *Experientia* 44:930-936, 1988.
41. Netter, FH (2006). Atlas of Human Anatomy (Fourth Edition). Saunders Elsevier, Elsevier LTD, Philadelphia, PA.
42. Morabito CJ, Kattan J, and Bristow J. Mechanisms of embryonic coronary artery development. *Curr Opin Cardiol* 17(3):235-241, 2002.
43. Sato TN. Transcriptional regulation of vascular development. *Circ Res* 88:127-128, 2001.
44. Crispino JD, Lodish MB and Thurberg BL. Proper coronary vascular development and heart morphogenesis depend on interaction of GATA-4 with FOG cofactors. *Genes Dev* 15:839-844, 2001.
45. Shiojima I, and Walsh K. Regulation of cardiac growth and coronary angiogenesis by the Akt/PKB signaling pathway. *Genes & Dev* 20:3347-3365, 2006.
46. Coultas L, Chawengsaksophak K, and Rossant J. Endothelial cells and VEGF in vascular development. *Nature* 438:3243-3248, 2007.
47. Riseau W, and Flamme I. *Vasculogenesis*. *Annu Rev Cell Dev Biol* 11: 73-91, 1995.

48. Ruiz-Ortega M, Lorenzo O, and Ruperez M. Role of the renin-angiotensin system in vascular diseases: expanding the field. *Hypertens* 38:1382-1387, 2001.
49. Kisch B. Electron microscopy of the atrium of the heart in guinea pig. *Exp Med Surg* 14:99-112, 1956.
50. de Bold AJ, Borenstein HB, Veress AT, and Sonnenberg H. A rapid and potent natriuretic response to intravenous injection of atrial myocardial extract in rats. *Life Sci* 28:89-94, 1981.
51. John SW, Krege JH, Oliver PM, Hagaman JR, Hodgins JB, Pang SC, Flynn TG, and Smithies O. Genetic decreases in atrial natriuretic peptide and salt-sensitive hypertension. *Science* 267(5198):679-681, 1995.
52. Levin ER, Gardner DG, and Samson WK. Natriuretic peptides. *New Eng J Med* 339(5):321-328, 1998.
53. Rosenzweig A, and Seidman CE. Atrial natriuretic factor and related peptide hormones. *Annu Rev Biochem* 60:229-255, 1991.
54. Cameron VA, and Richards AM. Natriuretic peptide system in fetal heart and circulation. *J Hypertens* 20:801-803, 2002.
55. Flynn TG, de Bold ML, and de Bold AJ. The amino acid sequence of an atrial peptide with potent diuretic and natriuretic properties. *Bioch Biophys Res Comm* 117:859-865, 1983.
56. Yan W, Wu F, Morser J, and Wu Q. Corin, a transmembrane cardiac serine protease, acts as a pro-atrial natriuretic peptide-converting enzyme. *PNAS* 97(15):8525-8529, 2000.

57. Cao L, and Gardner DG. Natriuretic peptides inhibit DNA synthesis in cardiac fibroblasts. *Hypertens* 25: 227-234, 1995.
58. Ellmers LJ, Scott NJA, Piuhola J, Maeda N, Smithies O, Frampton CM, Richards AM, and Cameron VA. Npr1-regulated gene pathways contributing to cardiac hypertrophy and fibrosis. *J Mol Endocrinol* 38(2):245-257, 2007.
59. Horio T, Nishikimi T, Yoshihara F, Matsuo H, Takishita S, and Kangawa K. Inhibitory regulation of hypertrophy by endogenous atrial natriuretic peptide in cultured cardiac myocytes. *Hypertens* 35:19-24, 2000.
60. Wu CF, Bisphopric NH, and Pratt RE. Atrial natriuretic peptide induces apoptosis in neonatal rat cardiac myocytes. *J Biol Chem* 272(23):14860-14866, 1977.
61. Sudoh T, Kangawa K, Minamino N, and Matsuo H. A new natriuretic peptide in porcine brain. *Nature* 332:78-81, 1988.
62. Ogawa Y, Nakao K, Mukoyama M, Shirakami G, Ito H, Hosoda K, Saito Y, Arai H, Suga S, Jougasaki M, Yamada T, Kambayashi Y, Inouye K, and Imura H. Rat brain natriuretic peptide-tissue distribution and molecular form. *Endocrinol* 126:2225-2227, 1990.
63. Kambayashi Y, Nakao K, Mukoyama M, Saito Y, Ogawa Y, Shiono S, Inouye K, Yoshida N, and Imura H. Isolation and sequence determination of human brain natriuretic peptide in human atrium. *FEBS Letters* 259:341-345, 1990.
64. Tamura N, Ogawa Y, Chusho H, Nakamura K, Nakao K, Suda M, Kasahara M, Hashimoto R, Katsuura G, Mukoyama M, Itoh H, Saito Y, Tanaka I, Otani H, Katsuki M, and Nakao K. Cardiac fibrosis in mice lacking brain natriuretic peptide. *PNAS* 97(8):4239-4244, 2000.

65. Sudoh T, Minamino N, Kangawa K, and Matsuo H. C-type natriuretic peptide (CNP): a new member of the natriuretic peptide family identified in porcine brain. *Biochem Biophys Res Comm* 168:863-870, 1990.
66. Nakao K, Ogawa Y, Suga S-i, and Imura H. Molecular biology and biochemistry of the natriuretic peptide system. I: natriuretic peptides. *J Hypertens* 10(9):907-912, 1992.
67. Kobayashi H, Ueno S, Tsutsui M, Okazaki M, Uezono Y, Yanagihara N, Yuhi T, and Izumi F. C-type natriuretic peptide increases cyclic GMP in rat cerebral microvessels in primary culture. *Brain Res* 648(2):324-326, 1994.
68. Chosho H, Tamura N, Ogawa Y, Yasoda A, Suda M, Miyazawa T, Nakamura K, Nakao K, Kurihara T, Komatsu Y, Itoh H, Tanaka K, Saito Y, Katsuki M, and Nakao K. Dwarfism and early death in mice lacking C-type natriuretic peptide. *PNAS* 98(7):4016-4021, 2001.
69. Horio T, Tokudome T, and Maki T. Gene expression, secretion, and autocrine action of C-type natriuretic peptide in cultured adult rat cardiac fibroblasts. *Endocrinol* 144:2279-2284, 2003.
70. Soeki T, Kishimoto I, Okumura H, Tokudome T, Horio T, Mori K, and Kangawa K. C-type natriuretic peptide, a novel antifibrotic and antihypertrophic agent, prevents cardiac remodelling after myocardial infarction. *JACC* 45(4):608-616, 2005.
71. Schweitz H, Vigne P, Moinier D, Frelin C, and Lazdunski M. A new member of the natriuretic peptide family is present in the venom of the Green Mamba (*Dendroaspis angusticeps*)*. *J Biol Chem* 267(20):13928-13932, 1992.
72. Hirose S, Hagiwara H, and Takei Y. Comparative molecular biology of natriuretic peptide receptors. *Can J Physiol Pharmacol* 79:665-672, 2001.

73. Chang MS, Lowe DG, Lewis M, Hellmiss R, Chen E, and Goeddel DV. Differential activation by atrial and brain natriuretic peptides of two different receptor guanylate cyclases. *Nature* 341:68-72, 1989.
74. Waldman SA, Rapoport RM, and Murad F. Atrial natriuretic factor selectively activates particulate guanylate cyclase and elevates cyclic GMP in rat tissues. *J Biol Chem* 259:14332-14334, 1984.
75. Kuno T, Andresen JW, Kamisaki Y, Waldman SA, Chang LY, Saheki S, Leitman DC, Nakane M, and Murad F. Co-purification of an atrial natriuretic factor receptor and particulate guanylate cyclase from rat lung. *J Biol Chem* 261:5817-5823, 1986.
76. Maack T, Suzuki M, Almeida FA, Nussenzveig D, Scarborough RM, McEnroe GA, and Lewicki JA. Physiological role of silent receptors of atrial natriuretic factor. *Science* 238:675-678, 1987.
77. Suga S, Nakao K, Hosoda K, Mukoyama M, Ogawa Y, Shirakami G, Arai H, Saito Y, Kambayashi Y, and Inouye K. Receptor selectivity of natriuretic peptide family, atrial natriuretic peptide, brain natriuretic peptide, and C-type natriuretic peptide. *Endocrinol* 130:229-239, 1992.
78. Fuller F, Porter JG, Arfsten AE, Miller J, Schilling JW, Scarborough RM, Lewicki JA, and Schenk DB. Atrial natriuretic peptide clearance receptor. Complete sequence and functional expression of cDNA clones. *J Biol Chem* 263:9395-9401, 1988.
79. Porter JG, Arfsten A, Fuller F, Miller JA, Gregory LC, and Lewicki JA. Isolation and functional expression of the human atrial natriuretic peptide clearance receptor cDNA. *Bioch Biophys Res Comm* 171:796-803, 1990.

80. Charles CJ, Espiner EA, Nicholls MG, Richards AM, Yandle TG, Protter A, and Kosoglou T. Clearance receptors and endopeptidase 24.11: equal role in natriuretic peptide metabolism in conscious sheep. *Am J Physiol Regul Integr Comp Physiol* 271:R373-R380, 1996.
81. Nishikimi T, Maeda N, and Matsuoka H. The role of natriuretic peptides in cardioprotection. *Cardiovasc Res* 69:318-328, 2006.
82. Gardner DG, Chen S, Glenn DJ, and Grigsby CL. Molecular biology of the natriuretic peptide system: Implications for physiology and hypertension. *Hypertens* 49:419-426, 2007.
83. Cameron VA, and Ellmers LJ. Minireview: natriuretic peptides during development of the fetal heart and circulation. *Endocrinol* 144(6):2191-2194, 2003.
84. Houweling AC, van Borren MM, Moorman AFM, and Christoffels VM. Expression and regulation of the atrial natriuretic factor encoding gene *Nppa* during development and disease. *Cardiovasc Res* 67:583-593, 2005.
85. Izumi T, Saito Y, Kishimoto I, Harada M, Kuwahara K, Hamanaka I, Takahashi N, Kawakami R, Li Y, Takemura G, Fujiwara H, Garbers DL, Mochizuki S, and Nakao K. Blockade of the natriuretic peptide receptor guanylyl cyclase-A inhibits NF- κ B activation and alleviates myocardial ischemia/reperfusion injury. *J Clin Invest* 108:203-213, 2001.
86. Pagel-Langenickel I, Buttgerit J, Bader M, and Langenickel TH. Natriuretic peptide receptor B signaling in the cardiovascular system: protection from cardiac hypertrophy. *J Mol Med* 85(8):797-810, 2007.
87. Oliver PM, Fox JE, Kim R, Rockman HA, Kim H-S, Reddick RL, Pandey KN, Milgram SL, Smithies O, and Maeda N. Hypertension, cardiac

- hypertrophy, and sudden death in mice lacking natriuretic peptide receptor A. *Proc Natl Acad Sci* 94:14730-14735, 1997.
88. Ellmers LJ, Knowles JW, Kim H-S, Smithies O, Maeda N, and Cameron VA. Ventricular expression of natriuretic peptides in Npr1^{-/-} mice with cardiac hypertrophy and fibrosis. *Am J Physiol Heart Circ Physiol* 283:707-714, 2002.
89. Tse MY, Watson JD, Sarda IR, Flynn TG, and Pang SC. Expression of B-type natriuretic peptide in atrial natriuretic peptide gene disrupted mice. *Mol Cell Biochem* 219:99-105, 2001.
90. Matsukawa N, Wojciech JG, Takahashi N, Pandey KN, Pang SC, Yamauchi M, and Smithies O. The natriuretic peptide clearance receptor locally modulates the physiological effects of the natriuretic peptide system. *PNAS* 96(13):7403-7408.
91. Walther T, Schultheiss HP, Tschöpe C, and Stepan H. Natriuretic peptide system in fetal heart and circulation. *J Hypertens* 20:785-791, 2002.
92. Vesely DL. Atrial natriuretic peptides in pathophysiological diseases. *Cardiovasc Res* 51:647-658, 2001.
93. Guan J, Mao C, Feng X, Zhang H, Xu F, Geng C, Zhu L, Wang A, and Xu Z. Fetal development of regulatory mechanisms for body fluid homeostasis. *Brazil J Med Biol Res* 41:446-454, 2008.
94. Tulassay T, and Rascher W. Role of atrial natriuretic peptide in sodium homeostasis of premature infants. *J Ped* 109(6):1023-1027, 1986.
95. Kurtz TW, Griffin KA, Bidani AK, Davisson RL, and Hall JE. Recommendations for blood pressure measurement in humans and experimental animals. *Hypertens* 45:299, 2005.

96. Brown ET, Umino Y, Loi T, Solessio E, and Barlow R. Anesthesia can cause sustained hyperglycemia in C57/BL6J mice. *Vis Neurosci* 22(5):615-618, 2005.
97. Tiemann K, Weyer D, Djoufack PC, Ghanem A, Lewalter T, Dreiner U, Meyer R, Grohe C, and Fink KB. Increasing myocardial contraction and blood pressure in C57BL/6 mice during early postnatal development. *Am J Physiol Heart Circ Physiol* 284:464-474, 2003.
98. Clubb FJ, Bell PD, Kriseman JD, and Bishop SP. Myocardial cell growth and blood pressure development in neonatal spontaneously hypertensive rats. *Lab Invest* 56:189-197, 1987.
99. Towbin JA, and Lipshultz SE. Genetics of neonatal cardiomyopathy. *Curr Opin Cardiol* 14(3):250, 1999.
100. Roberts P, and Burch M. Cardiomyopathy in childhood. *Peds & Child Health* 19(1):15-24, 2009.
101. Rich MW. Epidemiology, Pathophysiology, and etiology of congestive heart failure in older adults. *J Am Geriatr Soc* 45(8):968-974, 1997.
102. Liu Y, Leri A, Li B, Wang X, Cheng W, Kajstura J, and Anversa P. Angiotensin II stimulation in vitro induces hypertrophy of normal and postinfarcted ventricular myocytes. *Circ Res* 82:1145-1159, 1998.
103. Ruck A, Gustafsson T, Norrbom J, Nowak J, Kallner G, Soderberg M, Sylven C, and Drvota V. ANP and BNP but not VEGF are regionally overexpressed in ischemic human myocardium. *Biochem Biophys Res Comm* 322:287-291, 2004.

104. Gama EF, Liberti EA, and de Souza RR. Effects of pre- and postnatal protein deprivation on atrial natriuretic peptide- (ANP-) granules of the right auricular cardiocytes; an ultrastructural study. *Eur J Nutri* 46(5):245-250, 2007.
105. Melo LG, Veress AT, Chong CK, Pang SC, Flynn TG, and Sonnenberg H. Salt-sensitive hypertension in ANP knockout mice: potential role of abnormal plasma renin activity. *AJP Reg Integ Comp Physiol* 274(1):255-261, 1998.
106. Argentin S, Ardati A, Tremblay S, Lihrmann I, Robitaille L, Drouin J, and Nemer M. Developmental stage-specific regulation of atrial natriuretic factor gene transcription in cardiac cells. *Mol Cell Biol* 14(1):777-790, 1994.
107. Zeller R, Bloch KD, Williams BS, Arceci RJ, and Seidman CE. Localized expression of the atrial natriuretic factor gene during cardiac embryogenesis. *Genes Dev* 1: 693-698, 1987.
108. Wu JP, Deschepper CF, and Gardner DG. Perinatal expression of the atrial natriuretic factor gene in rat cardiac tissue. *Am J Physiol Endocrinol Metab* 255:E388-E396, 1988.
109. Minegishi T, Nakamura M, Abe K, Tano M, Andoh A, Yoshida M, Takagi T, Niskikimi T, Kojima M, and Kangawa K. Adrenomedullin and atrial natriuretic peptide concentrations in normal pregnancy and pre-eclampsia. *Mol Human Reprod* 5(8):767-770, 1999.
110. Smith FG, Sato T, Varille VA, and Robillard JE. Atrial natriuretic peptide during fetal and postnatal life: a review. *J Dev Physiol* 12(2):55-62, 1989.
111. Kuroski de Bold ML. Atrial natriuretic factor and brain natriuretic peptide gene expression in the spontaneous hypertensive rat during postnatal development. *Am J Hypertens* 11:1006-1018, 1998.

112. Christoffels VM, Habets PE, Franco D, Campione M, de Jong F, Lamers WH, Bao ZZ, Palmer S, Biben C, Harvey RP, and Moorman AF. Chamber formation and morphogenesis in the developing mammalian heart. *Dev Biol* 223:226-278, 2000.
113. Leu M, Ehler E, Perriard JC. Characterisation of postnatal growth of the murine heart. *Anat Embryol* 204:217-224, 2001.
114. Joseph DR. The ratio between the heart-weight and body-weight in various animals. *J Exp Med* 10(4):521-528, 1908.
115. Sabrane K, Kruse MN, Fabritz L, Zetsche B, Mitko D, Skryabin BV, Zweiner M, Baba HA, Yanagisawa M, and Kuhn M. Vascular endothelium is critically involved in the hypotensive and hypovolemic actions of atrial natriuretic peptide. *J Clin Invest* 115:1666-1674, 2005.
116. Yong T, Nyengaard JR, Baandrup U, and Gundersen HJG. A stereological study of capillaries, fibers and nuclei in left ventricles of normal and hypertrophic human autopsy hearts. In: Abstracts of the 9th International Congress for Stereology, August 20-25, 1996, Copenhagen. Stougaard Jensen/Scantryk (ISBN 87-984765-1-3). p.162
117. Stoker ME, Gerdes AM, and May JF. Regional differences in capillary density and myocyte size in the normal human heart. *Anat Rec* 202:187-191, 1982.
118. Kalinsnik M, Porenta OV, and Mattfeldt T. Stereological and morphometric studies of mammalian myocardium: a review. *Acta Stereol* 17:389-401, 1998.
119. Pang SC, and Scott TM. Stereological analysis of the tunica media of the aorta and renal artery during the development of hypertension in the spontaneously hypertensive rat. *J Anat* 133(4):513-526, 1981.

120. Silberbach M, Gorenc T, Hershberger RE, Stork PJS, Steyger PS, and Roberts CT. Extracellular signal-regulated protein kinase activation is required for the anti-hypertrophic effect of atrial natriuretic factor in neonatal rat ventricular myocytes. *J Biol Chem* 274(35):24858-24864, 1999.
121. Kishimoto I, Rossi K, and Garbers DL. A genetic model provides evidence that the receptor for atrial natriuretic peptide (guanylyl cyclase-A) inhibits cardiac ventricular myocyte hypertrophy. *PNAS* 98:2703-2706, 2001.
122. Vera N, Tse MY, Watson JD, Sarda S, Steinhilber ME, John SWM, Flynn TG, and Pang SC. Altered expression of natriuretic peptide receptors in proANP gene disrupted mice. *Cardiovasc Res* 46(3):595-603, 2000.
123. Stepan H, Leitner E, Bader M, and Walther T. Organ-specific mRNA distribution of C-type natriuretic peptide in neonatal and adult mice. *Regul Pept* 95:81-85, 2000.
124. Walther T, and Stepan H. C-type natriuretic peptide in reproduction, pregnancy and fetal development. *J Endocrinol* 180:17-20, 2004.
125. Kim SH, Han JH, Cao C, Kim SZ, and Cho KW. Postnatal changes in inhibitory effect of C-type natriuretic peptide on secretion of ANP. *Am J Physiol Regul Integr Comp Physiol* 282:1672-1679, 2002.
126. Navaratnam V, Woodward JM, and Skepper JN. Specific heart granules and natriuretic peptide in the developing myocardium of fetal and neonatal rats and hamsters. *J Anat* 163:261-273, 1989.
127. Toshimori H, Toshimori K, Oura C, and Matsuo H. Immunohistochemical study of atrial natriuretic polypeptides in the embryonic, fetal and neonatal rat heart. *Cell Tissue Res* 248:627-633, 1987.

128. Claycomb WC. Atrial-natriuretic-factor mRNA is developmentally regulated in heart ventricles and actively expressed in cultured ventricular cardiac muscle cells of rat and human. *Biochem J* 255:617-620, 1988.
129. Tamura N, Ogawa Y, Yasoda A, Itoh H, Saito Y, and Nakao K. Two cardiac natriuretic peptide genes (atrial natriuretic peptide and brain natriuretic peptide) are organized in tandem in the mouse and human genomes. *J Mol Cell Cardiol* 28(8):1811-1815, 1996.
130. Knowlton KU, Rockman HA, Itani M, Vovan A, Seidman CE, and Chien KR. Divergent pathways mediate the induction of ANF transgenes in neonatal and hypertrophic ventricular myocardium. *J Clin Invest* 96:1311-1318, 1995.
131. Kapoun AM, Liang F, O'Young G, Damm DL, Quon D, White RT, Munson K, Lam A, Schreiner GF, and Potter AA. B-type natriuretic peptide exerts broad functional opposition to transforming growth factor- β in primary human cardiac fibroblasts. *Circ Res* 94:453-461, 2004.
132. McGrath MN, and de Bold AJ. Determinants of natriuretic peptide gene expression. *Peptides* 26(6):933-943, 2005.
133. Chan JC, Knudson O, Wu F, Morser J, Dole WP, and Wu Q. Hypertension in mice lacking the proatrial natriuretic peptide convertase corin. *PNAS* 102:785-790, 2005.
134. Lepic E, Burger D, Lu X, Song W, and Feng Q. Lack of endothelial nitric oxide synthase decreases cardiomyocyte proliferation and delays cardiac maturation. *Am J Physiol Cell Physiol* 291:1240-1246, 2006.

135. Weil J, Benndorf R, Fredersdorf S, Griese DP, and Eschenhagen T. Norepinephrine upregulates vascular endothelial growth factor in rat cardiac myocytes by a paracrine mechanism. *Angiogenesis* 6:303-309, 2003.
136. Abdelaziz N, Colombo F, Mercier I, and Calderone A. Nitric oxide attenuates expression of transforming growth factor- β 3. *Hypertens* 38(2):261-266.
137. Kato T, Muraski J, Chen Y, Tsujita Y, Wall J, Gelmbotski CC, Schaefer E, Beckerle M, and Sussman MA. Atrial natriuretic peptide promotes cardiomyocyte survival by cGMP-dependent nuclear accumulation of zyxin and Akt. *J Clin Invest* 115(10):2716-2730, 2005.
138. DeBosch B, Treskov I, Lupa TS, Weinheimer C, Kovacs A, Courtois M, and Muslin AJ. Akt1 is required for physiological cardiac growth. *Circ* 113:2097-2104, 2006.
139. Pedram A, Razandi M, and Levin ER. Natriuretic peptides suppress vascular endothelial cell growth factor signalling to angiogenesis. *Endocrinol* 142(4):1578-1586, 2001.
140. Kojima T, Isozaki-Fukuda Y, Takedatsu M, Hirata Y, and Kobayashi Y. Circulating levels of endothelin and atrial natriuretic factor during postnatal development. *Acta Paediatr* 81:676-677, 1992.
141. Matsuura A, Yamochi W, Hirata K, Kawashima S, and Yokoyama M. Stimulatory interaction between vascular endothelial growth factor and endothelin-1 on each gene expression. *Hypertens* 32:89-95, 1998.
142. Glenn DJ, Rahmutula D, Nishimoto M, Liang F, and Gardner DG. Atrial natriuretic peptide suppresses endothelin gene expression and proliferation in cardiac fibroblasts through a GATA4-dependent mechanism. *Cardiovasc Res* 84(2):209-217, 2009.

143. Bernatchez PN, Soker S, and Sirois MG. Vascular endothelial growth factor effect on endothelial cell proliferation, migration, and platelet-activating factor synthesis is flk-1-dependent. *J Biol Chem* 274:31047-31054, 1999.
144. Pedram A, Razandi M, and Levin ER. Deciphering vascular endothelial growth factor/vascular permeability factor signalling to vascular permeability: inhibition by atrial natriuretic peptide. *J Biol Chem* 277(46):44385-44398, 2002.
145. Pedram A, Razandi M, Hu R-M, and Levin ER. Vasoactive peptides modulate vascular endothelial cell growth factor production and endothelial cell proliferation and invasion. *J Biol Chem* 272(27):17097-17103, 1997.
146. Ferrara N, and Davis-Smyth T. The biology of vascular endothelial growth factor. *Endo Rev* 18(1):4-25, 1997.
147. McBride K, and Nemer M. Regulation of the ANF and BNP promoters by GATA factors: lessons learned for cardiac transcription. *Can J Physiol Pharmacol* 79:673-681, 2001.
148. Jankowski M. GATA4, a new regulator of cardiac fibroblasts, is sensitive to natriuretic peptides. *Cardiovasc Res* 84(2):176-177, 2009.
149. D'Souza SP, Davis M, and Baxter GF. Autocrine and paracrine actions of natriuretic peptides in the heart. *J Pharm Thera* 101:113-129, 2004.
150. Niu P, Shindo T, Iwata H, Ebihara A, Suematsu Y, Zhang Y, Takeda N, Iimuro S, Hirata Y, and Nagai R. Accelerated cardiac hypertrophy and renal damage induced by angiotensin II in adrenomedullin knockout mice. *Hypertens Res* 26(9):731-736, 2009

151. Montuenga LM, Mariano JM, Prentice MA, Cuttitta F, and Jakowlew SB. Coordinate expression of TGF- β 1 and adrenomedullin in rodent embryogenesis. *Endocrinol* 139(9):3947-3957, 1998.
152. Shimokubo T, Sakata J, Kitamura K, Kangawa K, Matsuo H, and Eto T. Adrenomedullin: changes in circulating and cardiac tissue concentration in DAHL salt-sensitive rats on a high-salt diet. *Clin and Exper Hypertens* 18(7):949-961, 1996.
153. Tsuruda T, Kato J, Hatakeyama K, Masuyama H, Cao Y-N, Imamura T, Kitamura K, Asada Y, and Eto T. Antifibrotic effect of adrenomedullin on coronary adventitia in angiotensin II-induced hypertensive rats. *Cardiovasc Res* 65:921-929, 2005.
154. Tsuruda T, Kato J, Kitamura K, Kawamoto M, Kuwasako K, Imamura T, Koiwaya Y, Tsuji T, Kangawa K, and Eto T. An autocrine or a paracrine role of adrenomedullin in modulating cardiac fibroblast growth. *Cardiovasc Res*: 43(4): 958-967, 1999.
155. Horsthuis T, Houweling AC, Habets PEMH, de Lange FJ, el Azzouzi H, Clout DEW, Moorman AFM, and Christoffels VM. Distinct regulation of developmental and heart disease induced atrial natriuretic factor expression by two separate distal sequences. *Circ Res* 102:849-859, 2008.
156. Siu SC, Colman JM, Sorensen S, Smallhorn JF, Farine D, Amankwah KF, Spears JC, and Sermer M. Adverse neonatal and cardiac outcomes are more common in pregnant women with cardiac disease. *Circ* 105:2179-2184, 2002.
157. Gopinath B, Trent RJ, and Yu B. Molecular characterization of neonatal cardiac hypertrophy and its regression. *Cardiol Young* 14(15): 498-505, 2004.

158. Doust JA, Pietrzak E, Dobson A, and Glasziou P. How well does B-type natriuretic peptide predict death and cardiac events in patients with heart failure: a systematic review. *BMJ* 330:625-634, 2005.
159. Cataliotti A, Chen HH, Redfield MM, and Burnett JC. Natriuretic peptides as regulators of myocardial structure and function: pathophysiologic and therapeutic implications. *Heart Failure Clin* 2:269-276, 2006.
160. Holmstrom H, Hall C, and Thaulow W. Plasma levels of natriuretic peptides and hemodynamic assessment of patent ductus arteriosus in preterm infants. *Acta Paediatr* 90:194-189, 2001.
161. Choi BM, Lee KH, Eun BL, Yoo KH, Hong YS, and Son CS. Utility of rapid B-type natriuretic peptide assay for diagnosis of symptomatic patent ductus arteriosis in preterm infants. *Peds* 115:255-261, 2005.
162. Puddy VF, Amirmansour C, Willams AF, and Singer DRJ. Plasma brain-type natriuretic peptide as predictor of haemodynamically significant patent ductus areteriosus in preterm infants. *Clin Sci* 103:75-77, 2006.
163. Koch A, and Singer H. Normal values of B type natriuretic peptide in infants, children, and adolescents. *Heart* 89:875-878, 2003.
164. Reynolds EW, Ellington JG, Vranicar M, and Bada HS. Brain-type natriuretic peptide in the diagnosis and management of persistent pulmonary hypertension of the newborn. *Peds* 114:1297-1304, 2004.
165. de lab Graca RL, Hassinger DC, Flynn PA, Sison CP, Nesin M, and Auld PA. Longitudinal changes of brain-type natriuretic peptide in preterm neonates. *Peds* 117:2183-2189, 2006.

166. Mannarino S, Ciardelli L, Garofoli F, Perotti G, Mongini E, Damiano S, Tinelli C, Cerbo RM, Rondini G, and Stronati M. Correlations between cord blood, perinatal BNP values and echocardiographic parameters in healthy Italian newborns. *Early Hum Dev* 85(1):13-17, 2009.
167. Bouzegrhane F, and Thibault G. Is angiotensin II a proliferative factor of cardiac fibroblasts? *Cardiovasc Res* 53(2):304-312, 2002.
168. Tsujita Y, Muraski J, Shiraishi I, Kato T, Kajstura J, Anversa P, and Sussman MA. Nuclear targeting of Akt antagonizes aspects of cardiomyocyte hypertrophy. *PNAS* 103(32):11946-11951, 2006.
169. Catalucci D, and Condorelli G. Effects of Akt on cardiac myocytes; location counts. *Circ Res* 99:339-341, 2006.
170. DeBosch B, Treskov I, Lupu T, Weinheimer C, Kovacs A, Courtois M, and Muslin A. Akt1 is required for physiological cardiac growth. *Circ* 113:2097-2104, 2006.
171. Miquerol L, Langille GL, and Nagy A. Embryonic development is disrupted by modest increases in vascular endothelial growth factor gene expression. *Dev* 127: 3941-3946, 2000.
172. Austin A, Fagan DG, and Mayhew TM. A stereological method for estimating the total number of myocyte nuclei in fetal and postnatal hearts. *J Anat* 187:641-647, 1995.
173. Amann K, Wiest G, Zimmer G, Gretz N, Ritz E, and Mall G. Reduced capillary density in the myocardium of uremic rats – A stereological study. *Kidney Int* 42:1079–1085, 1992.

174. Weibel, E. and Gomez J. A principle for counting tissue structures on random sections. *J Appl Physiol* 17:343-348, 1962.

Appendix A

High Pure RNA Isolation

Table A.1. High Pure RNA Isolation Kit (Roche, Montreal QU) buffer recipes.

Lysis Binding Buffer pH 6.6	4.5M guanidine-HCl 50mM Tris-HCl 30% Triton X-100 (w/v)
DNase I	10 KU lyophilized Dnase I Resuspended in 0.55ml Elution Buffer
DNase Incubation Buffer pH 7.0	1M NaCl 20mM Tris-HCl 10mM MnCl ₂
Wash Buffer I pH 6.6	5M guanidine hydrochloride 20mM Tris-HCl
Wash Buffer II pH 7.5 made up to 10mL added to 40mL ethanol	20mM NaCl 2mM Tris-HCl
Elution Buffer	nuclease-free, sterile double distilled water

Appendix B

Gene Expression Analysis using LightCycler 480[®] real-time RT-PCR

General Background

Real-time RT-PCR allows cDNA gene products to be amplified and simultaneously quantified. Genes of interest were amplified using gene-specific primers, and the fluorescent mix containing the detection molecule SYBR Green I. The greater the number of gene copies, the sooner the reaction product will fluoresce. The crossing point is the measure of early expression, and is the fractional cycle number at which the fluorescence exceeds background fluorescence level (automatically collected by the LightCycler 480[®] software). This comparison is based on crossing point values, and essentially compares the rates of fluorescence between reference and target genes. Efficiency of the reaction is calculated based on slope of standard curve, and is a culmination of factors including primer and enzyme efficiency.

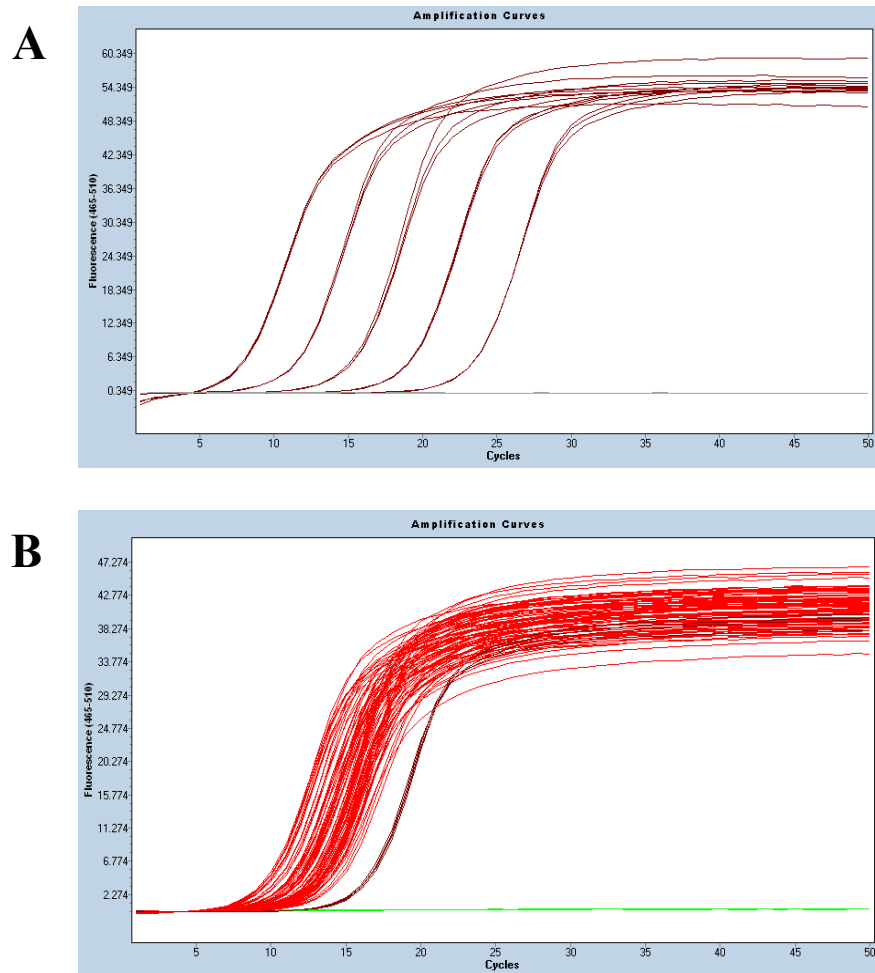


Figure B.1. (A) 18S ribosomal RNA standard curve. cDNA from each sample was pooled and serially diluted (5x, 1x, 1/10, 1/50, 1/100, 1/500) . Standards were run in triplicate. A flat line for the non-template controls, containing all reagents except for cDNA, confirms the absence of contaminating DNA. (B) 18S ribosomal RNA duplicate samples from pre-weaning and post-weaning ANP^{+/+} mice. Standards were run in triplicate. A flat line for the non-template controls, containing all reagents except for cDNA, confirms the absence of contaminating DNA. Quantification of 18s rRNA was determined by comparing standard samples with the corresponding 18S standard curve.

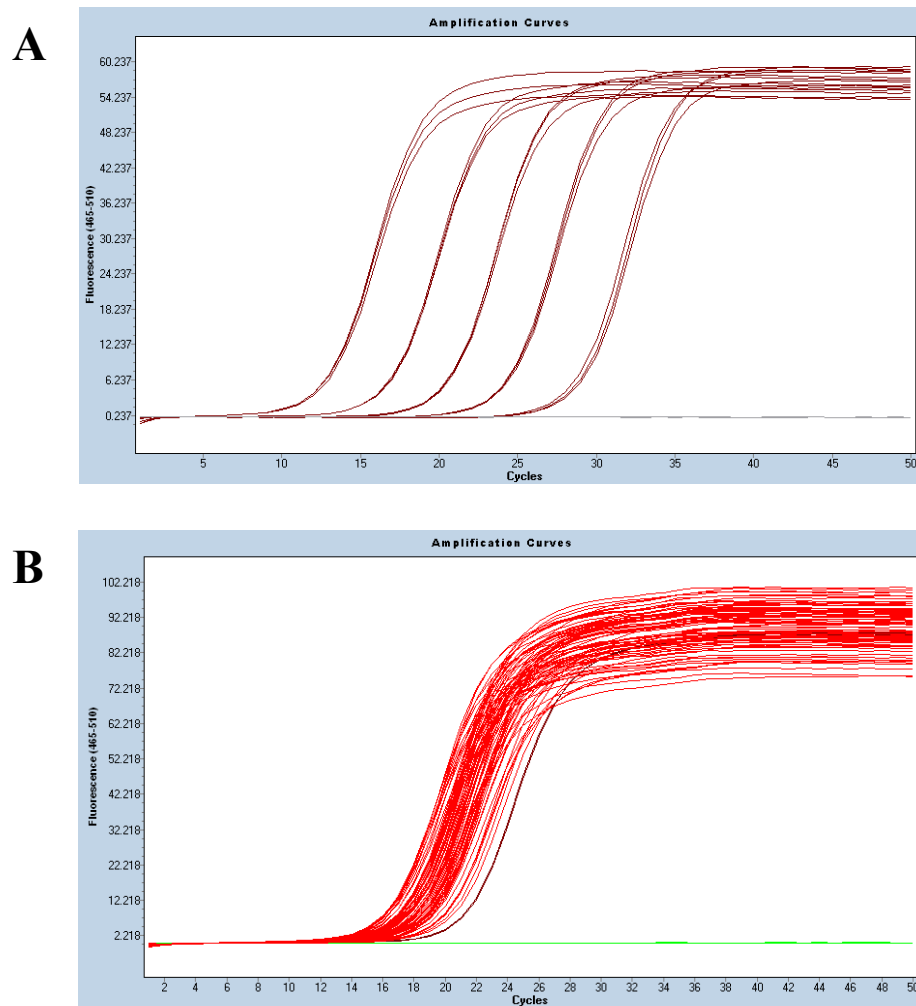


Figure B.2. (A) ANP standard curve. cDNA from each sample was pooled and serially diluted (5x, 1x, 1/10, 1/50, 1/100, 1/500). Standards were run in triplicate. A flat line for the non-template controls, containing all reagents except for cDNA, confirms the absence of contaminating DNA. (B) ANP duplicate samples from pre-weaning and post-weaning ANP^{+/+} mice (red). Standards were run in triplicate. A flat line for the non-template controls, containing all reagents except for cDNA, confirms the absence of contaminating DNA. Quantification of ANP was determined by comparing standard samples with the corresponding ANP standard curve.

Appendix C

Novel Experimental Vascular Casting Technique

Materials

Previous to polymer injection, systemic circulation is flushed with a preparatory perfusion solution. This perfusion buffer is comprised of NaCl (80g), KCl (7.45g), and EDTA (7.45g) made up to 1000mL at pH 7.4, and stored in this 10X concentrated form. Immediately preceding injection, the perfusion buffer was diluted with water to 1X concentration.

Batson's No 17 Plastic Replica and Corrosion kit comprises a partially polymerized monomer, catalyst, coloured dye (in powder form), and a promoter. These components are kept on ice, and added together immediately before injection into the designated vessel. Polymer is injected with a syringe and needle appropriate for the size of the vessel. The entire specimen is refrigerated to detract from the exothermic heat generating process of polymerization, which helps conserve structural integrity of injected tissues.

Depending on reagent proportions (increased volumes of catalyst or promoter results in faster polymerization), size of the organ, amount of total polymer injected, and temperature of polymerization environment, the injected specimen is ready for further processing between 2-3 hours and 3 days. At the time of injection, remaining polymer is put in a microcentrifuge tube to indicate when tissue-injected polymer is cured (polymer easily slides out of tube). Organs are then excised and submersed in a basic solution (5-10M NaOH), followed by an acidic solution (1M HCl), and finished with a detergent (industrial-use soap), for varying times depending on structural content and rigidity.

Experimental Modifications

Although vascular casting has been performed in alternate animal models by other research groups [99, 100], and previously on adult ANP^{-/-} mouse hearts by our research group (Pang Lab, Queen's University), this technique has never before been performed on neonatal mouse hearts. Progress was initially limited by the logistics of injecting into such a small area; actual overall body weight of these mice ranged from 1 to 25g, and the heart weight ranged from mg. In addition, the drastically reduced rigidity of cardiovascular tissues (heart, abdominal aorta) was also a major limitation during this time. However, these obstacles were overcome with a number of procedural modifications. Initially, it was apparent that each timepoint required a different needle gauge size (Table 2). In order to prevent the collapse of the abdominal aorta two sutures were put in place preliminary to needle insertion, and were delicately tightened around the needle/vessel complex once the needle was inserted. As well, a considerably smaller amount of polymer was needed for injection, and smaller amounts allowed for a more sensitive detection of the vascular injection volume capacity.

Because of the more collapsible vessels, we discovered that submersing the entire mouse corpse in refrigerated cold saline solution (0.9% NaCl/0.1% Azide) allowed the polymer in the vessels to form independent of the pressure from the weight of surrounding structures. In addition, the time for complete hardening of the polymer was drastically reduced in the neonates compared to adult mouse hearts (1-2 days compared to 2-3 days). Finally, the excised mouse heart required much less processing to remove surrounding tissues from the polymer cast. While the adult required stronger detergent NaOH, bleach and detergent solutions (each for multiple days), the older neonates required mild bleach and detergent (for less than 1 day each solution), and the younger neonates required only detergent (for 1 day).

Table C.1. Age, Weight, and Needle Size parameters for polymer injection technique.

Postnatal Timepoint	Average Weight (g)	Optimal Needle Size
1 Day	1.43 ± 0.15	N/A
1 Week	4.82 ± 0.82	25 gauge; 1 inch
2 Week	9.54 ± 0.83	25 gauge; 1 inch
3 Week	10.71 ± 1.51	23 gauge; 1 inch
4 Week	18.00 ± 2.13	21 gauge; 1.5 inch
5 Week	21.70 ± 2.45	21 gauge; 1.5 inch

Appendix D

Stereological Analysis of Cardiac Tissue

General Background

The use of stereological methods in cytology was originally established by the Delesse Principle and elaborated by Weibel [174], and applied to vascular tissue by Pang and Scott [119]. This principle is based on the assumptions that; every section is cut at random by a non-oriented section, and that an n-dimensional structure of tissue is represented on the section by an (n-1)-dimensional image. This principle allows bodies to be represented as areas, surfaces as lines and lines as points. By using a stereological grid over an image of a section of tissue, the corresponding number of times an “X” overlies or touches the structure of interest is actually representative of an estimated volume occupied by this structure. This is demonstrated by equation 1.

Equation D.1. V_x = the volume fraction of component “X”; V_t = the total volume of the organ containing “X”; P_x = the number of points overlying the profiles of “X”; P_t = the total number of points overlying the section of the organ containing “X”.

$$\frac{V_x}{V_t} = \frac{P_x}{P_t}$$

Application of Technique to Current Study

The sampling grid used for this analysis was a 10x10 regular point lattice, and gives direct percent values for volumetry (Figure 5).

Since the organization of vasculature within the heart is organized so that major blood vessels are traveling from the base to the apex, and the minor vessels branch out in a perpendicular fashion from these major vessels, and microvessels from there, the random sampling technique used in the present study may introduce a high variation in the estimates. In order to avoid extreme variations the sampling was still random, and completely blind, however areas were selected according to the presence of micro-vessels in cross section.

In order for a sample of analyzed micrographs to have minimal variability, and thus accurately represent the compositional features of the tissue, the variance between number of micrographs required for analysis was optimized. As such, a large selection of micrographs from a single tissue sample was analyzed to determine the minimum number of micrographs at which the variation of the estimates was stabilized. These variations were plotted against the number of micrographs counted. A total of 38 micrographs were analyzed according to established protocol, and it was determined that standard deviation of the estimates reached a plateau around the 5th micrograph (Figure 6, Figure 7). Thus, it was determined that each sample could be most accurately analyzed with at least 6 micrographs for minimized vessel volume error, and at least 7 micrographs for minimized myocyte volume error. As such stereological sampling consisted of counting the total number of vessel, myocyte and “other” profiles in 7 micrographs of each of 4 specimens.

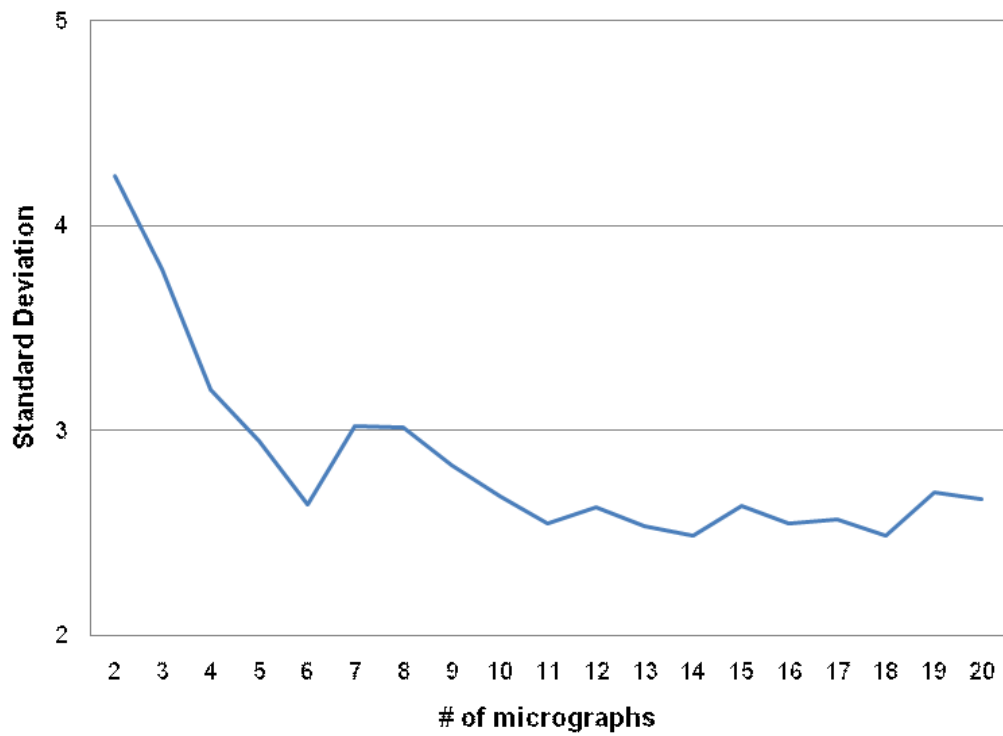


Figure D.1. Optimized number of micrographs for minimized vessel volume error.

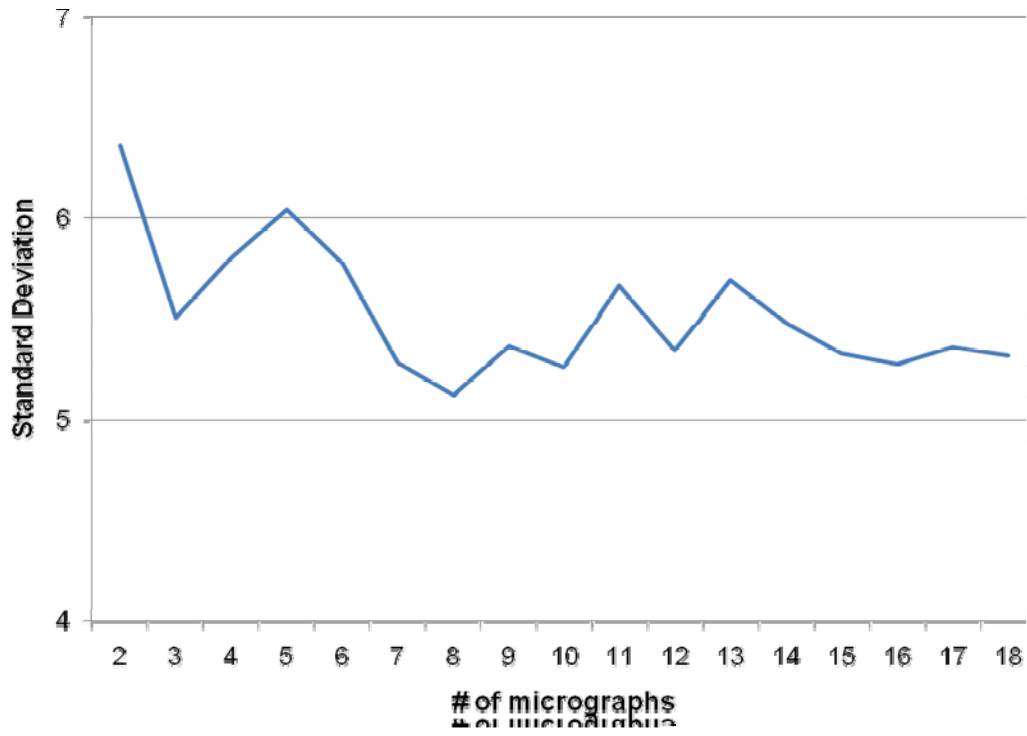


Figure D.2. Optimized number of micrographs for minimized myocyte volume error.

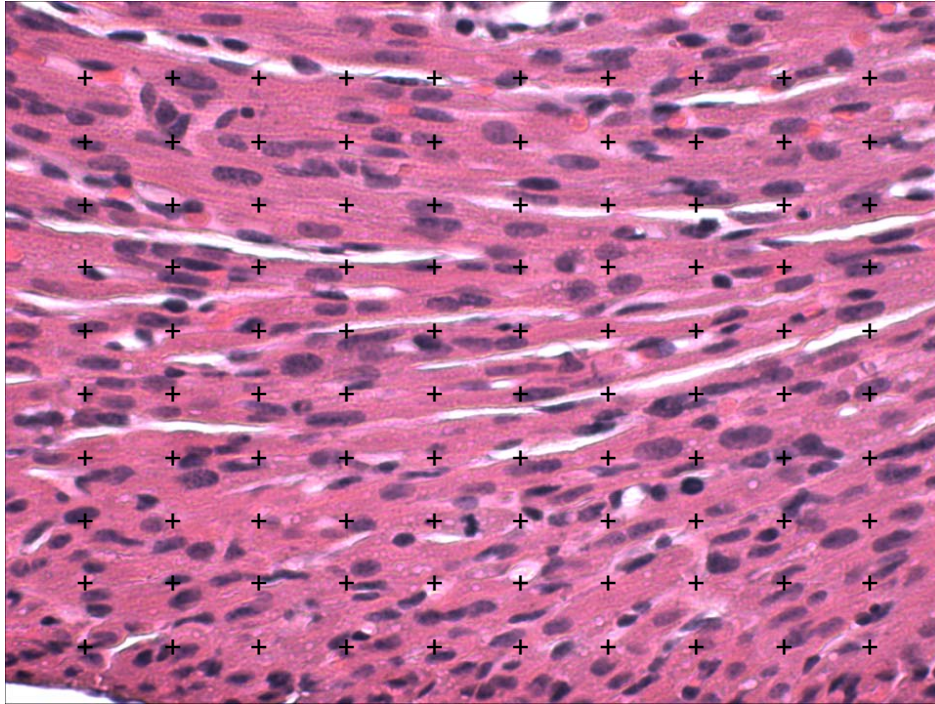


Figure D.3. Stereological grid overlying image demonstrating the stereological counting method. Any structure that is marked with any parts of the “+” indicates a count. Histological H&E stained section of 2 week ANP^{+/+} mouse heart.

Appendix E

Wet Lung Weight/Dry Lung Weight Analysis

Table E.1. Wet lung, dry lung, and wet-to-dry lung weight values for ANP^{+/+} and ANP^{-/-} male mice throughout postnatal development (day 1, weeks 1 to 5).

postnatal timepoint	ANP wildtype neonates (males)				ANP knockout neonates (males)			
		Wet lung	Dry lung	wet-to-dry		Wet lung	Dry lung	wet-to-dry
	<i>n</i>	weight (mg)	weight (mg)	weight	<i>n</i>	weight (mg)	weight (mg)	weight
day 1	10	34.48 ± 7.84	5.74 ± 1.34	16.65 ± 0.69	6	46.07 ± 8.30	8.43 ± 1.34	18.40 ± 1.33
week 1	6	106.67 ± 10.17	20.38 ± 1.82	19.15 ± 1.17	7	118.54 ± 12.23	22.40 ± 1.79	18.94 ± 0.61
week 2	5	134.7 ± 16.90	24.35 ± 2.66	18.11 ± 0.39	3	160.35 ± 20.34	36.83 ± 5.00	63.22 ± 3.22
week 3	5	111.60 ± 8.34	23.48 ± 1.82	21.04 ± 0.38	8	106.61 ± 30.63	23.95 ± 5.76	22.64 ± 0.86
week 4	7	120.81 ± 12.29	26.26 ± 2.65	21.74 ± 0.52	6	140.88 ± 30.37	33.22 ± 3.02	24.40 ± 4.96
week 5	7	129.96 ± 7.06	28.43 ± 1.14	21.93 ± 1.48	6	159.67 ± 19.22	36.02 ± 4.05	22.58 ± 0.48